RHEOLOGICAL OPTIMIZATION OF A CASTABLE PLASTIC BONDED EXPLOSIVE AND INVESTIGATION OF ITS MECHANICAL PROPERTIES

DÖKÜLEBİLİR PLASTİK BAĞLI BİR PATLAYICININ REOLOJİK OPTİMİZASYONU VE MEKANİK ÖZELLİKLERİNİN İNCELENMESİ

CANSU TUYGUN

ASSOC. PROF. DR. SELİS ÖNEL

Supervisor

Submitted to

Graduate School of Science and Engineering of Hacettepe University

as a Partial Fulfilment to the Requirements

for the Award of Degree of Master of Science in Chemical Engineering

2024

In loving memory of Asım Güngör (25.12.1994 – 25.09.2023), a dedicated lab technician and cherished friend, who made a difference and furthered our awareness. His meticulous work and kind heart left a lasting impact…

ABSTRACT

RHEOLOGICAL OPTIMIZATION OF A CASTABLE PLASTIC BONDED EXPLOSIVE AND INVESTIGATION OF ITS MECHANICAL PROPERTIES

Cansu TUYGUN

Master of Science, Department of Chemical Engineering

Supervisor: Assoc. Prof. Dr. Selis ÖNEL

June 2024, 122 pages

Efficient utilization of the available resources in the defense industry is crucial, particularly for castable polymer-bonded explosives (PBX) like PBXN-109 and -110. The rheology of PBX is strongly influenced by the properties of its components, and the initial post-mixing viscosity significantly impacts casting quality. PBXN-109 formulations employed at the Defense Industries Research and Development Institute (SAGE) of The Scientific and Technological Research Council of Turkiye (TUBITAK), achieve successful casting attributable to their low viscosity. However, certain PBXN-110 formulations exceed the designated viscosity constraints. In this study, rheological properties of a PBXN-110 formulation were optimized by adjusting the energetic powder content and particle size distribution in monomodal, bimodal, and trimodal mixtures to reduce viscosity. Micromeritic analysis of cyclotetramethylene-tetranitramine (HMX) energetic powders was conducted to identify key physical parameters influencing viscosity, a critical factor in the explosive production line Spherical HMX particles with low Hausner ratio and compressibility index, indicative of enhanced flowability, and multimodal particle size distributions were identified as key factors for achieving lower

viscosity. The influence of mean particle size on the initial viscosity was investigated, and it was shown that pre-coating the HMX particles with a plasticizer further reduces the initial viscosity. Mooney equation effectively showed the exponential dependence of initial viscosity of a bimodal Class 2 and Class 3 HMX suspension based on solid loading between 82–86%. The pseudoplastic shear thinning behavior of HMX suspensions was shown with the Oswald model based on a power law as a function of shear stress and shear rate. The non-Arrhenius temperature dependence of initial viscosity of HMX suspensions was presented by employing the Vogel-Fulcher-Tammann-Hess (VFTH) model. Statistical analyses based on micromeritic data highlighted that sphericity, bulk or tapped density, and mean diameter significantly influence the initial viscosity of the HMX suspension. These findings provide valuable insights for optimizing PBX casting processes by controlling the parameters that affect the initial viscosity of HMX suspensions.

ÖZET

DÖKÜLEBİLİR PLASTİK BAĞLI BİR PATLAYICININ REOLOJİK OPTİMİZASYONU VE MEKANİK ÖZELLİKLERİNİN İNCELENMESİ

Cansu TUYGUN

Yüksek Lisans, Kimya Mühendisliği Bölümü

Tez Danışmanı: Doç. Dr. Selis ÖNEL

Haziran 2024, 122 sayfa

Savunma sanayiinde mevcut kaynakların etkin kullanımı, özellikle PBXN-109 ve -110 gibi dökülebilir polimer bağlı patlayıcılar (PBX) için kritik öneme sahiptir. PBX reolojisi bileşen özelliklerine bağlıdır ve karıştırma sonrası elde edilen başlangıç viskozitesi döküm kalitesini büyük ölçüde etkilemektedir. Türkiye Bilimsel ve Teknolojik Araştırma Kurumu (TÜBİTAK) Savunma Sanayii Araştırma ve Geliştirme Enstitüsü (SAGE) bünyesinde uygulanan PBXN-109 formülasyonlarının düşük viskoziteleri nedeniyle başarılı bir döküm elde edilebilirken, bazı PBXN-110 formülasyonları belirlenen viskozite sınırlarını aşmaktadır. Bu çalışmada, optimum viskoziteyi düşürmek için bir PBXN-110 formülasyonunun reolojik özellikleri, enerjik toz içeriği ve monomodal, bimodal ve trimodal karışımlardaki enerjik toz içeriği ve parçacık boyutu dağılımı ayarlanarak optimize edilmiştir. Patlayıcı üretim hattında kritik bir faktör olan viskoziteyi etkileyen temel fiziksel parametreleri belirlemek için siklotetrametilen-tetranitramin (HMX) enerjik tozlarının mikromeritik analizi yapılmıştır. Düşük Hausner oranı ve sıkıştırılabilirlik indeksi ile akıcılığın arttığını gösteren küresel HMX parçacıkları ve çok modlu parçacık boyutu dağılımları, daha düşük viskozite elde etmek için kilit faktörler olarak belirlenmiştir. Ortalama parçacık boyutunun başlangıç viskozitesine etkisi araştırılmış ve HMX parçacıklarının bir plastikleştirici ile ön kaplama işleminin başlangıç viskozitesini daha da düşürdüğü gösterilmiştir. HMX süspansiyonlarının yalancı-plastik

iii

(ing. pseudo-plastic) kayma incelmesi davranışı, kayma gerilimi ve kayma hızının fonksiyonu olan ve kuvvet yasasına dayalı Oswald modeli ile gösterilmiştir. HMX süspansiyonlarının başlangıç viskozitesinin Arrhenius tipi olmayan sıcaklık bağımlılığı, Vogel-Fulcher-Tammann-Hess (VFTH) modeli kullanılarak belirlenmiştir. Mikromeritik verilere dayalı istatistiksel analizler, küreselliğin, yığın ya da sıkıştırılmış yoğunluğun ve ortalama parçacık çapının HMX süspansiyonlarının başlangıç viskozitesini önemli ölçüde etkilediğini göstermiştir. Bu bulgular, HMX süspansiyonlarının başlangıç viskozitesini etkileyen parametreleri ayarlayarak PBX döküm süreçlerini optimize etmek için değerli bilgiler sağlamaktadır.

Anahtar Kelimeler: Polimer bağlı patlayıcı süspansiyonu; Reoloji; Başlangıç viskozitesi; Modalite; Parçacık boyutu

GENİŞ TÜRKÇE ÖZET

DÖKÜLEBİLİR PLASTİK BAĞLI BİR PATLAYICININ REOLOJİK OPTİMİZASYONU VE MEKANİK ÖZELLİKLERİNİN İNCELENMESİ

Cansu TUYGUN

Yüksek Lisans, Kimya Mühendisliği Bölümü

Tez Danışmanı: Doç. Dr. Selis ÖNEL

Haziran 2024, 122 sayfa

Bu tez çalışmasında, polimer bağlı patlayıcıların (PBX) kalıplara güvenli ve etkili bir şekilde dökülebilmesinde kritik olan siklotetrametilen-tetranitramin (HMX) enerjik parçacıklarının polimer bir sıvı içinde süspansiyonlarının reolojik davranışı incelenmiştir. Standard PBXN-110 formülasyonunun Türkiye Bilimsel ve Teknolojik Araştırma Kurumu (TÜBİTAK) Savunma Sanayii Araştırma ve Geliştirme Enstitüsü (SAGE) bünyesinde uygulanan modifiye reçetesi kullanılmıştır. Bu süspansiyon şekillendirilmek üzere kalıba döküm için uygun bir başlangıç viskozitesine (ing. initial viscosity) sahip olmalıdır. Süspansiyonun viskozitesi, mekanik ve kimyasal etkiler nedeniyle HMX enerjik katı ve polimerik sıvı miktarına bağlı olarak değişmektedir. Bu tez kapsamında, PBX üretiminde son aşamada uygulanan kürleme maddesinin ilavesi yapılmadan önce, modifiye PBXN-110 katı-sıvı polimer süspansiyonunun başlangıç viskozitesini en aza indirmek ve kap ömrünü artırmak için gereken fiziksel etkenler araştırılmıştır. PBX'in döküm sürecini (ing. pot life) iyileştirmek amacıyla kürleme öncesi reolojik özellikleri etkileyen parametreler incelenmiştir. PBX süspansiyonunda bulunan HMX parçacık özelliklerinin, HMX parçacık-sıvı polimer süspansiyonunun başlangıç viskozitesi üzerindeki etkisi araştırılmıştır. HMX süspansiyonunun reolojisi çeşitli kayma hızlarında

(ing. shear rate) analiz edilmiştir. Sıcaklığın HMX süspansiyonunun reolojisi üzerindeki etkileri incelenmiştir.

Tezin ilk bölümünde, küçükten büyüğe doğru HMX Sınıf 5, Sınıf 2 ve Sınıf 3 HMX parçacıklarının karakterizasyonu yapılmıştır. Bu parçacıklar monomodal, bimodal ve trimodal formda farklı oranlarda kullanılarak elde edilen HMX karışımlarının ortalama parçacık boyutu, parçacık boyutu dağılımı ve modalitesi, parçacık şekli, küreselliği, sıkıştırılmış yoğunlu ve yığın yoğunluğu gibi mikromeritik özellikleri incelenmiştir. HMX parçacıklarının mikromeritik özelliklerinin, sıvı bir polimer içinde sabit süre karıştırma sonucu oluşan katı-sıvı süspansüyonunun reolojik özelliklerini nasıl etkilediği gösterilmiştir. Başlangıç viskozitesini düşürme ile ilgili bulgular şu şekildedir:

- Küresel HMX parçacıkları şekilleri nedeniyle akışa karşı asgari direnç göstererek karışımın daha kolay akmasını sağlar. Düşük Hausner oranı (HR) ve sıkıştırılabilirlik indeksi (CI), akış sırasında parçacıklar arasında düşük etkileşim ve kenetlenme olduğunu göstermektedir. Farklı boyutlarda HMX parçacıklarının kullanılması, yani multimodal dağılım, daha yoğun bir paketleme oluşmasına olanak tanımaktadır. Karışımdaki HMX miktarının artması başlangıç viskozitesini önemli ölçüde arttırmaktadır.

- İki farklı boyutta, Sınıf 2 ve Sınıf 3 HMX parçacıklarının, sırasıyla 1:2 oranında karıştırılması, 0,016 s-1 kayma hızında en düşük başlangıç viskozitesiyle sonuçlanmıştır. Bunun nedeni, küçük Sınıf 2 parçacıklarının daha büyük olan Sınıf 3 parçacıkları arasındaki boşlukları doldurarak daha yoğun bir paketlenmeye yol açmasıdır. HMX parçacıklarının izodesil pelargonat (IDP) plastikleştirici ile önceden kaplanması,

- Şekil *1*' de görüldüğü gibi nihai ürünün akış özelliklerini ve mekanik özelliklerini iyileştirmiştir.
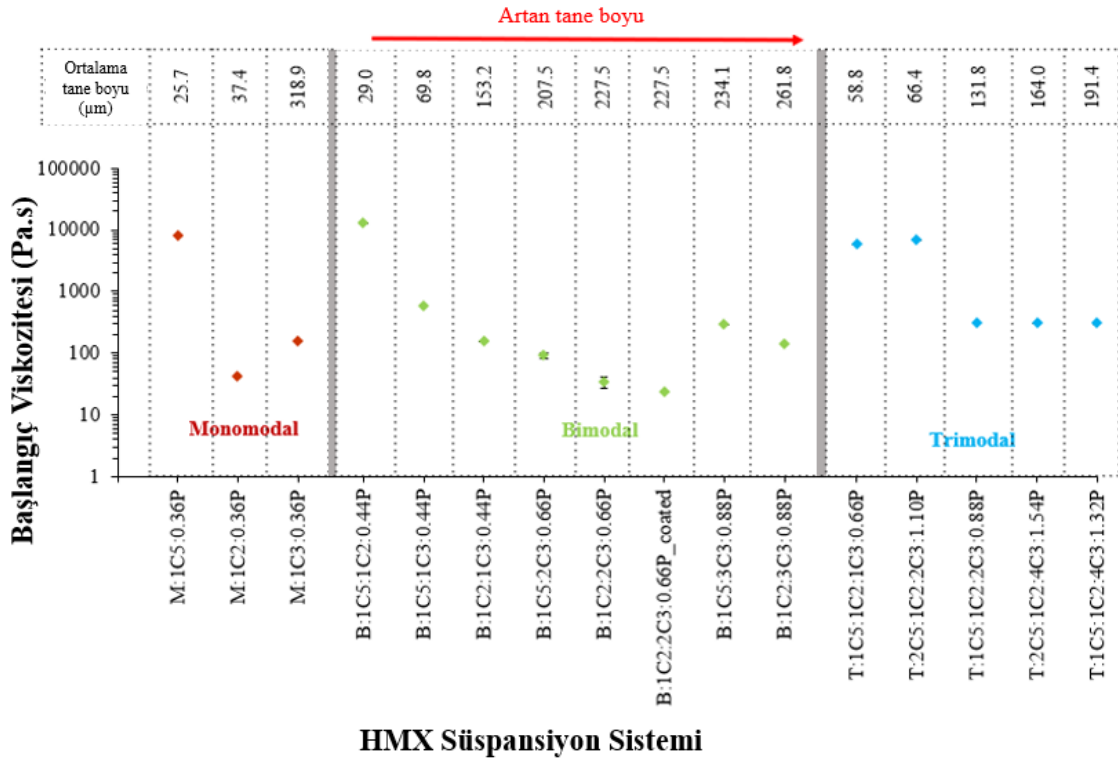
Şekil 1. 50 °C ve 0,016 s^{-1} kayma hızında mono, bi- ve tri-modal HMX süspansiyon sistemlerinin ortalama parçacık boyutuna bağlı başlangıç viskozitesi

Tezin üçüncü bölümünde, başlangıç viskozitesini tekli veya çoklu parametrelerin bir fonksiyonu olarak tahmin etmek için uygulanan çeşitli viskozite modelleri sunulmuştur. Bu modeller şu şekilde sıralanabilir:

1. Katı yüklemeye bağlı modeller,

2. Sıcaklığa bağlı; ancak Arrhenius tipi olmayan model,

3. Kayma gerilimi ve kayma hızına bağlı viskozite modelleri ve

4. Çoklu verilere dayalı karmaşık istatistiksel yöntemler.

İlk olarak başlangıç viskozitesinin %82 ve %86 arasında katı yüklemeye bağlı değişimi incelenmiştir. 50 °C sıcaklık ve 0,016 s^{-1} kayma hızı koşullarında, Sınıf 2-Sınıf 3 HMX kütle oranı 1:2 olan PBX süspansiyonunda katı yüklemesi arttırıldığında elde edilen bağıl viskozite Şekil 2'de siyah noktalarla gösterilmiştir. Bağıl viskozite, PBX süspansiyonunun başlangıç viskozitesinin aynı koşullardaki polimerin viskozitesine oranı olarak hesaplanmıştır. Deneysel sonuçlara göre PBX süspansiyonunda HMX yüklemesi

arttıkça viskozite üstel olarak artmaktadır. Literatürde, artan katı parçacık içeriği ile süspansiyon viskozitesinin arttığını gösteren birçok çalışma [40,71,78,79] bulunmaktadır. Döküm polimer bağlı patlayıcı PBXN-110'un gereklilikleri, Amerika Birleşik Devletleri Savunma Bakanlığı (US Department of Defense) tarafından yayınlanan bir askeri standart olan MIL-DTL-82901A'da [14] belirtilmiştir. Bu standartta işlenebilir azami viskozite 1000 Pa.s olarak belirtildiğinden, daha iyi sonuçlar alabilmek için modifiye PBXN-110 süspansiyonunda modalite çalışmaları %82 HMX yüklemesi ile gerçekleştirilmiştir.
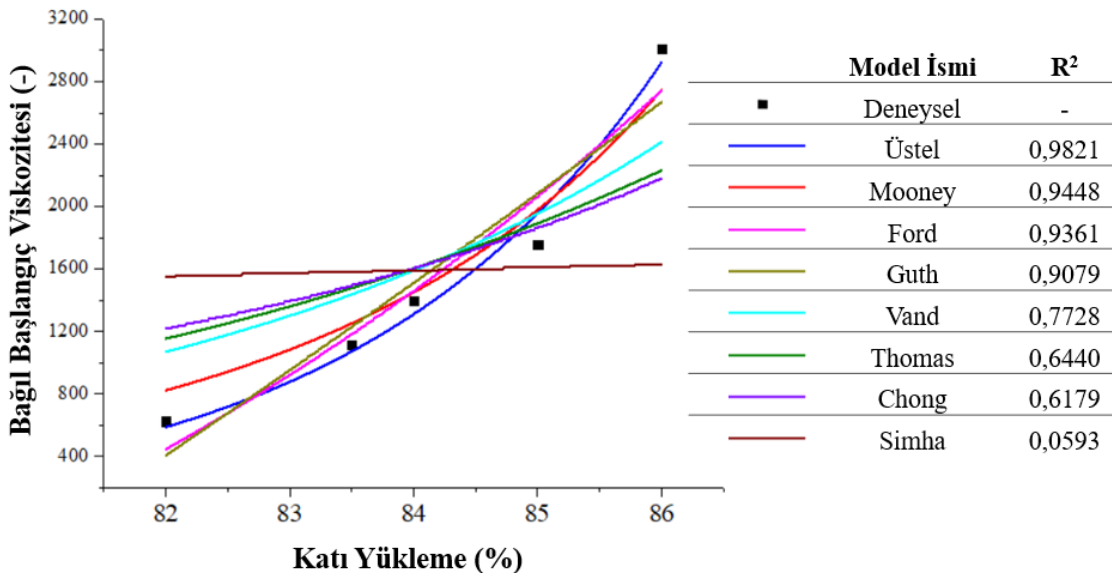
Şekil 2. Karışım sonundaki bağıl başlangıç viskozitelerinin 50 °C ve 0,016 s^{-1}' de farklı HMX yüklemesine (%) sahip PBX süspansiyonları için literatür ve deneysel verilerin karşılaştırılması

Katı parçacık-sıvı polimer süspansiyonlarının bağıl viskozitesi ile ilgili literatürde kullanılmış olan matematiksel modeller ve belirlilik katsayısı R^2 değerleri Şekil 2' de sunulmuştur. R^2 değerleri büyükten küçüğe doğru dizilmiştir. En iyi model $R^2 = 0,9448$ değeri ile Şekil 2' de kırmızı çizgi ile gösterilen Mooney modeli olmuştur. Çalışmada elde edilen deneysel sonuçlara uydurularak elde edilen sabit katsayılar ile Mooney denklemi $\eta_r = exp\left(\frac{2.5 \times \varphi}{1 - 0,8471 \times \varphi}\right)$ olarak belirlenmiştir.

İkinci olarak, sıcaklığın HMX süspansiyon sistemlerinin viskozitesi üzerindeki etkisi, kayma hızı sabit tutularak incelenmiştir. Şekil 3'te 0,005 s^{-1}, 0,016 s^{-1}, 0,05 s^{-1} ve 1 s^{-1} kayma hızlarında sıcaklığın 30 °C'tan 50 °C'a ve 70 °C'a yükseltilmesiyle viskozitedeki azalış görülmektedir. Düşük 0,005 s^{-1} ve 0,016 s^{-1} kayma hızlarında beklenenden farklı

sonuç veren iki sistem dışında tüm sistemler için viskozitenin artan sıcaklıkla azaldığı bulunmuştur. Bimodal B:1C5:1C3:0.44P ve IDP kaplı B:1C2:2C3:0.66P sistemlerinin, bu düşük kayma hızlarında sıcaklık 30 °C'tan 50 °C'a yükseltildiğinde viskozitelerinin arttığı görülmüştür. Sıcaklığın 70 °C'a yükseltilmesi her iki sistemde de viskozitenin düşmesine neden olmuştur, bu beklenen bir davranıştır.
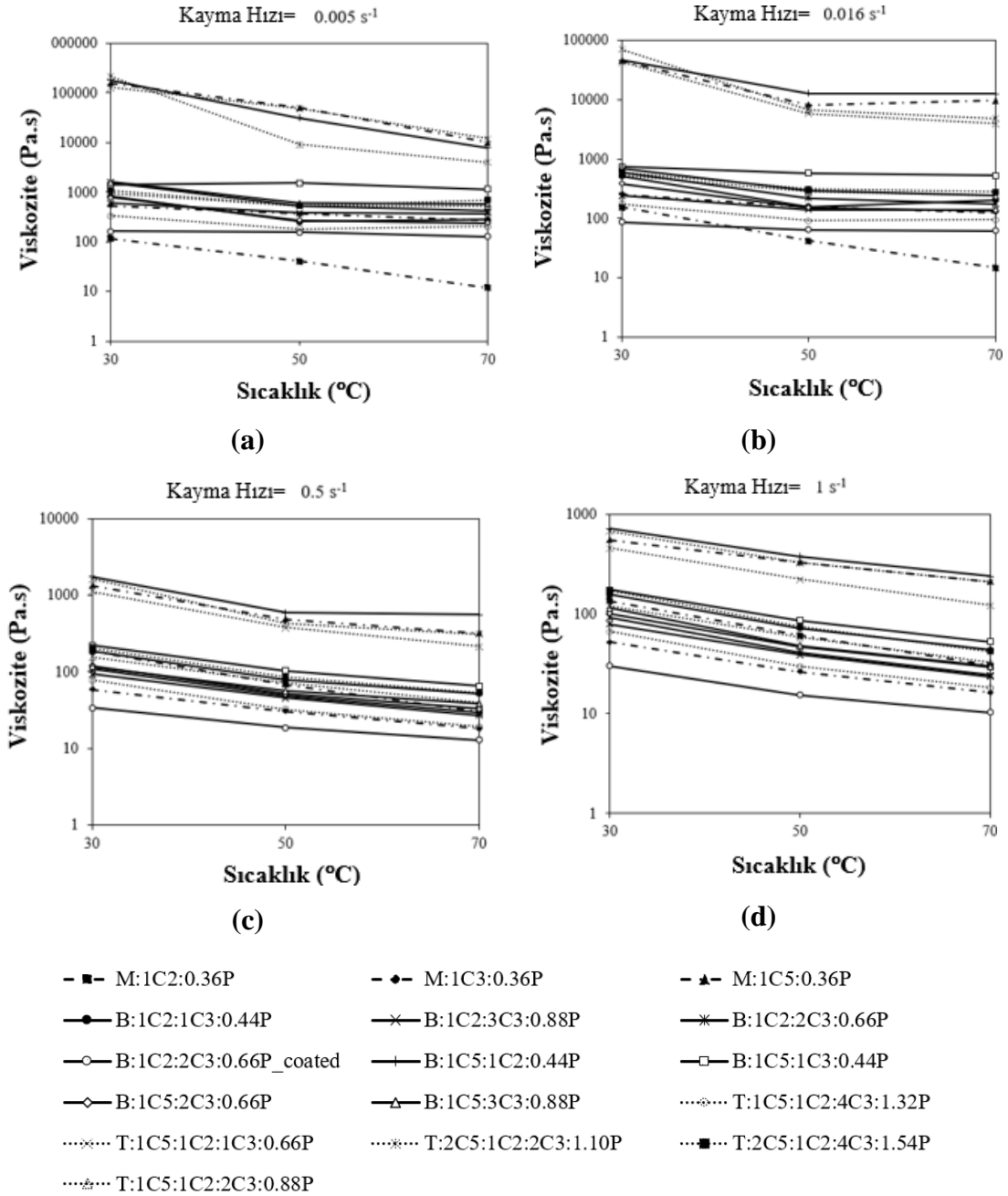
Şekil 3. (a) 0.005 s^{-1}, (b) 0.016 s^{-1}, (c) 0.5 s^{-1}, and (d) 1 s^{-1} olarak değişen kayma hızlarında sıcaklığa bağlı viskozite

Artan sıcaklıkla HMX süspansiyonlarının viskozitesindeki düşüş, Vogel-Fulcher-Tammann-Hess (VFTH) viskozite modeli ile gösterilmiştir. Bu model Arrhenius tipi olmayan bir sıcaklık ilişkisi ifade etmektedir. VFTH denkleminin A, B ve C sabitleri eğri uydurma (ing. curve fitting) yoluyla bulunmuş ve 0,005, 0,016, 0,5 ve 1 s^{-1} sabit kayma hızlarında her HMX süspansiyon sistemi için Tablo 1'de sunulmuştur. Her sistem için 1 veya 1'e çok yakın olarak hesaplanan R^2, HMX süspansiyon viskozitesinin, sıcaklığa bağlı VFTH modeline mükemmel bir şekilde uyduğunu göstermektedir. A, B ve C sabitlerinin HXM süspansiyonunun kayma hızına bağlı olduğu bulunmuştur.

Tablo 1. HMX-polimer süspansiyon sistemleri için farklı kayma hızlarında Vogel-Fulcher-Tammann-Hess (VFTH) modeli sabitleri

HMX Süspansiyon Sistemi	Kayma Hızı (s^{-1})	A (Pa.s)	B (K)	C (K)	R^2
M:1C5:0.36P	0.005	3	1250	-217	1.0000
	0.016	67	49	-7	1.0000
	0.5	0	992	-135	1.0000
	1	1	415	-71	1.0000
M:1C2:0.36P	0.005	2385	-1291	-596	1.0000
	0.016	2385	-1291	-596	1.0000
	0.5	2385	-1291	-596	1.0000
	1	2385	-1291	-596	1.0000
M:1C3:0.36P	0.005	0	1944	-153	0.9953
	0.016	0	1858	-129	1.0000
	0.5	0	1344	-123	1.0000
	1	0	2844	-228	1.0000
B:1C2:1C3:0.44P	0.005	0	3155	-139	0.9286
	0.016	1042	0	30	0.8585
	0.5	112	73	1	1.0000
	1	0	2130	-247	1.0000
B:1C2:2C3:0.66P	0.005	370	1	29	1.0000
	0.016	142	0	31	1.0000
	0.5	1	479	-76	1.0000
	1	1	385	-65	1.0000
B:1C2:2C3:0.66P$_{coated}$	0.005	276	22	17	1.0000
	0.016	124	18	18	1.0000
	0.5	2	290	-46	1.0000
	1	2	316	-50	1.0000

HMX Süspansiyon Sistemi	Kayma Hızı (s^{-1})	A (Pa.s)	B (K)	C (K)	R^2
B:1C2:3C3:0.88P	0.005	304	-3	33	1.0000
	0.016	243	-5	37	1.0000
	0.5	14	104	-11	1.0000
	1	4	294	-48	1.0000
B:1C5:1C2:0.44P	0.005	1	2905	-542	0.6665
	0.016	59	2	24	1.0000
	0.5	2	180	-38	1.0000
	1	2	152	-28	1.0000
B:1C5:1C3:0.44P	0.005	0	2589	-133	1.0000
	0.016	12184	1	29	1.0000
	0.5	521	3	28	1.0000
	1	10	491	-85	1.0000
B:1C5:2C3:0.66P	0.005	0	7680	-845	0.0225
	0.016	409	18	1	1.0000
	0.5	9	213	-36	1.0000
	1	3	353	-60	1.0000
B:1C5:3C3:0.88P	0.005	199	8	24	1.0000
	0.016	114	8	24	1.0000
	0.5	8	124	-15	1.0000
	1	3	233	-39	1.0000
T:1C5:1C2:4C3:1.32P	0.005	569	1	29	1.0000
	0.016	176	17	18	1.0000
	0.5	10	112	-16	1.0000
	1	6	147	-19	1.0000
T:1C5:1C2:1C3:0.66P	0.005	225	-3	37	1.0000
	0.016	98	-1	32	1.0000
	0.5	3	199	-28	1.0000
	1	2	212	-33	1.0000
T:2C5:1C2:2C3:1.10P	0.005	0	2971	-147	0.9060
	0.016	2267	28	20	1.0000
	0.5	34	155	-15	1.0000
	1	0	1429	-159	1.0000
T:2C5:1C2:4C3:1.54P	0.005	961	77	16	1.0000
	0.016	3149	21	23	1.0000
	0.5	188	27	18	1.0000
	1	39	167	-29	1.0000
T:1C5:1C2:2C3:0.88P	0.005	797	-4	41	1.0000
	0.016	249	6	23	1.0000
	0.5	10	145	-19	1.0000
	1	2	386	-57	1.0000

Üçüncü olarak, çalışmada elde edilen deneysel sonuçlar, kayma gerilimi ve kayma hızına bağlı viskozite modelleri ile incelenmiştir. Literatürde içeriği PBX ile benzeyen kompozit katı yakıt süspansiyonları üzerine yapılan araştırmalara göre, katı-sıvı süspansiyonlarının kayma ile incelen (ing. shear thinning) yalancı-plastiklik (ing. pseudo-plasticity) indeksi *n*'nin 0,6 - 1 arasında değiştiği görülmüştür [37, 38]. Bu çalışmada Şekil 4'te en düşük viskoziteli B:1C2:2C3:0.66P, B:1C5:2C3:0.66P ve T:1C5:1C2:4C3:1.32P HMX süspansiyonları için 30 °C, 50 °C ve 70 °C' ta kayma gerilimine karşı kayma hızı eğrileri Oswald modeli (ing. Power Law Model PLM) kullanılarak elde edilmiştir. Tablo 2'de PLM modelinin sabit sayıları olan yalancı-plastiklik indeksi (*n*) ve tutarlılık katsayısı (*K*) ve R^2 değerleri gösterilmiştir. Buna göre PBX süspansiyonunun, *n* değerlerinin genellikle 0,61 ile 0,89 arasında değiştiği ve kompozit katı yakıt süspansiyonu ile ilgili literatürle uyumlu olarak kayma ile incelen yalancı-plastik davranış gösterdiği doğrulanmıştır. Ayrıca 0,98'i aşan R^2 değerleri ile PLM modelinin PBX süspansiyonu ile uyumlu olduğu anlaşılmaktadır. Özellikle, *n* değerlerinin sıcaklıkla birlikte arttığı görülmektedir. 70 °C'ta daha düşük R^2 değerleri elde edilerek tutarsızlıklar gözlenmiştir.

.
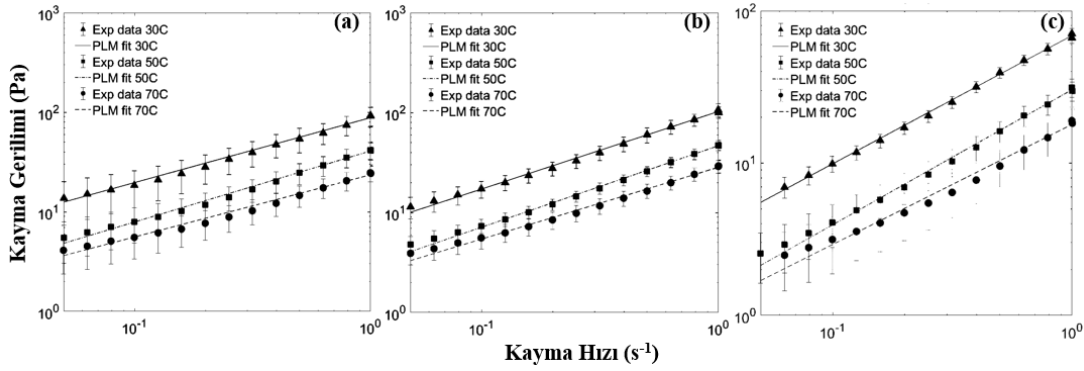
Şekil 4. (a) B:1C2:2C3:0.66P, (b) B:1C5:2C3:0.66P, (c) T:1C5:1C2:4C3:1.32P HMX süspansiyon sistemlerinde kayma geriliminin (ing. shear stress) kayma hızına bağlı değişiminin deneysel sonuçları ve Oswald viskozite modeli (ing. Power law model, PLM) ile elde edilen eğriler

Tablo 2. En düşük viskoziteye sahip üç HMX süspansiyon sisteminin farklı sıcaklıklarda Oswald modeli (Power Law Model, PLM) sonuçları

HMX Süspansiyonu	Sıcaklık (°C)								
	30			50			70		
	n	K (Pa.s^n)	R^2	n	K (Pa.s^n)	R^2	n	K (Pa.s^n)	R^2
B:1C2:2C3:0.66P	0.65	88	0.9870	0.71	41	0.9922	0.62	24	0.9841
B:1C5:2C3:0.66P	0.78	100	0.9967	0.82	47	0.9978	0.72	28	0.9952
T:1C5:1C2:4C3:1.32P	0.84	69	0.9982	0.89	30	0.9964	0.79	18	0.9848

Dördüncü olarak, karmaşık istatistiksel yöntemler kullanılarak yapılan analiz, HMX süspansiyonunun başlangıç viskozitesinin birden fazla parametreden önemli ölçüde etkilendiğini göstermiştir. Şekil 5.(a)'da görüldüğü gibi 30 °C, 50 °C ve 70 °C'taki reometre ölçümlerinden elde edilen viskozite sonuçları yüksek bir korelasyona sahiptir. Bu sonuç, üç sıcaklık değerinden herhangi birinin diğerlerini temsil etmek üzere kullanılabileceğini göstermektedir. Reometreden elde edilen viskozite sonuçları Brookfield viskometreden elde edilen viskozite sonuçları ile nispeten zayıf bir

korelasyona sahiptir. Bu nedenle, Brookfield viskometre ile ölçülen sonuçlar istatistiksel analiz için kullanılmamıştır. İstatistiksel analizlerde sadece reometre ile 50 °C'de yapılan viskozite ölçümleri kullanılmıştır. Şekil 5.(b)'de sıkıştırılmış yoğunluk ve yığın yoğunluğun %96 korelasyon ile bağımlı ve neredeyse tamamen doğru orantılı oldukları görülmektedir. Sonuç olarak, sıkıştırılmış yoğunluk değeri çıkarılmıştır ve analizde bağımsız değişken olarak yığın yoğunluk kullanılmıştır. Ortalama çap, yığın yoğunluk ve küresellik kullanılarak reometreyle 50 °C'ta ölçülen viskozite sonuçları ile Pyton Charm kullanılarak regresyon analizi yapılmıştır.
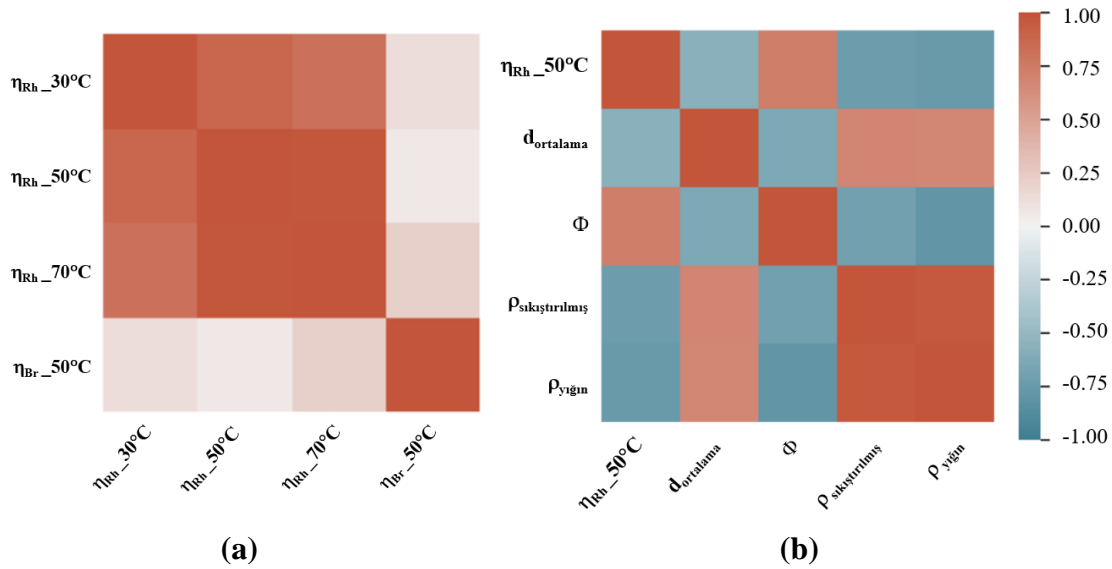
Şekil 5. (a) Reometre ve Brookfield viskometre ile ölçülen viskozitenin ıraksak ısı haritası, **(b)** Reometre ile 50°C'ta ölçülen viskozitenin ve diğer mikromeritik parametrelerin (ortalama çap $d_{ortalama}$, küresellik Φ, sıkıştırılmış yoğunluk $\rho_{sıkıştırılmış}$, and yığın yoğunluk $\rho_{yığın}$) ıraksak ısı haritası

Şekil 6'da rastgele orman modeli (ing. random forest model) ile yapılan veri analiz sonuçları gösterilmiştir. HMX parçacık küreselliğinin, 50 °C sıcaklıkta ve 0,016 s^{-1} kayma hızında ölçülen başlangıç viskozitesi üzerinde %58 oranda en etkili parametre olduğu tespit edilmiştir. Bunu %31 ile yığın veya sıkıştırılmış yoğunluk ve %11 ile ortalama partikül çapı izlemektedir. Bu sonuç, süspansiyonun başlangıç viskozitesini ayarlayabilmek için bu özelliklerin birlikte etkisinin dikkate alınmasının önemini vurgulamaktadır.
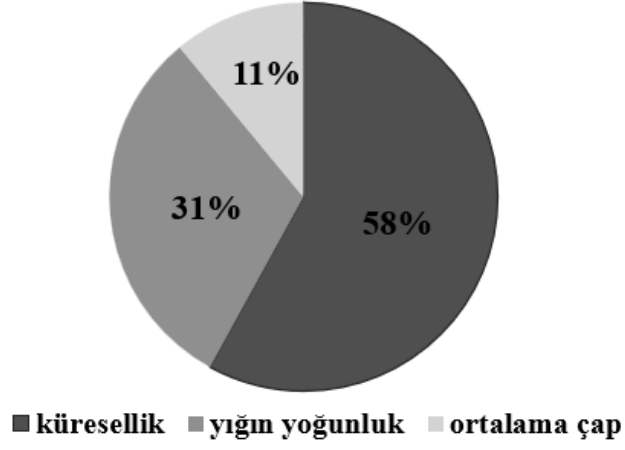
Şekil 6. Rastgele orman modeline göre değişkenlerin reometrede 50 °C sıcaklıkta ölçülen başlangıç viskozitesi üzerindeki etki yüzdeleri

Sonuç olarak, bu tez çalışması HMX parçacıklarının çoklu mikromeritik özelliklerinin HMX süspansiyonunun başlangıç viskozitesi üzerindeki kritik rolünü ortaya koymaktadır. Araştırmacılar ve üreticiler bu mikromeritik özellikleri optimize ederek etkili döküm süreçleri elde edebilir ve PBXN-110 ürününün nihai kalitesini artırabilir.

Anahtar Kelimeler: Polimer bağlı patlayıcı süspansiyonu; Reoloji; Başlangıç viskozitesi; Modalite; Parçacık boyutu

ACKNOWLEDGEMENTS

TABLE OF CONTENTS

LIST OF TABLES

LIST OF FIGURES

LIST OF ABBREVIATIONS

CI : Compressibility Index

°C : Degree Celsius

DBTDL : Dibutyltin dilaurate

HMX : Cyclotetramethylene-tetranitramine, Octogen

HR : Hausner Ratio

HTPB : Hydroxyl-Terminated Polybutadiene

IDP : Isodecyl Pelargonate

IPDI : Isophorone Diisocyanate

K : Kelvin

m$_{eq}$: Milliequivalent

P : Poise

PBX : Polymer Bonded Explosive

PBXN : Polymer Bonded Explosive Navy

R^2 : The coefficient of determination

RDX : Siklotrimetilen-trinitramin, Royal Demolition Explosive

SAGE : Defense Industries Research and Development Institute

SEM : Scanning Electron Microscopy

St. Dev. : Standard deviation

TNT : Trinitrotoluene

wt% : Weight percentage

VFTH : Vogel-Fulcher-Tammann-Hess

LIST OF SYMBOLS

η **:** The apparent viscosity or dynamic viscosity (Pa.s)

η_r **:** The relative viscosity ((Pa.s)/(Pa.s))

η_{Br} **:** The viscosity from Brookfield viscometer (Pa.s)

η_{Rh} **:** The viscosity from rheometer (Pa.s)

φ **:** The volumetric concentration of solid particles (vol./vol.)

Φ **:** Sphericity

$\dot{\gamma}$ **:** The shear rate (1/s)

τ **:** The shear stress (Pa)

n   **:** The pseudoplasticity index (unitless)

K   **:** The consistency coefficient (Pa.s^n)

k   **:** Experimental crowding factor for particles

d_{mean} **:** The mean diameter (μm)

ρ_{bulk} **:** The bulk density (g/ml)

ρ_{tapped} **:** The tapped density (g/ml)

1.   INTRODUCTION

Research in the defense industries has become essential for technological development and competition between countries. Today's world economic crisis requires each country to use its resources in the most efficient and practical ways. TUBITAK SAGE is one of the leading research and development companies in Turkiye working in the defense industry, where studies on explosives, propellants, and pyrotechnics are carried out. The two types of explosive materials used at SAGE are the most commonly used castable polymer bonded explosives (PBXs), Navy 109 (US code PBXN-109) and Navy 110 (US code PBXN-110). The rheology of PBXs depends significantly on the contents and their micromeritic properties. The initial viscosity of the PBX following the completion of mixing of the contents right before casting is significant as it affects the process of casting and, thus, the quality of the final product. The formulations of PBXN-109 employed at SAGE result with relatively low initial viscosities after mixing and can be cast easily resulting in high quality products. Some of the formulations for PBXN-110 have been observed to have initial viscosities above the limits required for a high-quality casting.

Within the scope of this thesis, we worked on optimizing the rheological properties of one of the formulations of PBXN-110 to improve the casting process. We modified the formulation of PBXN-110 by adjusting the contents of the energetic powder. We aimed at reaching an optimum viscosity by using energetic particles of different sizes in monomodal, bimodal, and trimodal mixtures. We did a micromeritic analysis, which are the properties of micro particles, such as particle size, packing, porosity, cohesion between micro particles and flowability of HMXs, to investigate the physical parameters that affect the viscosity of the final product, which is a critical parameter in the production line of an explosive.

Energetic materials can be classified as sensitive and insensitive based on their vulnerability to explosion under external stimuli. Sensitive energetic materials used in military munitions have a high risk of out-of-control explosion due to friction heating or pressure build-up as a result of an impact. Energetic materials can be deafened by making them insensitive by homogeneously distributing them in a polymer liquid and binding the particles to this polymer with chemical bonds [1,2]. The term "plastic/polymer bonded explosive" (PBX), refers to energetic particles suspended in a polymer liquid, i.e., a composite material. PBXs are insensitive explosives and frequently utilized in insensitive

munition (IM) applications [3]. They are relatively safer and less likely to explode during storage, transit, or usage. PBXs are thermoset plastics and they cannot be recycled or reprocessed [4]. PBXs have several potential benefits over the commonly used explosives [5], which are either difficult to make or cannot be quickly melted into a cast, such as warheads [6]. Due to their high level of safety, simplicity of operation, and superior strength, PBXs are frequently employed in both civil and military applications. Nowadays, PBXs are used in development studies to benefit from their insensitivity and high energy density properties, and improved mechanical integrity [1,7].

PBXs can be produced in three ways: 1. Pressing, 2. Extrusion, and 3. Casting. In the former method, powders of PBX are pressed into a mold with a certain shape at room temperature [1]. In the second, the formulation is combined and then fed straight into an extruder, where pressure is applied to force it through a die [4]. In the latter case applied in this study, an insensitive energetic material is mixed with a polymer and cured at a specified temperature and time, so that the energetic powders can stand together to form a flexible and insensitive polymer-bonded castable explosive [4]. A planetary rotating double-blade vertical stirrer is commonly used in the production of PBXs to evenly distribute the solid particles within a low molecular weight polymer liquid. These explosives should be cast easily into the munition and no air gap should be formed. If an air gap forms inside the explosive, undesirable situations, such as hot spots, may form due to adiabatic jams, where regional energetic reactions may develop. A hot spot can cause non-impact ignition when stimulated externally, which poses a major threat to the stability of the charge that might result in an uncontrolled explosion. Such undesired results must be prevented by providing solutions to increase the safety of explosives [8][9][10].

Castable polymer bonded explosives should be thermally and chemically stable. PBXN-109 is a general-purpose explosive used in defense industry applications. PBXN-110 is an explosive used to achieve high particle impact. Table 1.1 shows the specifications of PBXN-109 and PBXN-110. The percent solid loading in PBXN-109 and PBXN-110 should be 84 % and 88 %, respectively. The energetic materials included in PBXN-109 are research department explosives (RDX) or hexogens, i.e. organic compounds with the formula $(O_2N_2CH_2)_3$, such as RDX Class 1 and RDX Class 5 and aluminum (Al) powder. Class is based on particle size, which is ~150 micron for RDX Class 1 that is larger than

RDX Class 5 with ~25 micron particle size [11]. The energetic materials that make PBXN-110 are high melting explosives (HMX) or octogens, i.e. cyclotetramethylene-tetranitramine, such as Grade B HMX Class 2 (~35 microns) and HMX Class 3 (~350 microns) [12]. HMX is obtained by nitrolysis of RDX and is a more powerful explosive. Grade refers to the mass ratio of RDX in HMX, for example, Grade B HMX contains 2% of RDX and thus a HMX purity of 98%. PBXN-109 contains hydroxy-terminated polybutadiene (HTPB) as a binder, dioctyl adipate (DOA) as a plasticizer, dimethylhydantoin (DHE) as a bonding agent, triphenyl phosphate (TPB) as a catalyst, and isophorone diisocyanate (IPDI) as a curing agent [13]. The military standard with the code MIL-DTL-82901A(OS) describes Polymer Bonded Explosive Navy-110 (PBXN-110) as a copolymer-bonded material [14]. PBXN-110 contains HTPB as a binder, isodecyl pelargonate (IDP) as a plasticizer, lecithin as a surfactant, dibutyltin dilaurate (DBTDL) as a catalyst and IPDI as a curing agent. The NCO group from IPDI and OH group from HTPB are the groups that make up the polyurethane reaction. The NCO/OH (wt/wt) value is given Table 1.1 below. The parameter that is effective in determining the mechanical properties of the product, which is the ratio of binder to plasticizer, is given in Table 1.1.

Energetic materials are in general thermally and mechanically sensitive, i.e., they have high autoignition temperatures, as well as high sensitivity to friction, shock, and impact. Energetic materials should be compatible with each other and be processable. They should have a high performance, i.e., a high velocity of detonation (VOD).

Table 1.1. PBX types using polyurethane (PU) liquid according to military standards of PBXN-109 and PBXN-110

PBX Type	Solid Loading (%)	NCO/ OH	Binder / Plasticizer	Bonding Agent / Surfactant	Energetic Material (solid)
PBXN-109 [13]	80–88	1.0–1.1	HTPB-to-DOA 0.95 – 1.05	DHE (B.A.[*])	RDX / Al
PBXN-110 [14]	86–89	1.0–1.1	HTPB-IDP 0.95 – 1.05	Lecithin (S.[**])	Grade B, HMX

[*]B.A.: bonding agent

[**]S.: surfactant

PBXN-109 and PBXN-110 have physical and mechanical differences. The initial viscosity of PBXN-110 mixture is greater than that of PBXN-109. It is crucial to prevent the problems caused by a high initial viscosity value, such as air spaces and hot spots created during compression packing of munition. It is known that PBXN-109 can form a more compact structure, while powdery particles can be spilled out from PBXN-110 samples after the curing procedure. Curing causes the crosslinking of the polymer and, thus, stiffening the PBX. One of the problems with PBXN-110 is that even though the energetic material particles can be homogeneously distributed in the polymer liquid, they cannot be completely covered by the polymer due to weak bonding. Thus, desensitization, avoiding contact between the particles becomes impossible. Interactions between the uninsulated particles in the polymer liquid result in friction between the particles causing the formation of heat and high pressure and, thus, uncontrolled explosions. Solutions for such a problem require the study of a more appropriate binder and surfactant combination, which may form the core of another research study.

Within the framework of the thesis, we modified the formulation of PBXN-110 towards optimizing the initial viscosity after mixing by adjusting the contents and micromeritic properties of the energetic powder.

The initial viscosity [14] or end-of-mixing viscosity [15][16][17] of a combination of energetic powder and liquid polymer is defined as the viscosity right after mixing. The mixture must be cast into the case immediately after mixing, while it is still in the liquid

phase [18]. The viscosity and consistency of the mixture increase with time due to the formation of new chemical bonds, which transform the mixture into a non-castable solid. In this study, the viscosity of the uncured PBX is defined as the initial viscosity or the end-of-mixing viscosity. This is the viscosity of the suspended mixture before the curing agent is added. Curing naturally starts at room temperature after mixing, is dependent on the viscosity, and determines the pot life.

Pot life is the period between the time when the mixing process of the polymer with the energetic powder is stopped and the time when the material attains such a high viscosity that it cannot be cast anymore [14][18]. A high viscosity is not desired as the solid - liquid suspension loses its fluid nature and high-quality loading becomes impossible [19]. The period during which the mixture's viscosity doubles is also known as the "pot life" [3]. Another definition stated by the NATO standards describes pot life as the period until the viscosity of the suspension reaches 10 kP equivalent to 1000 Pa.s [14]. If the initial viscosity of the PBX suspension is more than 1000 Pa.s, the military specification of PBXN-110 [14] advises modification of the 1:3 mass ratio of HMX Class 2 (~35 microns)-to-HMX Class 3 (~350 microns) by changing the amount of Class 2 HMX or lowering the total HMX content to 86% to optimize the pot life and reduce the viscosity. The limit value of the initial viscosity strongly depends on the geometrical properties of the energetic powder. Sphericity and the shape of the particles affect flow characteristics, where a high sphericity makes flow easier by decreasing the viscosity due to minimum contact between the particles. A study conducted on heterogeneous rocket propellants [20] consisting of particles with high sphericity has set the technological limit of the initial viscosity as 1500 Pa.s., a value much higher than the military specification for PBXN-110. Mean particle size is another parameter effective on the initial viscosity of a solid-liquid polymer suspension. Studies based on achieving maximum packing and minimum initial viscosity of composite propellants have been carried out using particles, such as of ammonium perchlorate (AP) [21], of different sizes. A study based on the effect of both particle size and modality on the initial viscosity of a solid-liquid suspension does not exist for explosives to our knowledge. This thesis work involves the study of the effect of mean particle size and shape as well as modality on the initial viscosity and true density of the solid-liquid polymer suspension and flowability of the powders that depends on the tapped and bulk densities of the solid powder.

Preliminary studies in SAGE were carried out in this work to determine the initial viscosity for bimodal HMX mixtures with a Class 2-to-Class 3 mass ratio of 1:2 with a total HMX content of 82%, 83.5%, 84%, 85%, and 86%. Results showed that a total HMX content larger than 82% should not be employed leading to an initial viscosity higher than 1000 Pa.s, the standard criterion for optimal casting [14]. 82% by mass was selected as the maximum possible HMX content. Modality studies involved mixing HMX of various particle sizes to reduce the initial viscosity following mixing and achieve a good casting performance. Rheological studies to optimize the initial viscosity of Grade B HMX were based on three different particle sizes selected as Class 5, Class 2, and Class 3, from fine to coarse. A total of 15 experiment sets involved 3 monomodal, 7 bimodal, and 5 trimodal combinations of the selected three classes of HMX.

The modality studies were aimed at improving particle packing to reduce the initial viscosity and to increase the pot life for a constant HMX content of 82% by mass, which is smaller than the 86-89% range listed in Table 1.1. The formulation of the modified PBXN-110 was adjusted to have an NCO-to-OH molar ratio of 1.1 and a HTPB-to-IDP mass ratio of 0.95 specified by TUBITAK SAGE.

A modified PBXN-110 solid-liquid polymer suspension mixture involves energetic particles dispersed in a polymeric liquid and must have an optimum initial viscosity suitable for casting. The viscosity of the suspension might change based on the amounts of the energetic solid and polymeric liquid due to mechanical and chemical effects. Within the scope of this thesis, we focused the research on physical factors to minimize the initial viscosity and maximize the pot life of the modified PBXN-110 solid-liquid polymer suspension prior to addition of curing agent towards production of PBX.

- Find optimum loading for minimum viscosity and maximum pot life
- Use the optimum loading to investigate the effect of modality on viscosity based on a fixed amount of energetic solid and polymeric liquid.

We studied the micromeritic properties of energetic particles, such as mean particle size, particle size distribution and modality, particle shape, sphericity, tapped density, and bulk density. We showed how the micromeritic properties of the HMX particles affect the rheological properties of the suspended solid-liquid mixture they form when they are added to a liquid polymer and mixed for a fixed amount of time, i.e., the modified PBXN-110 solid-liquid polymer suspension. We determined the viscosity of the product PBX

samples using both a rheometer, which allows for variation of shear rate, and a viscometer, where measurements are conducted at a fixed shear rate. We understood the effect of coating HMX particles with plasticizer before production on the process results such as initial viscosity, pot life, mechanical properties etc.

The scientific empirical data obtained in this thesis will allow us to:

- Determine the relationship between the relative viscosity of HMX suspension and the solid HMX loading (%) of the bimodal HMX system with Class 2 and Class 3.

- Determine the modality and combinations of the particles that provide the minimum initial viscosity and maximum pot life at 82% solid HMX loading.

- Determine the shear stress vs. shear rate relationship for uncured PBX system mixture at three different temperatures to measure the effect of temperature on initial viscosity and compare the viscosity and temperature relation VTFH equation.

Employ statistical analysis tools to understand the effects of micromeritic parameters such as mean diameter, sphericity, tapped density and bulk density on the initial viscosity of the modified PBXN-110 suspension.

2.   GENERAL INFORMATION

2.1.   History of Explosives

The invention of explosives by the Chinese, who used a black powder gun containing carbon, sulfur, and saltpeter, goes back to the 7th century. After the Chinese, Arabs, Europeans, and the whole world worked on the development of explosives. In World War I, heat-effect explosives were developed and used. Explosives containing trinitrotoluene (TNT) were studied in the 20th century and were first used in TNT Russo – the Japanese War (1904-1905). The first use of TNT by the US military is in 1912. In World War II, pentaerythritol tetranitrate (PETN) and cyclotrimethylene trinitramine (RDX) were used in filling hand and antitank grenades. TNT, which has a high velocity of detonation around 6700 m/s, was used due to its high explosive property [4]. Black powder, TNT, nitroglycerine, dynamite, and nitrocellulose (NG) are the types of energetic materials with various properties used in history. The types of energetic materials that have been used most commonly in the recent years are research department explosives (RDX) or in other words cyclonite and high melting explosives (HMX) or in other words octogen, whose velocity of detonation values are 8600 m/s and 9100 m/s, respectively [4]. Depending on where explosives are used, they are classified as either civil or military. Commercial explosives are another name for civil explosives. They are mostly utilized in building, mining, quarrying, and tunnel construction projects. Military weapons including bombs, bullets, grenades, missiles, and rocket warheads employ military explosives as their explosives [4].

2.2.   Plastic Bonded-Castable Explosives

Energetic filler, plasticizer, binder, catalyst, surfactant, and curing agent are the major ingredients of castable PBXs. Chemically, HMX, which is polynitramine, is known as cyclotetramethylene tetranitramine, 1,3,5,7 - tetranitro - 1,3,5,7 - tetraazacyclooctane, or octogen. In 1941, HMX also known as Her Mejesty's Explosive was discovered by Bachmann [4]. In the 1960s, HMX was developed for use in lunar seismic studies [1][22]. HMX has undergone extensive research as a component of explosives and propellants throughout the past few decades. It is a well-known energetic component that may enhance the effectiveness of munitions. Only a few fundamental research findings

concerning HMX's military applications are accessible from publicly available sources because of the insufficiency of knowledge about this topic [1][23].

Table 2.1 shows the granulation requirements that specified by the military standards for HMX of different classes, that is, different particle sizes.

Table 2.1. Granulation of HMX classes according to military standards [12]

U.S. Mesh No.	Mesh Size (µm)	HMX Class 2	HMX Class 3	HMX Class 5
8	2380	-	-	-
12	1680	-	min. 99 %	-
35	500	-	-	-
50	297	min. 100 %	min. 40 %	-
100	149	-	min. 20 %	-
120	125	min. 98 %	-	-
200	74	-	min. 10 %	-
325	44	min. 75 %	-	min. 98 %

The binder is a thermoset polymer, which is a primary component for PBXs. The mechanical properties of the binder can be manipulated by adding a plasticizer. Binder provides the mechanical and thermal strength of PBXs, aging stability, and desired viscosity [4]. It provides the formation of an elastomeric fuel core after pre-polymer curing, which initially has low molecular weight. The energetic filler crystals are protected by the polymeric network, which prevents the explosive crystals from rubbing against one another and creating a hot spot in response to an external stimulus, such as a collision. In addition, binder provides carbon and hydrogen to the environment during the combustion reaction. The binder must be liquid with processable viscosities between 20 °C and 70 °C. Moreover, it has to be turned into an elastomer with effective compressive, tensile, and elastic properties [24]. The most important feature of polybutadiene-type binder polymer and copolymer derivatives is that they can be operated at high temperature ranges. With superior processability, increased mechanical qualities, low cost, and stability, hydroxyl-terminated polybutadiene (HTPB) is a commonly used binder because of its high solid loading capability up to 90% [25,26]. HTPB is combined with isophorone diisocyanate (IPDI) using a plasticizer, dioctyl adipate (DOA) or isodecyl pelargonate

(IDP) based on stoichiometry (NCO/OH ratio). Hydroxyl groups (OH$^-$) are attached to the ends of the polymer chains of the polymer containing HTPB. Hydroxyl groups can cure very quickly due to their high reactivity. Urethane elastomer is obtained as a result of the bonding of hydroxyl ends to isocyanates. For this reason, they have good mechanical properties, such as high tensile strength, abrasion resistance and oil resistance at high temperatures, which are possessed by polyurethane (PU) elastomers. In addition, they are the primarily preferred polymers for explosives due to their properties, such as low moisture permeability and, therefore, good electrical insulation, and low glass transition temperature.

Plasticizers are used in PBX to improve the rheological properties of polymer chains, reduce interactions by entering between polymer chains, increase the elasticity of the explosive. Plasticizers improve the flow properties by reducing the viscosity during production and improve mechanical properties by increasing elongation and decreasing tensile strength, increasing flexibility, and reducing the glass transition temperature (T_g) by creating free volume [27]. At low temperatures, an explosive without a plasticizer may break. It facilitates the free mobility of binder molecules without the need for chemical reactions. One of the most serious issues with PBXs is plasticizer migration. Depending on the rate of migration or diffusion, plasticizer migration can cause polymers to lose their flexibility. Ester-type plasticizers, such as dioctyl adipate (DOA) and isodecyl pelargonate (IDP), are included in the explosive composition. DOA and IDP are the most commonly used plasticizers in PU-based thermoset explosive formulations. DOA has been discovered to be a good and appropriate plasticizer for HTPB binders [24].

Catalysts help to accelerate the reaction between the binder and the curing agent and decrease the curing time of polyurethane at high temperatures without a negative impact on pot life. The ability of the explosive mixture to remain castable long enough during its transfer into the warhead after the completion of the production is crucial when deciding how many catalysts should be included in the explosive. Dibutyltin dilaurate (DBTDL) is added to obtain the optimum catalytic activity.

Surfactants, in general, reduce the viscosity of a solid-liquid suspension mixture by decreasing the surface tension between the solid and the liquid. The pot life of uncured explosives is increased as a result of this characteristic. They play an important role in increasing the solid loading in the suspension mixture [28]. Wetting agents are a type of

zwitterionic surfactant that reduces surface tension by allowing liquid droplets to spread over a solid surface. Wetting of explosive particles can be hampered by the liquid binder's high surface tension. In that circumstance, proper product mixing and casting are impossible. The use of a surface-active agent, also known as a wetting agent, to lower the surface tension is advised to solve this problem by increasing the interaction between the binder and the solid energetic filler [29]. The most common wetting agent used in PBXN-110 is Lecithin. Lecithin consists of a kind of glycerophospholipid that has a polar head and nonpolar long-chain fatty acids [30]. The nitramine containing HMX has polar groups, whereas the binder HTPB has nonpolar groups in the PBX. The polar head in lecithin interacts with polar groups in HMX and nonpolar groups in the structure of nonpolar long-chain HTPB. Therefore, lecithin plays a crucial role in wetting the HMX surfaces of HTPB by enhancing the interaction of HMX and HTPB.

Isocyanates combine with binders to form a highly stable polyurethane bond that is resistant to hydrolytic degradation and is suitable for auto-oxidative bonding. Isophorone diisocyanate (IPDI) is one of the most used isocyanates and contains two isocyanate groups (NCO$^-$) in its structure. Isocyanates with several uses can serve as a crosslinking agent or curative. The chemical structure of the isocyanate influences the kinetics of the polyurethane process. Aromatic structured isocyanates are more reactive and preferred for interactions between polyols with secondary hydroxyl groups [2][31]. IPDI is more suitable to react with the primary hydroxyl group, OH$^-$ in HTPB, although aliphatic or cycloaliphatic isocyanates, such as IPDI, are less reactive. The types and quantity of isocyanate utilized in the reaction, as well as the reaction temperature, directly correlate with pot life and curing time. Curing time ranges from a few hours to 7–10 days.

The chemistry of the polymeric matrix in the PBX is based on the condensation polymerization between the isocyanate groups (NCO$^-$) in the curing agent and the hydroxyl groups (OH$^-$) in the binder structure. The condensation polymerization process creates cross-links between the NCO and OH$^-$ groups in the polyurethane are created. The ratio of the amount of NCO-to-OH, which is crucial for designing an explosive, is calculated using the milliequivalents of IPDI and HTPB molecules. The NCO-to-OH ratio is crucial for the mechanical properties of the polyurethane (PU) system. For instance, a high NCO-to-OH ratio increases the hardness and modulus of the cured PU system while it reduces the elongation of the cured PU system [32]. The PU reaction formed by the

chemical crosslinking bonds between HTPB and IPDI used as a curing agent is given in Figure 2.1 [24][33].
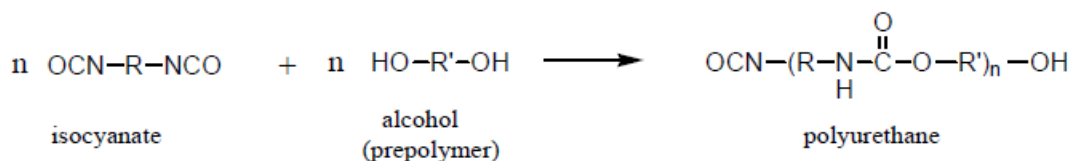
Figure 2.1. Polyurethane (PU) reaction [2]

The system is called "cured" after NCO^- from the curing agent and OH^- from the binder are mixed in the appropriate stoichiometry and the PU reaction is completed. After mixing the binder that contains OH^- groups and the curing agent that contains NCO^- groups in the PBX, the mixture is cast into the mold before it hardens and maintained in the oven at the preset curing temperature and time. The "curing time" is the period it takes for the formation of the crosslink bonds to be completed. A three-dimensional polymer network (3D network) is created during the curing process due to the chemical reactions that are triggered by temperature. The length of the curing process is crucial in establishing the material's physical characteristics. The flow characteristics of the PBX that has not yet been fully cured at the time of casting are crucial since they have an immediate impact on the mechanical, physical, chemical, and performance qualities of the PBX [34]. The PU reaction cannot be started in the absence of any of the reactants of the PU reaction, such as the curing agent or curative. Such systems are referred to as "uncured."

2.3. Rheology of Uncured Explosives

The word "rheo" derives from the Greek word "rhein," which means flow, while the phrase "rheology" means "theory of deformation" or "flow of matter". The constitutive theory of very viscous liquids and solids with viscoelastic and viscoplastic characteristics is sometimes referred to as rheology [35]. An emulsion, liquid, suspension, etc. may all be measured using a rheometer to see how they flow or deform in response to stress [36].

According to some researches on slurry of composite propellants [37][38], pseudoplasticity index (n) varies between $0.6 - 1$. The viscosity of most of the propellant slurry component decreases with increasing shear rate due to pseudoplastic behavior. The molecular structure of the binder and the packing of the filler are what lead to this

behavior. The polyurethane is produced by the reaction of the binder and the curing agent [39].

Studies for different explosive formulations consider the rheological properties of the mixture in order to ensure accurate filling and loading. At the same time, process settings and filling processes are adjusted considering the sensitivity and stability of explosive compounds. The time and space scales of observation and experimentation determine a material's rheological behavior [40].

The rheology of PBX is related to the rheology of solid-liquid polymer suspension mixtures. The solid content, particle shape and size, particle gradation, temperature, and chemical additives all have an impact on the non-Newtonian viscous behavior of solid-liquid polymer suspensions [41]. The rheological viscosity of the PBX explosive solid-liquid polymer suspension decreases, but the explosive's performance improves as the amount of the energetic powder in the solid-liquid polymer suspension is increased. Rheological properties, such as the initial viscosity, pot life, and particle size distribution play a direct role in PBX rheology due to attractive and repulsive interactions between particles. The initial viscosity of a PBX mixture refers to the thickness or resistance to flow of the PBX material after it has been fully processed and prepared [42]. The viscosity of the PBX mixture is a critical parameter in the production of PBX, as it can affect the handling, processing, and performance of the material. The initial viscosity of a PBX mixture can be influenced by several factors, including the type and concentration of the polymer binder used, the particle size distribution and loading of the energetic powder, and the processing conditions, such as the mixing time and the temperature. Achieving the optimal viscosity is important to ensure that the PBX material can be easily handled and processed during production, while also providing the desired level of explosive performance and stability. To determine the initial viscosity of a PBX mixture, various analytical techniques can be used, such as rheometer or viscosity measurement. These techniques can provide quantitative data on the viscosity of the PBX material, which can be used to assess its suitability for specific applications.

2.4. Flow Behavior of Fluids

Fluids either display Newtonian or non-Newtonian viscous flow characteristics [43]. Fluids that conform to Newton's law of linear friction are known as Newtonian fluids.

Non-Newtonian fluids are defined as those that do not conform to this linear rule. These fluids, which are often highly viscous, draw attention due to their elastic characteristics. Rheology is recognized to include the theory of non-Newtonian fluids. Thermoplastics, polymeric liquids, paints, and biological fluids are a few examples of non-Newtonian fluids [20,21]. The function of shear stress (τ) depending on the shear rate ($\dot{\gamma}$) (a), the function of viscosity (η) depending on the shear rate ($\dot{\gamma}$) (b) and the time-dependent function of shear stress (τ) with respect to time (c) are shown in Figure 2.2.

(a)　　　　　　　**(b)**　　　　　　　**(c)**
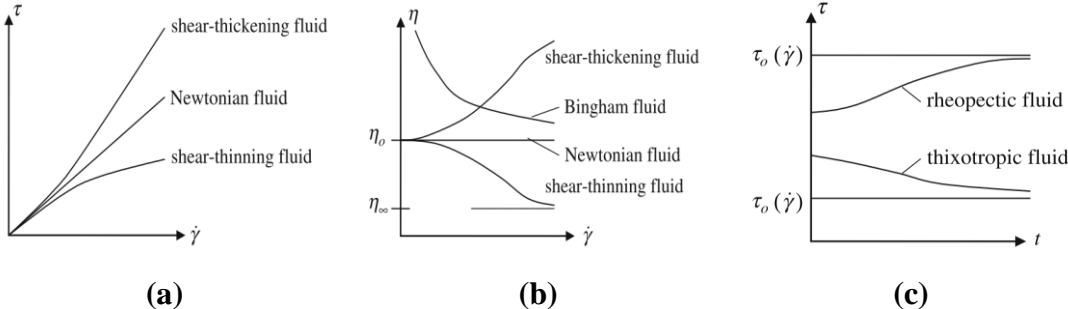
Figure 2.2. Types of fluids based on their rheological behavior according to the power law defined by graphs of (a) shear stress τ vs shear rate $\dot{\gamma}$, (b) viscosity η vs shear rate at constant shear stress, and (c) shear stress τ vs time t [43]

The pseudoplasticity index of Newtonian fluid equals 1. A non-Newtonian fluid behaves as shear thinning or shear thickening according to its pseudoplasticity index that may have a value smaller than 1 or higher than 1, respectively. In shear thinning (pseudoplastic) behavior, the non-Newtonian viscosity decreases with increasing shear rate e.g. paint, and polymer liquids [43–48]. For fluids with shear thickening behavior, the non-Newtonian viscosity increases with increasing shear rate, such as in the starch-water mixture. Bingham fluids, such as asphalt and chewing gum, have no flow until yield stress [43,44]. Fluids that behave non-Newtonian may be categorized into two. The first category includes fluids that do not need yield stress, where the flow curve passes through the origin. The category includes fluids that need yield stress, where the flow occurs when the shear rate is greater than the yield stress. In the studies of Izdebska [45] and Koleske [46] non-Newtonian flow behavior was seen without yield stress. In thixotropic fluids, time-dependent breakdown takes place with shear; therefore, the viscosity is decreasing over time. However, in rheopectic fluid shear-induced structure formation; thus, the viscosity is increasing with stress over time [44–46].

When solid energetic elements are dispersed in a liquid, castable concentrated explosive solid-liquid polymer suspensions are formed. Castable explosive suspensions exhibit non-Newtonian behavior, i.e. shear rate dependent viscosity [5][49] influenced by several factors, such as temperature, chemical additives, solid content, average particle size distribution, and grain geometry [41]. Solid particles are added to and dispersed inside a liquid polymeric plastisol to form a suspended mixture. When the number of particles in a suspension rises, so does its viscosity. This is due to an increase in the amount of energy needed for the liquid to flow around the solid particles [50]. The viscosity of particle suspensions in Newtonian fluids becomes shear dependent as the amount of suspended particles increases leading to the fact that the majority of uncured PBX materials display non-Newtonian flow characteristics [51].

A technical term used to describe the rheological behavior of suspended mixtures is the relative viscosity η_r. It is defined as the ratio of the viscosity of the solid-liquid polymer suspension η to that of the liquid phase η_s, given as:

$$\eta_r = \frac{\eta}{\eta_s} \tag{2.1}$$

Data from empirical studies to determine the viscosities of different materials under varying conditions have led researchers to derive mathematical formulations for faster prediction of viscosity.

Table *2.2* shows a list of the major mathematical formulations (Equation from 2.2 to 2.12) used in the literature.

Table 2.2. Major viscosity models

Model, Reference	Equation Type	Equation	Properties
Newtonian model, 1687 [44]	Linear	$\eta = \dfrac{\tau}{\dot{\gamma}}$ (2.2)	Newtonian with constant viscosity and shear rate is not dependent viscosity
Power Law (Oswald) model, 1925 [52]	Power law	$\tau = K \times \dot{\gamma}^n$, $\eta = \dfrac{\tau}{\dot{\gamma}}$ (2.3) $\eta = K \times \dot{\gamma}^{n-1}$ (2.4)	Non-Newtonian, Viscosity is a function of shear rate
Bingham Model, 1916 [53]	Linear	$\tau = \tau_{yield} + \eta \times \dot{\gamma}$ (2.5)	Newtonian when $\tau > \tau_{yield}$
Casson Model, 1959 [54]	Linear	$\sqrt{\tau} = \sqrt{\tau_{yield}} + \sqrt{K \times \dot{\gamma}}$ (2.6)	Newtonian when $\tau \gg_{yield}$
Hershel-Bulkley Model, 1925 [55]	Power law	$\tau = \tau_{yield} + K \times \dot{\gamma}^n$ (2.7)	Newtonian, Power Law, Bingham fluid
Sisko Model, 1958 [56]	Power law	$\eta = \eta_{\infty} + K \times \dot{\gamma}^{n-1}$ (2.8)	Newtonian when high shear rates where the power law model is not applicable
Cross Model, 1965 [57]	Power law	$\dfrac{\eta - \eta_{\infty}}{\eta_0 - \eta_{\infty}} = \dfrac{1}{1 + (K \times \dot{\gamma})^n}$ (2.9)	Newtonian viscosity is low, infinite viscosity is high at wide shear rate range
Ellis Model, 1927 [58]	Power law	$\dfrac{\eta - \eta_{\infty}}{\eta_0 - \eta_{\infty}} = \dfrac{1}{1 + (K \times \tau)^n}$ (2.10)	Newtonian viscosity is low
Carreau Model, 1972 [59]	Power law	$\dfrac{\eta - \eta_{\infty}}{\eta_0 - \eta_{\infty}} = \dfrac{1}{(1 + (K \times \tau)^2)^{n/2}}$ (2.11)	Newtonian viscosity is low, infinite viscosity is high
Carreau-Yasuda Model, 1981 [60]	Power law	$\dfrac{\eta - \eta_{\infty}}{\eta_0 - \eta_{\infty}} = (1 + (K \times \tau)^a)^{\frac{n-1}{a}}$ (2.12)	Infinite viscosity is high or low, transition between the Newtonian region and the power law region

The Newtonian model of viscosity explains the most basic type of flow behavior, in which the material's viscosity is constant regardless of shear rate. This model depends on the ratio of shear stress and shear rate as shown in Equation 2.3.

Mathematically, the Oswald model (or power law model, PLM) and the apparent viscosity (η) are defined in literature with respect to the pseudoplasticity index (n), the consistency coefficient (K) and shear rate ($\dot{\gamma}$) as Equation 2.4.

In the solid-liquid polymer suspension rheology, the volumetric concentration of solid particles (φ) is proportional with the particle packing of the solid particles [61]. Moreover, the maximum solid particle volume fraction (φ_{max}) correlates with the maximum particle packing of the solid particles. The relative solid volume (vol./vol.) is calculated from the ratio of the volumetric concentration of solid particles (φ) to the maximum solid particle volume fraction (φ_{max}), as below:

$$V_r = \frac{\varphi}{\varphi_{max}} \tag{2.13}$$

2.5. Mathematical Models for Viscosity

The majority of research studies on particle suspension rheology in the literature concentrate on the effects of particle volume fraction on fluid viscosity in free-flow situations and suspended particles in Newtonian fluids where the boundary effect is negligible for particle behavior. The Table 2.3 presents some of the models (Equations from 2.14 to 2.24 developed to describe the rheological behavior of solid-liquid polymer suspensions viscosity under certain conditions.

Table 2.3. Mathematical models for the relative viscosity of solid particle-liquid polymer suspensions

Model, Reference	Equation Type	Equation	Properties
Einstein, 1906 [62]	Linear	$\eta_r = 1 + 2.5 \times \varphi$ (2.14)	Takes into account interactions between two moving spheres
Guth, 1936 [63]	2nd order polynomial	$\eta_r = 1 + 2.5 \times \varphi + 7.8 \times \varphi^2$ (2.15)	Assumes two moving spheres interact with each other
Vand, 1948 [64]	Exponential, Taylor series	$\eta_r = \exp\left(\frac{2.5 \times \varphi + 2.7 \times \varphi^2 + \cdots}{1 - k \times \varphi}\right)$ (2.16)	Assumes incremental the volume fraction of the spheres (d φ)
Mooney, 1951 [65]	Exponential	$\eta_r = \exp\left(\frac{2.5 \times \varphi}{1 - k \times \varphi}\right)$ (2.17)	Assumes that rigid and spherical particles with k constant (crowding factor) is in between 1.35 – 1.91

Model, Reference	Equation Type	Equation	Properties
Simha, 1952 [66]	Polynomial	$\eta_r = 1 + 1.5 \times \varphi(1 + (1 + 6.25f^{-3}) \dots)$ (2.18)	Assumes that having highly concentrated Newtonian polymer suspensions with f constant is in between $1.30 - 2.00$
Brinkman, 1952 [67]	Power law	$\eta_r = \frac{1}{(1 - \varphi_{max})^{[\eta]}}$ (2.19)	Assumes that infinite polydispersity as φ goes to 1. $[\eta]$ is intrinsic viscosity.
Krieger and Dougherty, 1959 [68]	Power law	$\eta_r = 1 - \left(\frac{\varphi_{max}}{\varphi}\right)^{[\eta]\varphi_{max}}$ (2.20)	$[\eta]$ represents the intrinsic viscosity.
Ford, 1960 [69]	Polynomial	$\eta_r = 1 - 2.5 \times \varphi + 11 \times \varphi^5 - 11.5 \times \varphi^7$ (2.21)	Assumes only closely packed uniform spheres occupy the volume fraction
Thomas, 1965 [70]	Polynomial, exponential	$\eta_r = 1 + 2.5 \times \varphi + 10.05 \times \varphi^2 + 0.00273 \times \exp(16.6 \times \varphi)$ (2.22)	There is no theoretical explanation provided for the additional term of the polynomial
Chong, 1971 [71]	Polynomial	$\eta_r = \left(1 + \frac{0.75 \times \left(\frac{\varphi}{\varphi_{max}}\right)}{1 - \left(\frac{\varphi}{\varphi_{max}}\right)}\right)^2$ (2.23)	Assumes that viscosity data greater than 0.75 Pa.s. Applicable to crosslinked, amorphous viscoelastic materials packed with spherical particles of variable sizes and size distributions
Senapati, 2010 [72]	Power law	$\eta_r = \frac{10C_u}{d_{50}} \times \left(1 + \frac{[\eta]}{\dot\gamma^{0.4}}\right) \times \left(\frac{\frac{\varphi}{\varphi_{max}}}{1 - \frac{\varphi}{\varphi_{max}}}\right)^{3.5}$ (2.24)	C_u represents particle diameter distribution. d_{50} represents median particle diameter.

Einstein [62]'s model shown in Equation 2.14 is simple and good enough to estimate the viscosity of Newtonian fluids containing a small number of scattered particles.

η_r (Pa.s/Pa.s), φ (vol./vol.) and φ_{max}(vol./vol.) are the relative viscosity, fraction of volumetric concentration of solid spherical particles and maximum fraction of volume of solid spherical particles, respectively. Assuming that the flow around a particle has no

impact on the flow around other particles, this model offers a reliable linear approximation for suspensions under consideration. In a completely laminar flow, the linear equation simply takes into account the no-slip boundary condition on the particle sphere. Particle diameter, d, has a very narrow range of acceptable values. Einstein's concept of suspension viscosity works well for low concentrations and does not apply to high concentrations. New models have been developed since Einstein to improve the precision of the models on fluids with a wider range of viscosities.

Exponential equations can be listed as Vand [64], Mooney [65] and Thomas [70] in Table 2.3 chronologically. Mooney [65] derived the following model by considering the successive addition of two monodispersed spheres to a pure fluid in Equation 2.17. In this model, η_r (Pa.s/Pa.s) represents the relative viscosity, φ (vol./vol.) represents the volumetric concentration of solid spherical particles and k constant (crowding factor) is the experimental value and in between 1.35 and 1.91 for purely geometric particles.

2.6.   Parameters Affecting the Rheology of the Uncured Explosive

Parameters, such as the amount of HMX contained in the mixture, the micromeritic properties of HMX, production temperature, mixing time, and mixing rate are effective on the rheology of the mixture and therefore on the viscosity and the pot life of the mixture. These parameters, as presented schematically in Figure 2.3. affect the viscosity and pot life of the mixture.
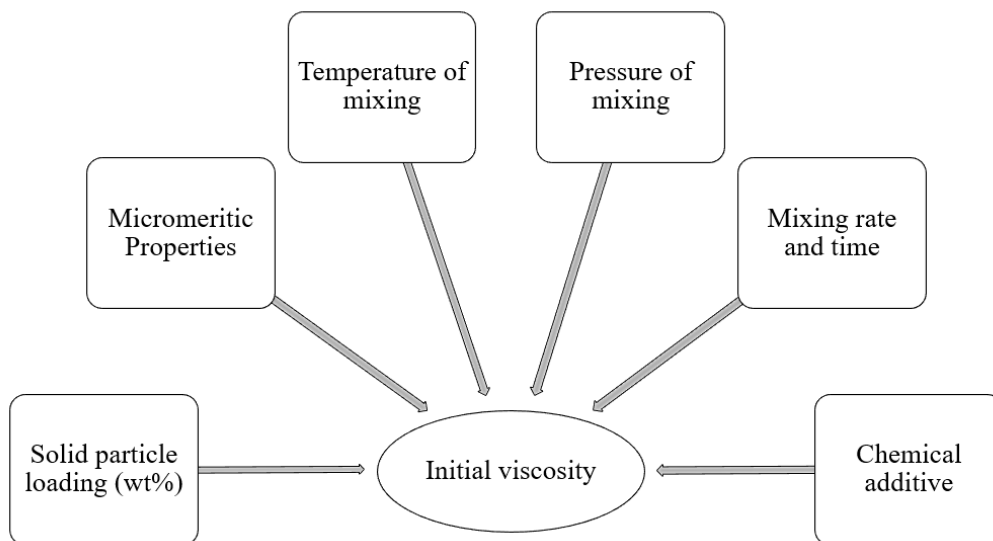
Figure 2.3. Parameters affecting rheology of PBX of the uncured explosive

2.6.1. Mixing Rate and Mixing Time

All of the raw materials, such as energetic powder and polymeric liquid, are combined during the mixing process to form a homogenous mixture by dispersing and distributing the powder particles throughout the polymer liquid. The fundamental reason for the poor flow characteristics in such polymer systems is interaction between solid-solid particles dominates over the interaction between solid-liquid (i.e. the energetic powder and polymeric matrix) above a specific energetic powder content [73]. These polymer systems are mixed by low-rpm mixers and require high shear rates to be deformed. The energetic suspension needs to have sufficient pot life and rheological characteristics that allow for enough flow for perfect casting. Mixing rate and mixing time also significantly affect the rheological properties. The initial viscosity of the mixture is reduced when the mixing rate is increased, causing coarse particles to break apart and become finer. The initial viscosity of a solid-liquid suspension rises when the mixing rate increases, and coarse particles begin to break apart. Therefore, it is important to maximize the mixing rate [35,40,73]. Increased total mixing time except for the addition of the curing agent reduces the viscosity due to improved polymer liquid -energetic powder interaction (i.e. wetting) [74].

2.6.2. Temperature

The initial viscosity of the suspended solid-liquid mixture decreases as the temperature rises before the polyurethane reaction starts. However, after the completion of the polyurethane reaction, the viscosity of the suspension increases as the temperature rises. For example, Joshi et al. [40] examined the behavior of the mixture at various temperatures to explain the differential tendency of the initial viscosity of the suspension to decrease with increasing temperature. It is common for liquids to have lower viscosity at higher temperatures [35,42,48].

The Vogel-Fulcher-Tammann-Hess (VFTH) equation describes the non-Arrhenius temperature dependence of viscosity with three parameters [75–77]. This equation explains the viscosity decreases caused by increasing temperature. The VFTH equation is shown below:

$$\eta = A * exp\left(\frac{B}{T-C}\right) \tag{2.25}$$

A is in Pa.s, B in K and C in K are constants of the VFTH equation and T is the absolute temperature in Kelvin.

2.6.3. Pressure

Upon completion of the mixing process, the explosive suspension is poured into molds or warheads under low pressure conditions to avoid the formation of voids or air bubbles. The amount of vacuum determines the porosity and increased vacuum conditions cause the initial viscosity of the suspended solid-liquid mixture to be high after curing.

2.6.4. Solid Particle Loading

The addition of solid material to a suspension is well known to enhance the viscosity of the fluid because of the increasing forces of collision and friction between the solid particles [78]. According to the study of Chong et al. [71], increasing the volume fraction of uniform glass spheres from 0.5 to 0.6 increases the relative viscosity of the suspension, i.e. the ratio of the viscosity of the suspension to that of the suspension medium, by 200 units (**Figure 2.4**).
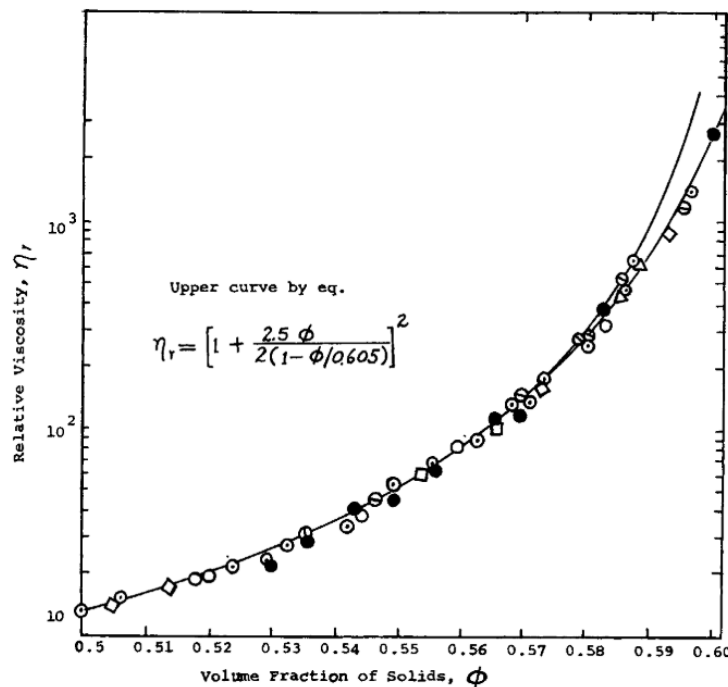
Figure 2.4. The effect of the volume fraction of monodispersed particles on the relative viscosity of the suspension [71]

According to Liu et al.' s research [79] on a suspension of spherical silica particles in deionized fruit sugar solution, increasing the solid particle volume fraction from 0.25 to 0.50 produces a 677% increase in relative viscosity at a shear rate of 1 s^{-1} (Figure 2.5).
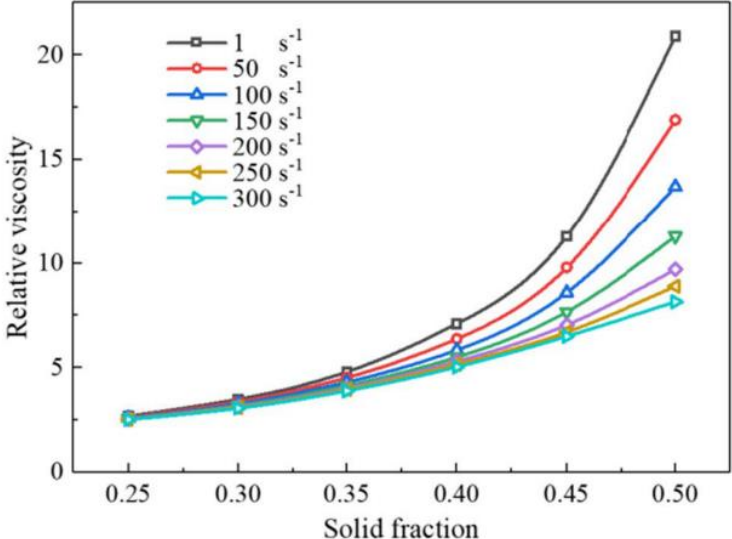
Figure 2.5. The effect of particle volume fraction on suspension relative viscosity [79]

An et al. [78] worked with a suspension of Fe-C powder in acrylonitrile butadiene styrene (ABS) melt. They found that increasing the Fe-C concentration from 0% to 30% by volume led to an increase in the apparent viscosity from 0.1 Pa.s to 0.6 Pa.s at a shear rate of 12.7 s^{-1}, as shown in Figure 2.6.
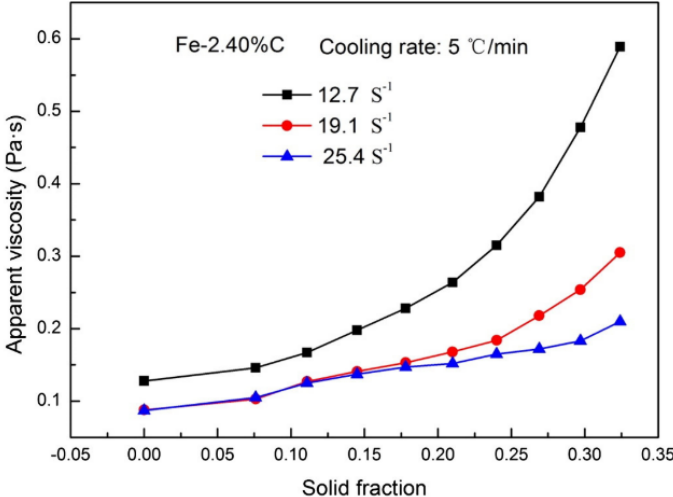
Figure 2.6. The effect of particle volume fraction on suspension apparent viscosity [78]

22

According to Joshi et al. [40], increasing the percentage of HMX from 0% to 70% by volume resulted in an approximately 5 Pa.s increase in initial viscosity for an energetic combination including HMX and TNT. According to Figure 2.7 below, the viscosity of the HMX/TNT mixture increases as the HMX concentration rises.
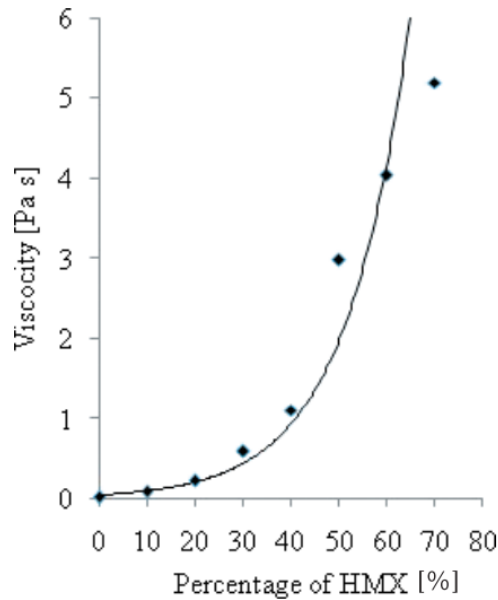
Figure 2.7. Effect of HMX percentage on the viscosity of HMX/TNT mixture [40]

2.6.5. Micromeritic Properties

"Micromeritics" refers to the science and technology of powders and minute particles and investigation of their characteristics and behavior. It may be utilized to enhance the manufacturing of powders and improve their functionality in a variety of applications. Micromeritics studies the properties of micro particles, such as size, packing, porosity, cohesion between micro particles, flowability, and interaction of particles with fluids and binders [80]. Particle size analysis with laser diffraction, surface area analysis, porosity analysis, and density measurements are a few methods often used in micromeritic investigations. With the help of these methods, it is possible to understand and regulate the behavior of powders in a variety of applications by getting extensive information on their physical traits and features. The bulk density, the tapped density, compressibility index ratio or Carr's index (CI), and Hausner ratio (HR) are the properties obtained using micromeritic analysis methods [81].

2.6.5.1.　　　　Particle Size Distribution

The size of the solid particles has been considered the most important factor affecting the viscosity of the mixtures [35]. A suspension involving coarse spherical particles has a greater bulk density and a lower viscosity compared to a suspension with fine particles. It is also anticipated that the cohesivity of the powder would decrease as the particle size increases [82]. Fine particles are employed to enhance the performance parameters in explosive components because of their large surface area. Measurement, control, and optimization of particle size and distribution are crucial. To reach the maximum theoretical density and, thus, the required performance, solids with two or more particle sizes are dispersed to produce a mixture in bimodal, trimodal, or multimodal forms [81].

The viscosity of suspensions with a specific quantity of solid particle load typically increases when the particle size of the particles is decreased [36,71,79,83]. It is well known that suspensions with particles of the same size and shape have a lower viscosity [84]. In high-concentration suspensions, bimodal or multimodal particle gradation is frequently employed to lower the viscosity [83,85]. In a review study carried out by Kamal and Mutel [43], the relative viscosity of the suspensions is shown to increase linearly with concentration at extremely low concentrations, but the relation deviates from linearity at moderate concentrations. The relative viscosity rises sharply with a concentration near the maximum packing. Another critical term important in understanding the effects of particle size distribution is modality. Modality indicates the number of ranges of sizes of particles in a suspension [86]. For instance, monomodal systems have one particle size range, bimodal systems have two different particle size ranges, and trimodal systems have three different size ranges. Bimodal or multimodal particle grading systems are based on the particle packing theory. This hypothesis is based on selecting the proper proportions and size of the particulate material to fill the big voids with coarser particles and the remaining tiny voids with finer particles. Parameters that affect the packing can be grouped as particle properties, such as size, size distribution, shape, and surface characteristics, and mixture properties, such as modality, mass proportions of the different sizes of particles used in the mixture or simply the coarse-to-fine ratio for bimodal systems, average (mean) diameter of the particles, interactions between particles, and interactions between the particles and the suspension liquid. Stacking coarse and fine particles together is usually the preferred strategy to optimize

the density and viscosity of the mixture. The fine particles must be small enough to fit in the spaces between coarse particles [87].

Blott et al. [88] showed in 2009 that mean diameter provides a more reliable results for bimodal and truncated systems when analyzing the broader particle size distributions.

2.6.5.2.   Particle Shape and Sphericity

The particle shape has been considered one of the most important factors affecting the viscosity of the mixtures [35]. A measurement of a particle's sphericity is its circularity. The degree of sphericity or sphericity index is determined by its deviation from perfect circularity indicated by a value of 1. Circularity for noncircular objects is less than one [81]. Irregular or angular particles can lock up more easily than round particles. For this reason, spherical particles have higher fluidity than irregular or angular particles [78,89–91] Another study that explains the relationship between particle shape and viscosity is Hudson' s study [92]. According to this study, spherical and elliptical energetic particles i.e., RDX crystals are proven to decrease formulation viscosity.

2.6.5.3.   Flowability

Flowability of a suspension is affected by both the bulk and tapped densities of the suspended powder mixture. Bulk density (random loose packing) allows the dispersed powder to fall to the bottom of a container with a given volume under the influence of gravity [82]. A suspension with a large bulk density allows for the flow of a coarse spherical particle from the top to the bottom of the container at a faster rate [93]. Higher bulk density causes the fraction of solid content to be high and the voidage to be low [94]. Tapped density (random dense packing) is obtained by tapping a graduated cylinder containing an aerated sample. The volume of a highly cohesive powder particle is drastically decreased when the graduated cylinder is tapped. The action of tapping helps the powder particles to get rearranged that leads to higher packing [82].

In 1969, Gray et al. formulated the Hausner ratio, HR, defined as the ratio of tapped density to bulk density [95] as below:

$$HR = \frac{tapped\ bulk\ density\ (\frac{g}{ml})}{bulk\ density\ (\frac{g}{ml})}$$ (2.26)

It was concluded that the decrease in the cohesiveness of the powder particles reduces the Hausner ratio. The Hausner ratio declines as packing increases. According to Zou et al., Hausner ratio decreases as sphericity increases [96].

The compressibility index, also called as the Carr's index, CI, was formulated for the same amount of powder particles (in grams) by Carr in 1965 [97], as shown below:

$$CI = \left(1 - \frac{bulk\ density\ (\frac{g}{ml})}{tapped\ bulk\ density\ (\frac{g}{ml})}\right) \times 100\% \tag{2.27}$$

According to Gupta et al. [98], both the compressibility index (Carr's index) and the Hausner ratio (HR), which are standardized ratios, are used to analyze the material's flow behavior. Flow properties improve when the CI is less than 15%, while flow characteristics deteriorate when it exceeds 25%. A HR of 1.25 or less indicates good flow, whereas an HR of 1.25 or more indicates poor flow [98] as shown in Table 2.4.

Table 2.4. The effect of HR and CI values on flowability according to Gupta [98]

Values	Flowability
CI (%) < 15	improved flowability
HR < 1.25	improved flowability
CI (%) > 25	poor flowability
HR > 1.25	poor flowability

It is known that flowability improves due to less cohesive forces between the particles as particle size increases [81]. The concept of flowability of powders was associated by Carr with the Hausner ratio, which is the ratio of tapped and bulk density, as in the Table 2.5 below [97].

Table 2.5. Flowability of powders according to Carr [97]

Hausner Ratio	Flowability
1.00 – 1.11	Excellent
1.12 – 1.18	Good
1.19 – 1.25	Fair
1.26 – 1.34	Passable
1.35 – 1.45	Poor
1.46 – 1.59	Very poor
> 1.60	Very, very poor

2.6.5.4.   Particle Packing

The particle packing theory, which examines how particles are arranged and packed in a suspension, can significantly affect the suspension's viscosity. In accordance with this theory, the arrangement and size of the particles can have an impact on how they interact with one another and the fluid around them, which in turn affects how the suspension flows and how viscous it is. The two categories of particle packing are regular (ordered) packing and random packing. Random packing can be measured using a densitometer or calculated roughly as [94]:

$$Random\ Packing = \frac{bulk\ density}{tapped\ density} = \frac{volume\ of\ powder\ particles}{volume\ of\ powder\ particles\ with\ voids} \qquad (2.28)$$

Random packing can be classified as: (1) dense random packing, when the tapped density is dominant, and (2) loose random packing, when the bulk density is dominant. When the particles have higher bulk density, the suspension is more fluid-like and has lower viscosity [99]. Utilizing the idea of packing, which shows the volume percentage of voids in a bed that is occupied by solid particles, is one technique to enhance the solid content with a minimal change in the rheological and mechanical characteristics [18,86]. The principle of particle packing is contingent on choosing the right sizes and ratios of particulate material. This principle suggested that large spaces are filled with matching-sized particles, and the new, smaller voids that are generated are then filled with smaller particles [21].

The fine-coarse ratios of the particles in the mixture are very effective on the packing of the particles. Moreover, solid loading is typically high with coarse explosives and low with fine explosives. Particle size is meticulously managed, and bi- and tri-modal mixes of various particle sizes are employed in order to obtain the highest solids loading. In this manner, smaller particles fill the interstices between larger ones to obtain maximum particle packing. Also, incorporating spheroidized explosive/oxidizer (solid fillers) into formulations reduces viscosity, resulting in a larger solid loading in terms of the particle shape of the filler [4].

In a study by Joshi [40], the optimum packing that gives the minimized voids and initial viscosity in systems created using a bimodal HMX mixture that had 60/40 coarse/fine ratio and a trimodal HMX mixture that had 25/40/35 coarse/fine ratio are given in Figure 2.8 (a) and (b).
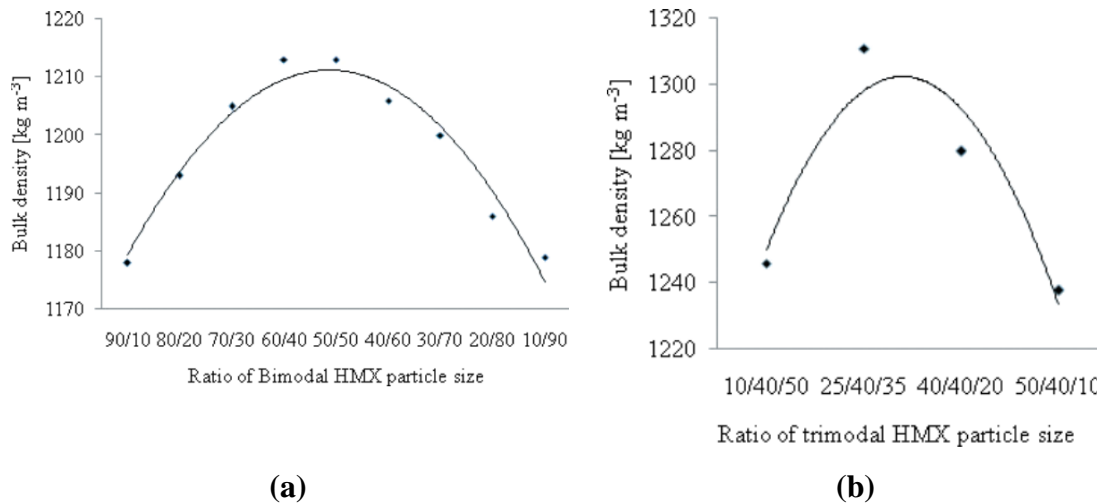
Figure 2.8. Effect of particle size ratios of bimodal (a) and trimodal (b) HMX mixture on bulk density [40]. HMX particle sizes are (125 – 250) μm / (125 – 0) μm in the bimodal system and (500 – 800) μm / (250 – 500) μm / (250 – 0) μm in the trimodal system.

In a study by Chong [71], it was stated that the minimum viscosity is obtained from a system in which 25-35 % of the solid particles in a bimodal suspension system are fine particles and the remaining 75-65 % is coarse particles.

The packing of powders increases as the difference between the tapped and bulk density decreases and thus, the flowability of powders increases as the literature [15,96–99].

2.6.5.5. Density And Porosity

True density is the volume occupied by the material, omitting open and closed pores. It is a crucial characteristic that contributes to product characterization and may also aid in the detection of polymorphs or pseudo-polymorphs. Furthermore, skeletal density, which corresponds to the total of the solid material's volumes and closed (or blind) pores inside the particles, is an essential measure in describing powders in terms of porosity. As a result, it is critical to define the material for its density, which also indicates the porosity of a solid [81].

2.6.6. Effect of Wetting Agent

Liquid binders might have high surface tension, which hinders the wetting of the explosive particles. In such a situation, proper mixing of the product and casting becomes impossible. The use of surface-active agents, also known as wetting agents, lowers the

surface tension and is advised to solve this problem by increasing the interaction between the binder and the solid energetic filler [100]. The most common wetting agent used in PBXN-110 is lecithin [14].

3. MATERIALS, EXPERIMENTAL, AND CHARACTERIZATION METHODS

3.1. Materials

Modified PBXN-110 is produced by mixing HMX (NITRO-CHEM, Poland) particles with a polymeric liquid. HMX particles act as the energetic filler. The energetic raw material used in this study is Grade B cyclotetramethylenetetranitramine (Grade B HMX). Its physical and chemical information is listed in Grade B cyclotetramethylenetetranitramine (Grade B HMX) is the energetic raw material used in production. Its physical and chemical information is listed in Table 3.1.

The polymeric liquid comprises of IDP (SAE Manufacturing Specialties Corp., Bayville, NY) as the plasticizer (Table 3.2), HTPB (SAE Manufacturing Specialties Corp., Bayville, NY) as the binder (Table 3.3), DBTDL (Island Pyrochemical Industries (IPI), Mineola, NY) as the catalyst (Table 3.4), lecithin (American Lecithin Company, Oxford, US) as the wetting agent or surfactant (Table 3.5), and IPDI (Island Pyrochemical Industries (IPI), Mineola, NY) as the curing agent (Table 3.6). The milliequivalent of IPDI was calculated based on the NCO^- content.

Table 3.1. Physical and chemical properties of HMX supplied from NITRO-CHEM
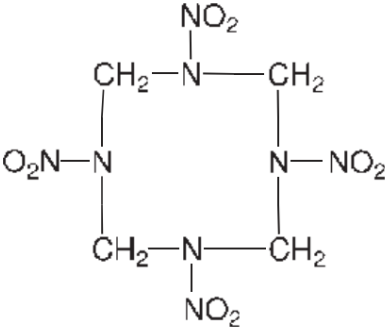
Properties	HMX (s)	Ref.
Chemical formula	$C_4H_8O_8N_8$	[1,101] [12]
Specification	Cyclotetramethylene tetranitramine	[12]
Molecular weight (g/mol)	296.16	[12,101]
Components (Purity of HMX) (%)	Min. 98%HMX and 2%RDX in Grade B HMX	[12]
Min. melting point (°C)	277	[12]
Storage temperature (°C)	2-8	[12]
Maximum % moisture	0.05	[12]
Maximum % acidity (wt/wt)	0.02	[12]
Impact sensitivity (per 2.5kg, min)	17	[12]
Molecular Structure		[4]
Hazard class	1.1D	[12]

Table 3.2. Physical and chemical properties of IDP supplied from SAE Manufacturing Specialties Corp.
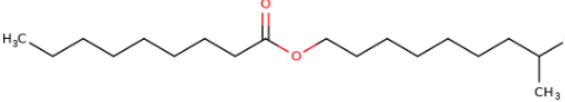
Properties	IDP (l)	Ref.
Chemical formula	$C_{19}H_{38}O_2$	[102]
Specification	Isodecyl pelargonate	[102]
Molecular weight (g/mol)	298.5	[102]
Appearance	Transparent oily liquid	[102]
Acidity	≤0.01 mg KOH/g	[103]
Boiling Point (°C)	312	[102]
Flash Point (°C)	172	[102]
Moisture (wt%)	≤0.1	[104]
Density (g/cm^3 @20°C)	0.855–0.866	[105]
Dynamic Viscosity (Pa.s @20°C)	0.007	[106]
Molecular Structure		[102]

Table 3.3. Physical and chemical properties of HTPB supplied from SAE Manufacturing Specialties Corp.
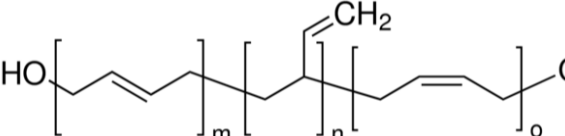
Properties	HTPB (l)	Ref.
Specification	Hydroxy- terminated polybutadiene	[107]
Molecular weight (g/mol)	Mw ~6200 & Mn ~2800	[107]
Hydroxyl value (m_{eq}/g)	0.79	[108]
Moisture (wt%)	≤0.1	[109]
Dynamic Viscosity (Pa.s @30°C)	0.04–0.06	[107]
Antioxidant content (wt%)	0.7–1.3	[107]
Molecular Structure		[107]

Table 3.4. Physical and chemical properties of DBTDL supplied from Island Pyrochemical Industries (IPI)
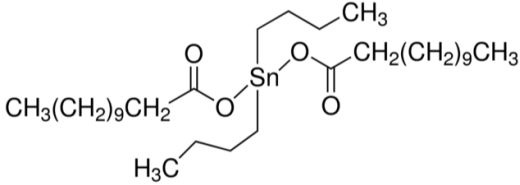
Properties	DBTDL (l)	Ref.
Chemical formula	$C_{32}H_{64}O_4Sn$	[110]
Specification	Dibutyltin dilaurate	[110]
Molecular weight (g/mol)	631.56	[110]
Tin Content (wt%)	17.7–19.5	[111]
Molecular Structure		[110]

Table 3.5. Physical and chemical properties of Lecithin supplied from American Lecithin Company Inc.
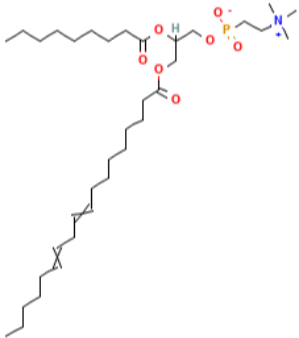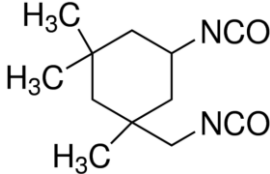
Properties	Lecithin (l)	Ref.
Chemical formula	$C_{42}H_{80}NO_8P$	[112]
Specification	Lecithin from Soybean	[112]
Appearance	Light yellow waxy	[112]
Acid number (mg KOH/g)	≤32	[113]
Moisture (wt%)	<1.0	[104]
Molecular weight (g/mol)	758.1	[112]
Molecular Structure		[112]

Table 3.6. Physical and chemical properties of IPDI supplied from Island Pyrochemical Industries (IPI)

Properties	IPDI (l)	Ref.
Chemical formula	$C_{12}H_{18}N_2O_2$	[114]
Specification	Isophorone diisocyanate	[114]
NCO⁻ content (wt%)	37.5	[115]
Appearance	Yellowish liquid	[114]
Molecular weight (g/mol)	222.28	[114]
Freezing Point (°C)	-60	[114]
Flash Point (°C)	155	[114]
Dynamic viscosity (Pa.s @25°C)	0.009-0.013	[116]
Molecular Structure		[114]

3.2.   Characterization of HMX

HMX powders were characterized by measuring bulk density and tapped density and scanning electron microscopy (SEM) analyses to determine the particle size and shape of the HMX powders. HMX samples were prepared monomodal with a single size range of particles or as mixtures of two or three size ranges in the bimodal or trimodal forms, respectively. Table 3.7 shows the mass ratios and the percentage of solids in monomodal, bimodal, and trimodal combinations of Class 5 (C5), Class 2 (C2), and Class 3 (C3) type HMX samples. Each modality category in Table 2.1 lists the combinations in order of increasing particle size. The notation "M", "B", and "T" represent mono-, bi-, and tri-modal systems, respectively. The total mass of the powder-polymer suspension is fixed at 300 grams. The mono-modal system uses 72.6 grams (24.2 wt%) of liquid polymer (P), while bi- and tri-modal systems utilize 54 grams (18 wt%). The remaining mass constitutes the total solids, which is 227.4 grams (75.8 wt%) for mono-modal and 246 grams (82 wt%) for bi- and tri-modal systems. The mass ratio between each HMX class and the polymer is based on the HMX class with the lowest mass. For example, a mixture containing 41 grams each of HMX Class 5 and Class 2, 164 grams of Class 3, and 54 grams of polymer is denoted as (41/41)C5:(41/41)C2:(164/41)C3:(54/41)P, which

simplifies to 1C5:1C2:4C3:1.32P. The final notation for this tri-modal system is T:1C5:1C2:4C3:1.32P. The notation of "i" added after the P stands for PBX produced by adding the curing agent IPDI.

Table 3.7. Mass composition of suspended HMX suspension mixtures

Modality	Product Name	C5:C2:C3 Mass (g)		C5:C2: C3 Mass Ratio	Solid Loading (wt %)	Content (wt %) Total mass = 300 g			
		Particles	Poly mer			HMX Class 5	HMX Class 2	HMX Class 3	Poly mer Liqu id
Monomodal	M:1C5:0.36P	227.4 : 0 : 0	72.6	1 : 0 : 0	75.8	75.8	-	-	24.2
	M:1C2:0.36P	0 : 227.4 : 0		0 : 1 : 0		-	75.8	-	
	M:1C3:0.36P	0 : 0 : 227.4		0 : 0 : 1		-	-	75.8	
Bimodal	B:1C2:1C3:0.44P	0 : 123 : 123	54	0 : 1 : 1	82.0	-	41.0	41.0	18.0
	B:1C2:2C3:0.88P	0 : 82 : 164		0 : 1 : 2		-	27.3	54.7	
	B:1C2:3C3:0.88P	0 : 61.5 : 184.5		0 : 1 : 3		-	20.5	61.5	
	B:1C5:1C2:0.44P	123 : 123 : 0		1 : 1 : 0		41.0	41.0	-	
	B:1C5:1C3:0.44P	123 : 0 : 123		1 : 0 : 1		41.0	-	41.0	
	B:1C5:2C3:0.66P	82 : 0 : 164		1 : 0 : 2		27.3	-	54.7	
	B:1C5:3C3:0.88P	61.5 : 0 : 184.5		1 : 0 : 3		20.5	-	61.5	
Trimodal	T:1C5:1C2:4C3:1.32P	41 : 41 : 164	54	1 : 1 : 4	82.0	13.7	13.7	54.6	18.0
	T:1C5:1C2:1C3:0.66P	82 : 82 : 82		1 : 1 : 1		27.3	27.3	27.3	
	T:2C5:1C2:2C3:1.10P	98.4 : 49.2 : 98.4		2 : 1 : 2		32.8	16.4	32.8	
	T:2C5:1C2:4C3:1.54P	70.2 : 35.1 : 140.7		2 : 1 : 4		23.4	11.7	46.9	
	T:1C5:1C2:2C3:0.88P	61.5 : 61.5 : 123		1 : 1 : 2		20.5	20.5	41.0	

3.2.1. Bulk and Tapped Density

The bulk density test was performed as shown in Figure 3.1.(a) according to MIL-DTL-650 standard [117].
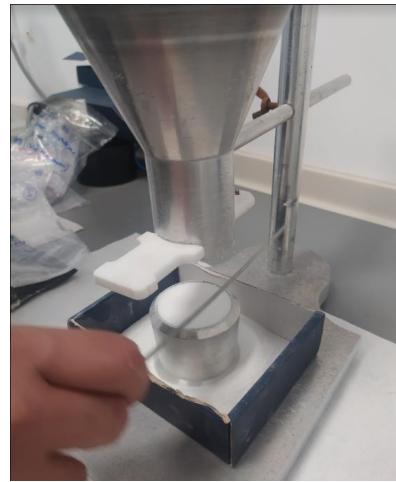
Figure 3.1. (a) The bulk density setup (b) Cup of bulk density

The bulk density cup is filled with water at room temperature in such a way that there is a convex meniscus on top and no water bubbles. The weight of the water-filled cup is measured after the outside pockets of the cup are placed. The volume of water is determined by subtracting the mass of the cup from the total mass of the water and the cup and dividing it by the density of water since the density of water is considered to be 1 g/ml. The cup volume estimate is given in ml. After that, the conditioned at 50°C sample is freely poured into the density cup. The excess portion of the sample is scraped with a spatula softly so that the top section of the cup and the sample are at the same level as shown in Figure 3.1.(b). The lower lid of the cup is opened, the sample is placed in the little weighing cabinet, and its weight is measured. The mass of the cup is subtracted from the mass of the sample combined with the cup, and the resulting value (g) is divided by the volume of the cup to get the bulk density (g/ml) of the sample (ml).

The tapped density measurement is done by using the jolting volumeter (Jolting Volumeter Type STAV II, J. Engelsmann AG, Deutschland) shown in Figure 3.2.

Figure 3.2. J. Jolting volumeter (Jolting Volumeter Type STAV II, J. Engelsmann AG, Deutschland) setup for measurement of tapped density

The conditioned at 50°C sample is weighed with 0.1 g accuracy and placed in a µml graduated cylinder. The volume of the sample within the cylinder is measured and recorded. The graduated cylinder is put inside the tapped density testing device and tapped 1250 times, depending on the results. The final volume is recorded after each tapping process. Tapped density data is obtained in g/ml by dividing the weight difference between the full and empty version of the cylinder (g) by the volume after the tamping and compaction process is completed (ml).

3.2.2. Particle Size and Shape Distribution

0.5 grams of conditioned at 50°C HMX mixture sample is mixed with 50 ml of distilled water (Figure 3.3.(a)). All HMX samples are dispersed in water for 10 seconds in 10-Watt ultrasonic mixer at room temperature (Figure 3.3(b)).
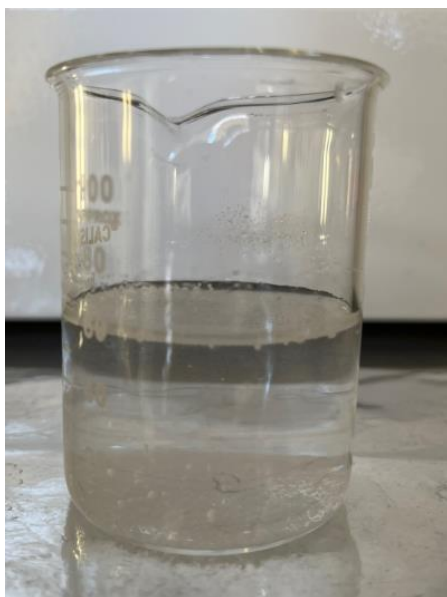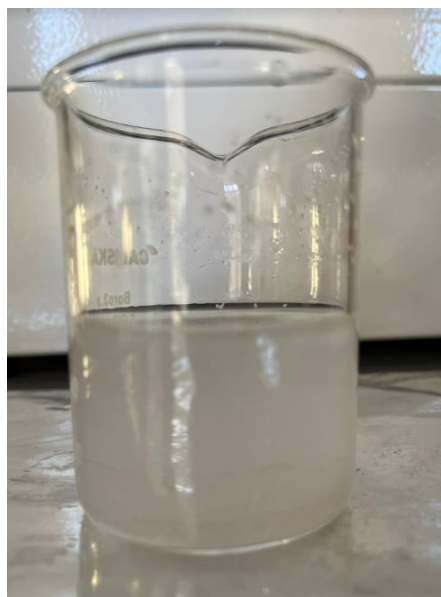
(a)	**(b)**

Figure 3.3. (a) HMX added to distilled water sinks and (b) gets dispersed using an
ultrasonic mixer

The average particle sizes (mean size) of HMXs are investigated by using the wet module
of laser diffraction particle size analyzer instrument (LA-960S, HORIBA, Japan), shown
in Figure 3.4.(a). Particle shape analysis is done by using the wet module of laser
diffraction and dynamic particle shape analyzer (Microtrac, SYNC, USA), seen in Figure
3.4.(b).

(a)	**(b)**

Figure 3.4. (a) Laser diffraction particle size analyzer (LA-960S, HORIBA, Japan)
(b) Laser diffraction and dynamic particle shape analyzer (Microtrac, SYNC, USA)

Sphericity analysis is performed for monomodal, bimodal and trimodal HMX systems.
The refractive index of water, which is used as the dispersion medium, is taken as 1.333

and the refractive index of HMX samples is taken as 1.693 and used for both the particle size and shape analysis methods.

The reservoir of the instrument is filled with 300 ml of the HMX-water mixture drop by drop using a Pasteur pipette until the back transmittance exceeded the threshold at 96–97 %. The average size and sphericity results of the particles are reported from the laser diffraction analyzer on a volume basis. The volume weighted (De Brouckere Mean Diameter) indicating the size of the particles that constitutes the bulk of a sample volume, is calculated by the laser diffraction particle size analyzer instrument based on the D[4,3] formulation given as:

$$D[4,3] = \frac{\sum_1^n D_i{}^4 v_i}{\sum_1^n D_i{}^3 v_i} \qquad (3.1)$$

Where n is the number of particles, D_i is the diameter of the ith particle, and v_i is the frequency of occurrence of particles in size class i with a mean diameter of D_i.

3.2.3. Particle Geometry

The morphological structures of HMX energetic powders were examined using scanning electron microscopy (SEM) (GAIA3+Oxford XMax 150 EDS, Tescan, Czech Republic) at HUNITEK, Hacettepe University. The device was operated at a voltage of 3 kV at magnification rates of 100x, 250x, 500x, and 1000x.

3.3. Production of PBX

The precoating procedure of HMX and production procedure of PBX are explained in this section.

3.3.1. Precoating of HMX

MIL-DTL-82901A (OS) [14] recommends IDP coating of HMX Class 2 and HMX Class 3 powders and use of their mixtures in certain ratios to adjust the initial viscosity. Aggregation of the small particles of HMX Class 5 prevents efficient wetting of the sample with the IDP liquid. To prepare 5-kilograms of coated products, dry HMX Class 2 or HMX Class 3 powders were mixed with IDP in a water slurry in the mixer shown in Figure 3.5. The wet HMX particles from the mixer were collected on a sieve as shown in Figure 3.6. and transferred to an oven for drying.

Figure 3.5. 50-liter jacketed reactor

Figure 3.6. IDP-coated HMX collected on a sieve before drying

3.3.2. Production Method

The production parameters including the mass of the product, molar ratio of NCO-to-OH and mass ratio HTPB-to-IDP and solid loading (wt%) were set as 300 grams, 1.1, 0.95, and 82%, respectively, before the production and kept constant in all productions made within the scope of this thesis. According to the viscosity results obtained when the HMX loading in the PBX suspension with a Class 2-to-Class 3 mass ratio of 1:2 was reduced from 86% to 82%, the HMX content that gave results below 1000 Pa.s [14], which is the processability limit of relative viscosity, was preferred. The production recipe is formed when the types of solids in the mixture are decided in accordance with this formula and the modality (mono, bi, or tri-modal) as shown in Table 3.7 for the HMX content of 82%.

M:, B: and T: represent the monomodal, bimodal, and trimodal mixture compositions, respectively.

As can be seen in Table 3.7, 82% could not be reached at the solid loading step during the production steps of the monomodal systems mentioned below. Since the viscosity increased too much during production, production was completed at the maximum solid loading limit i.e., 75.8% that the mixer blades could mix.

Production details and mixing steps are listed below:

1.   All the materials used in the production of PBX, except for DBTDL and IPDI, must be cleaned of moisture and conditioned at the production temperature prior to PBX production.

2.   HMX samples were dried at 80 °C for 48 hours. HMX samples, HTPB, IDP and lecithin are kept in different ovens at the production temperature of 50 °C for 18 hours.

3.   DBTDL, lecithin, HTPB, and IDP were added together to prepare the polymer mixture and mixed with a rotating blade at 150 rpm in an electric mixer (RZR 2102, Heidolph, Deutschland) at 50 °C for 25 minutes in a water bath (BM 15, Müve). This mixture was added to the 1-pint planetary mixer set at 50 °C and regularly heated with a heating jacket.

4.   HMX classes were added batch-by-batch to the planetary mixer.

5.   After a total of 2.5 hours of mixing, some of the sample was removed for rheological tests using a rheometer (HMX suspension sample). We note here that measurements done with the rheometer are based on samples that do not contain the curing agent.

6.   IPDI was added in the order ppm to the mixer to complete production.

7.   Some of the sample was removed immediately (PBX suspension) for measurement of viscosity using a Brookfield Viscometer and determination of pot life.

8.   The explosive mixture was cast into the molds to cure and is held under vibration and vacuum at 55 °C for approximately one hour, during which the air in the explosive mixture was eliminated.

9.   The molds were left in an oven set at 55 °C to cure.

3.4. Characterization of PBX

Methods used to characterize PBX samples include rheological, mechanical, and physical analyses. Rheological measurements are done on samples excluding the curing agent using a rheometer and on PBX samples upon addition of the curing agent using a viscometer. The mechanical testing involves the shore A hardness test and the uniaxial tensile test, and the physical test is done by true density measurement.

3.4.1. Viscosity Measurement of PBX-Excluding Curing Agent via Rheometer

The initial viscosity and shear stress of a total of sixteen (16) HMX suspension samples, prior to addition of the curing agent IPDI, were analyzed based on shear rate. One of the samples was composed of coated bimodal HMX powders as explained in Section 3.3.1. Rheological measurements were applied once on each PBX sample and three samples that attain the lowest viscosities were selected. Measurements were repeated four times on the selected samples for accuracy. A rheometer (Kinexus Pro, Malvern Instruments Ltd., UK) with an upper plate (PU20 SC0177 SS) and lower plate (PL65 S0733 SS) located in parallel are used for the rheological analysis of HMX suspension mixtures as shown in Figure 3.7.(a) and (b), respectively.

(a)   **(b)**
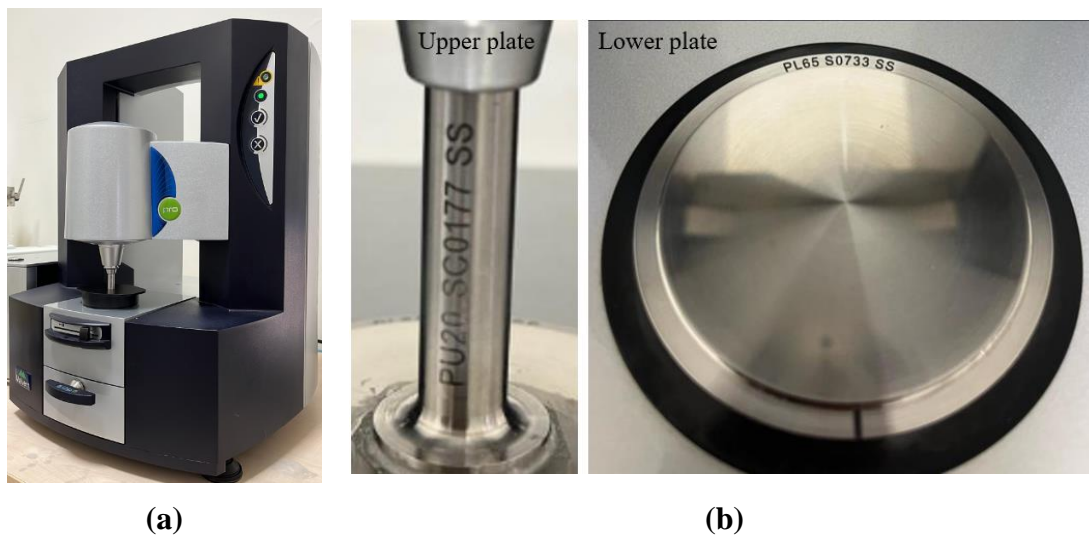
Figure 3.7. Rheological analysis using a (a) Kinexus Pro rheometer with (b) PU20 SC0177 SS upper and PL65 S0733 SS lower plates

The upper plate with the code PU20 SC0177 SS and the lower plate with the code PL65 S0733 SS are placed after the device is turned on. The thermal cover of the device is removed to load the sample. A zero gap is made to reset the distance between the plates.

42

We set the distance between the rotating plate (upper plate) and the fixed plate (lower plate) as 1 mm. During the production of PBX mixtures, a 20–30 g sample was taken and mixed by hand for 2.5 minutes. This sample was placed on the lower plate. The upper plate compresses the sample to the preset 1 mm distance from the lower plate. The placement of the sample in the instrument is finalized when the thermal cover is closed. The rheometer operates based on the computer software named rFinder, which includes several modules. We used the module titled "Viscometry_0010 Table of shear rates with Power law model fit". The temperature of the bottom plate, which is controlled by a Peltier heating system, is set to the assigned temperature. In this study, we tested the viscosity of each PBX sample at three different temperatures, 30 °C, 50 °C, and 70 °C. We set the shear rate between 0.005 s^{-1} and 1 s^{-1} and the number of measurements to 10 data points per decade. The measurement is started after the temperature reaches steady state. The desired data is exported from the computer program.

3.4.2. Viscosity Measurement of PBX via Viscometer

Viscosities of the PBX samples including the curing agent are measured after completion of the production process using a Brookfield DV2T Extra viscometer (AMATEK, US ET) shown in Figure 3.8 and T-bar (T-E) spindle shown in Figure 3.9.

Figure 3.8. Brookfield DV2T Extra viscometer [118]

Figure 3.9. T-bar spindles with helipath [118]

The water bath is switched on and the temperature is set to the production temperature at 50 °C at least an hour before the non-flow test. A sample of around 450–500 ml is obtained from a 600 ml beaker and a test pen at the conclusion of production. The sample-filled beaker is positioned in a water bath. The initial temperature of sample is checked. The sample temperature is tested to see if it matches the production temperature. Bubble levels on the viscometer and the helipath adapter are checked, and if required, modifications are made. The T-E spindle is attached to the device and the length of the path that the T-E spindle will follow through the sample is adjusted with the helipath adapter by leaving a gap of 1-2 cm below and above the upper and lower surfaces of the sample (one turn of the T-E spindle up and down the sample). Measurements are made in such a way that 1800 data is obtained every 5 seconds. The speed of the spindle is determined as 0.016 s^{-1}. The software in the viscometer keeps track of the non-flow value. The program must show a torque value that is at least 10%. In the event that the torque falls below this level, the measurement speed is initially raised until the torque value is at least 10%. A spindle that is one size larger is utilized if the torque value is still out of the 10% to 100% range. If the torque value is more than 100%, the measurement speed is slowed down until the torque value is 10% to 100%. The data were smoothed using the Savitzky-Golay method since the data from the Brookfield viscometer had a very high level of noise.

The slope of time dependent viscosity curves varied based on the specific curing rate. The initial viscosity value was determined by identifying the point of intersection between the curve and the y-axis on the Brookfield viscometer data. This approach aimed to capture the viscosity of the PBX suspension immediately after mixing, which represents the initial state of interest. It is important to note that the entire observed trend is attributed to the

curing reaction, and a detailed analysis of the complete curing process falls outside the scope of this study. To ensure consistency and prevent potential complications, neither a reduction in shear rate nor a change in spindle was implemented for samples with viscosity exceeding the measurable range of the T-F spindle at a shear rate of 0.016 s^{-1} i.e., 1 rpm. This approach ensured that all samples were measured under identical conditions.

3.4.3. Hardness Test

Shore A hardness test was done by using durometer (BS61 II, Bareiss, UK) (Figure 3.10).

Figure 3.10 Shore A hardness durometer (BS61 II, Bareiss, UK)

A test sample of 50 mm width, 20 mm length, and 12.5 mm thickness is sliced from the test pen. The sample was placed on the test stand. The measurement indicator on the hardness tester is adjusted according to the surface of the sample and the device height is adjusted. The measuring needle on the device is kept on the 2 main surfaces of the explosive sample (50 mm x 20 mm) for 15 seconds. Ten measurements were made on different locations on the surface of the sample. The average value of the measured 10 data is recorded as the Shore A hardness value

3.4.4. Uniaxial Tensile Test

Uniaxial Tensile Test was done by using the Universal Testing Instrument (5900 Series, INSTRON, US) (Figure 3.11). Military standards [14] recommend a minimum of three dog-bone samples for tensile testing, raising concerns about the validity of the single

result. The uniaxial tensile test was performed at a temperature of 25±3 °C based on STANAG 4506 Edition 1, the agreement prepared by NATO to standardize the uniaxial tensile test for explosive materials [119]. A layer with a thickness of 12.5±1 mm was cut from the test sample using a guillotine. The cutting punch was attached to the guillotine and the explosive material was cut with the guillotine as a test specimen as shown in Figure 3.12.(a) in the shape of a dogbone. The width and length of each test specimen were measured using a caliper at the points specified in the STANAG 4506 agreement and the acquired width and thickness values were individually recorded. The device was set to a cross-head speed of 50±1 mm/minute and the process was performed at this speed until the test specimen fractured as shown in Figure 3.12.(b) and Figure 3.12.(c). Load-elongation (Newton-mm) data was recorded by the device software during the tensile test.

Figure 3.11. Universal Testing Instrument (5900 Series, INSTRON, US)

| (a) | (b) | (c) |
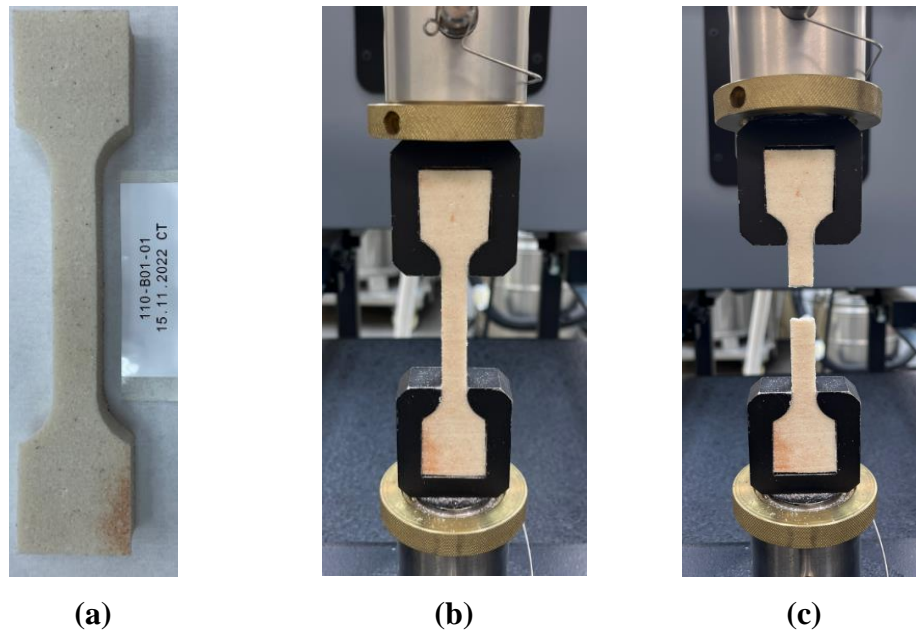
Figure 3.12. The dogbone test specimen as (a) prepared, (b) placed in the tensile tester, and (c) fractured

3.4.5. True Density Test

True density test was done by using pycnometer (Accupyc II, Micromeritics, GA) (Figure 3.13).

Figure 3.13. Pycnometer for determination of true density (Accupyc II, Micromeritics, GA)

True density test was performed at a temperature of 25±3 ° C in line with the AOP-7 standard [120]. The sample cabinet in the density measurement device is filled up to 80-90% with the samples obtained from the test pen. The sample weight is calculated using the difference between the empty and filled weights of the sample container with an accuracy of 0.1 mg. This information is entered as an input in the device software. The

container device is filled with the sample and closed. The valve of the helium tube is opened, and the gas regulator is adjusted to 20 psig. The instrument is used to test the sample density at least five times. Average density is calculated in g/cm^3 at the end of the test.

3.5. Models for Prediction of Viscosity

The data from measurements in this study was used to predict the viscosity as a function of single or multiple parameters. We used three approaches by employing:

1.   Viscosity models as a function of solid loading,
2.   Viscosity models as a function of shear rate,
3.   Complex statistical methods based on multiple data.

3.5.1. Comparison of Viscosity Models as a Function of Solid Loading

We investigated the relation between the relative viscosity and solid loading based on initial viscosity data. The main aim is to determine the model that most accurately fits the experimental initial viscosity data. The steps of the analysis are listed below:

1.   The relative viscosities were calculated as the ratio of the initial viscosity of the PBX suspension, i.e. the suspension viscosity at 0.016 s^{-1} and 50 °C, to the viscosity of the polymer liquid or the suspension medium at the same conditions.

2.   PBX suspensions with HMX content of 82%, 83.5%, 84%, 85%, and 86% by weight were prepared with a Class 2-to-Class 3 mass ratio of 1:2.

3.   The Curve Fitting tool in MATLAB R2016B was used to find the trend between solid loading and relative viscosity. Viscosity models by Guth [63], Vand [64], Mooney [65], Simha [66], Ford [69], Thomas [70] and Chong [71] listed in Table 2.3 were used and compared to find the best fit to the experimental data based on R^2, coefficient of determination. The R^2 value explains how well the data fits the regression model i.e., the goodness of fit. The R^2 has a positive value from zero to one.

4.   HMX suspensions with relative viscosities below 1000 Pa.s were selected for comparison of viscosity models as a function of shear stress and shear rate.

3.5.2. Comparison of Viscosity Models as a Function of Shear Rate

Table *2.2* lists eleven different Newtonian and non-Newtonian models to predict viscosity based on shear stress and shear rate. According to the graphs of initial viscosity changing with changing shear rate, we decided that we should use non-Newtonian models from

Table *2.2*. We used these models on the viscosity data obtained from the Rheometer measurements. The steps of the analysis are listed below:

1.   The Oswald model (Power Law Model, PLM), shown in Equations 2.3 and 2.4 [52], was used to analyze the initial viscosity with respect to the shear stress and shear rate.

2.   Three PBX systems with the lowest initial viscosity, which were two bimodal and one trimodal and consisted of different HMX particles i.e., B:1C2:2C3:0.66P, B:1C5:2C3:0.66P and T:1C5:1C2:4C3:1.32P were selected.

3.   The rheological analysis for each system was repeated four times and measured the initial viscosity of the suspension. The mean and standard deviation of the 4 measurement results were calculated for each parameter i.e., shear rate, shear stress, initial viscosity.

4.   The relative viscosity was obtained by dividing the measured initial viscosity of the suspension by the measured viscosity of the suspension medium i.e., polymer liquid.

5.   The relative viscosity in the Oswald model (Power Law Model, PLM) was used to find the model constants, namely, the consistency coefficient, K, and the pseudoplasticity index, n.

3.5.3.   Statistical Estimation of Viscosity Based on Multiple Data

The micromeritic parameters that affect the initial viscosity of the samples in 15 experimental data sets were investigated statistically. The main drawback of this statistical study is that it is based on a limited amount of viscosity measurement data. A Python code was created for statistical analysis and run in PyCharm Community Edition, which is an integrated development environment (IDE). The steps of the analysis can be listed as:

1.   A bell curve graph was used to determine if the data are normally distributed. For all data, the histogram approach was used to plot the distribution of numerical variables.

2.   Tree analysis was used for data that was not regularly distributed. The independent variables (predictors) were selected as amount of HMX Class 5, Class 2, and

Class 3, mean size, sphericity, tapped density, and bulk density. The dependent variables, i.e., the responses, were determined as the viscosity measurement results at temperatures of 30 °C, 50 °C, and 70 °C, using either a rheometer or the Brookfield viscometer.

3.   Diverging heatmap of the viscosity values from Rheometer measurements at 30 °C, 50 °C, and 70 °C was obtained based on the tree analysis.

4.   Diverging heatmap of the viscosity results from rheometer measurements at 50 °C, mean diameter, sphericity, tapped density, and bulk density was obtained based on the tree analysis.

5.   The Kolmogrov test was applied after the design of experiment analysis assuming a normal distribution. The Shapiro test was applied to compare multiple groups. Levene's test was performed to see if the variances were homogeneous.

6.   We applied multilinear regression based on the Mann Whitney (MW) non-parametric estimator and random forest regression based on the Kolmogorov Smirnov (KS) non-parametric estimator. Random forest is a supervised learning algorithm that uses ensemble learning methods for classification and regression. The trees in random forests run in parallel. There is no interaction between these trees while building the trees. Random forest regression operates by constructing a multitude of decision trees at training time and outputting the class that is the mean prediction of the individual trees [121,122].

4. RESULTS and DISCUSSION

The results presented in this section can be classified as follows:

1. Micromeritic characterization and comparison of Class 5, Class 2, and Class 3 HMX energetic powders and their bimodal and trimodal mixtures.

2. Rheological and mechanical testing of modified PBXN-110 systems

3. Estimation of viscosity as a function of single or multiple parameters.

4.1. Properties of Raw Material: HMX Particles

Class 5, Class 2, and Class 3 HMX energetic powders, listed in order of increasing particle size, used in explosive systems at TUBITAK SAGE were investigated for their micromeritic parameters, such as bulk and tapped density, particle size and shape distribution, and particle geometry.

4.1.1. Bulk and Tapped Density

Average bulk density and tapped density measurements resulted with maximum 0.0036% standard deviation and was regarded as highly accurate. Tapped density and bulk density values are directly proportional to each other as expected. The measured values of the tapped density were found to be on the average 1.44 times the measured values of the bulk density. This is an expected result as the tapping results in compaction and densification of the particles. The measured bulk and tapped densities of the mono-, bi-, and trimodal HMX systems prepared based on the ratios shown in Table 3.7 are presented in Figure 4.1. The results for each modality group are presented based on increasing mean particle size. The mono-, bi-, and trimodal systems were found to have a particle size range of 25.69–318.89 µm, 29.00–261.78 µm, and 58.80–191.36 µm, respectively. Tapped and bulk densities of the HMX systems were observed to increase with increasing mean particle size for each modality caused by better packing due to nonspherical particle geometry. The monomodal system defined by M:1C5 with the smallest mean particle size of 25.69 µm attained the minimum tapped density of 0.9592 g/ml and bulk density of 0.5435 g/ml. The bimodal system defined by B:1C5:3C3 with the largest mean particle size of 261.8 µm attained the maximum tapped density of 1.0213 g/ml amongst all the samples.

B:1C5:3C3, T:1C5:1C2:4C3, B:1C2:3C3, B:1C2:2C3, and B:1C5:2C3 are the first five systems overall in terms of highest tapped density and bulk density. These five systems are expected to have the highest particle packing density as the bulk density is directly proportional to HMX packing density as shown in Equation 2.28. The tapped and bulk densities of these four bimodal systems and one trimodal system including a mixture of fine and coarse particles are greater than those of the monomodal systems.
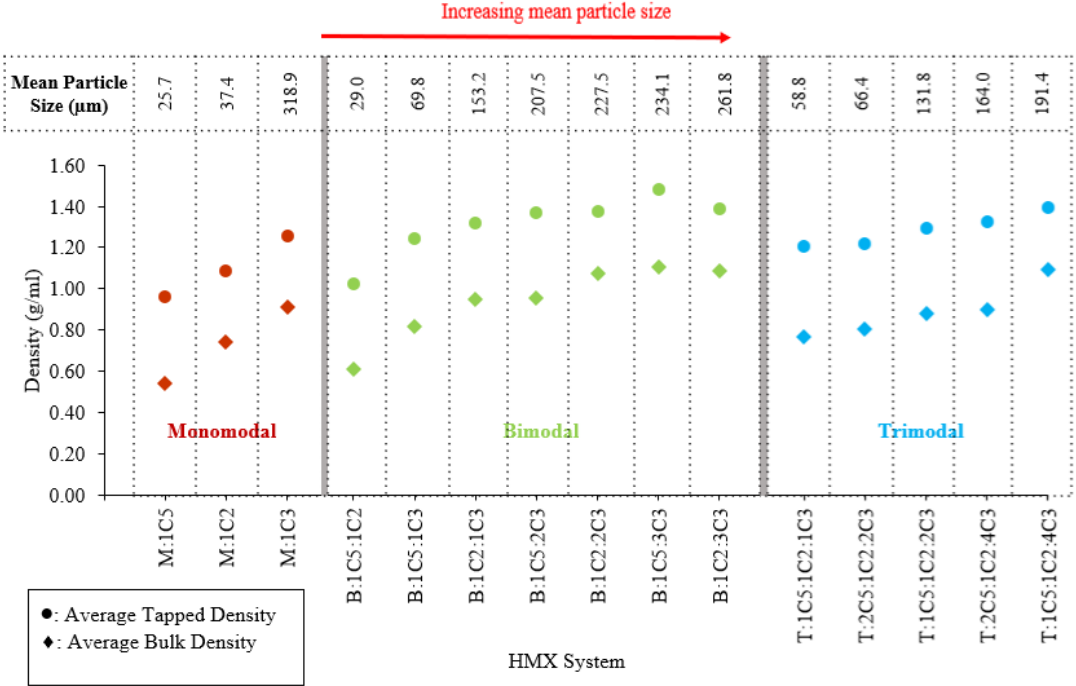
Figure 4.1. Average tapped (spheres) and bulk density (squares) of monomodal (red), bimodal (green), and trimodal (blue) HMX systems listed in Table 3.7

The appropriate packing of the HMX particles to achieve the most effective HMX packing, and the highest density requires an ideal fine-to-coarse ratio. A study by Joshi et al. [40] compares the bulk densities of bimodal and trimodal mixtures of HMX particles shown in the graphs in Figure 2.8. The ranges of HMX particle sizes used in the bimodal system are 0–125 μm and 125–250 μm and the highest bulk density can be obtained with a 1:1 ratio of these particles. The ranges of HMX particle sizes used in the trimodal system are 0–250 μm, 250–500 μm, and 500–800 μm and the maximum bulk density is obtained at a 0.35:0.40:0.25 ratio of these particles. This shows that using particles with different mean diameters at the right ratios will minimize the interparticle voids to optimize the packing. The results for random packing, i.e. the ratio of bulk density to tapped density as shown in Equation 2.28, are shown in Figure 4.2. Random packing is found to increase

52

in each modality with respect to mean particle size. The monomodal system defined by M:1C5 with the smallest mean particle size of 25.69 μm attained the minimum random packing of 0.5666. The bimodal system defined by B:1C5:3C3 with the largest mean particle size of 261.8 μm attained the maximum random packing of 0.7831 amongst all the samples.
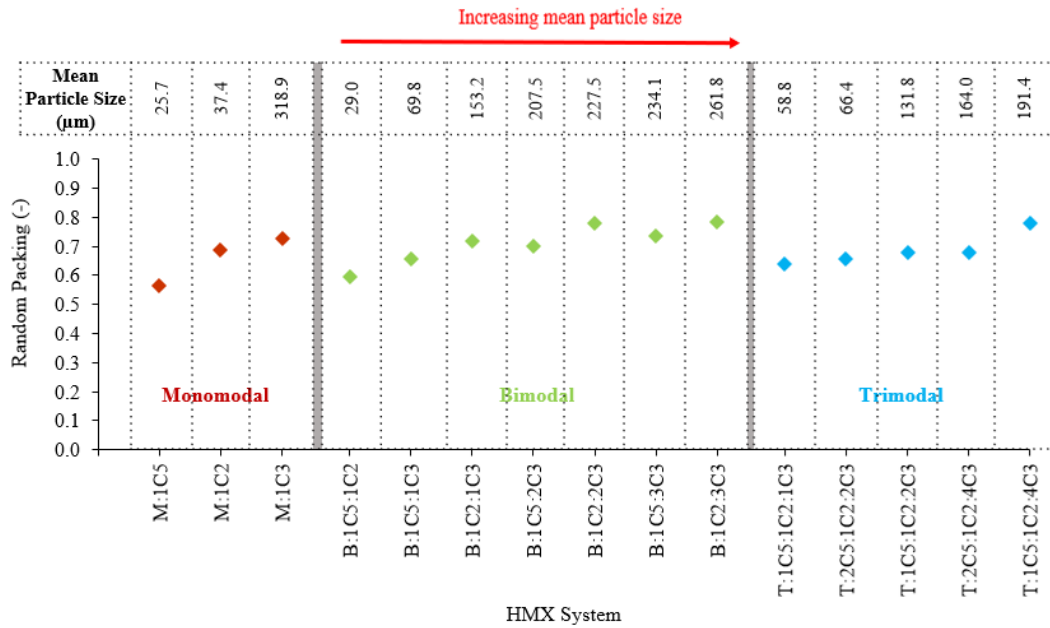
Figure 4.2. Random packing for monomodal (red), bimodal (green), and trimodal (blue) HMX systems listed in Table 3.7

An increase in the random packing of powders in the solid-liquid suspensions has been shown to increase their flowability [15, 93–96]. Figure 4.3 shows the flowability characteristics of all samples based on definitions created by Carr [97] and Gupta [98] using results of Hausner ratio (HR) and compressibility index (CI), respectively. HR results for all HMX systems are found to be higher than the maximum limit value of 1.18 for good flowability defined by Carr [97], indicating none of the samples could attain good or excellent flowability. Similarly, the compressibility indices (CI) most of the HMX systems are found to be higher than the maximum limit value of 25% for poor flowability and there are only three HMX systems with CI between 15%−25% and passable flowability defined by Gupta [98].

Increasing mean particle size

Powder Flowability	Carr= f(HR)	VVP	VP	P	VVP	VP	P	P	Ps	P	Ps	VP	VP	VP	VP	Ps
	Gupta= f(CI)	P	P	P	P	P	P	P	Ps	P	Ps	P	P	P	P	Ps
Mean Particle Size (µm)		25.7	37.4	318.9	29.0	69.8	153.2	207.5	227.5	234.1	261.8	58.8	66.4	131.8	164.0	191.4

HMX System: M:1C5, M:1C2, M:1C3 (Monomodal); B:1C5:1C2, B:1C5:1C3, B:1C2:1C3, B:1C5:2C3, B:1C2:2C3, B:1C5:3C3, B:1C2:3C3 (Bimodal); T:1C5:1C2:1C3, T:2C5:1C2:2C3, T:1C5:1C2:2C3, T:2C5:1C2:4C3, T:1C5:1C2:4C3 (Trimodal)

●: Hausner Ratio
♦: Compressibility Index (%)

Figure 4.3. Powder flowability, Hausner ratio, HR, (circles) and compressibility index, CI, (diamonds) based on particle size for the monomodal (red), bimodal (green), and trimodal (blue) HMX systems listed in Table 3.7. Powder flowability is based on indices defined by Carr [97] on HR and Gupta [98] on CI, where Ps: passable, P: poor, VP: very poor, VVP: very very poor

The CI value in Figure 4.3, i.e. the compressibility of HMX particles, decreases as the tapped density and bulk density values in Figure 4.1 approach each other. In this case, we can see that the packing of HMX particles in Figure 4.2 increases.

All the measured data for tapped density and bulk density and the calculated data for Hausner ratio, compressibility index, and random packing of HMX systems are presented in APPENDIX A.

4.1.2. Particle Size and Shape Distribution

The particle size distributions of the mono-, bi-, and trimodal HMX systems, prepared based on the ratios shown in Table 3.7, were measured by using the wetted laser diffraction method and are shown in Figure 4.4.

Figure 4.4.(a) shows the peaks around the mean diameters for the monomodal HMX systems of M:1C5, M:1C2, and M:1C3 as 25.69 µm, 37.41 µm and 318.89 µm, respectively. HMX powders defined by M:1C5 and M:1C2 with small particle size have a narrow size distribution, whereas M:1C3 including larger particles has a broader size distribution. Particle mean size results are expected when compared to the values listed in the HMX Class 5, Class 2, and Class 3 standards [12].

Figure 4.4.(b) shows the particle size distributions for seven different bimodal systems. All systems, except for the B:1C5:1C2 system that is a combination of two systems of fine particle size, exhibit two-humps as expected. The B:1C5:1C2 system behaves monomodal and presents a single combined distribution curve as the mean particle sizes of class C5, 25.69 µm, and class C2, 37.41 µm, are close to each other. Standard deviation is higher in the bimodal HMX systems. The density distribution obtained in the low particle size region gets larger as the mass ratio of fine-particle HMX classes C5 or C2 in the bimodal HMX systems increases. The density distribution in the larger particle size region is observed to increase as the coarse particle size ratio increases, though this rise is not proportional with the ratio of the amounts of HMX classes used, i.e. we do not see the peak three times as large as the first one for a mixture of B:1C5:3C3 and B:1C2:3C3.

Figure 4.4.(c) shows that the mixtures involving HMX samples of three different mean particle sizes result with two peaks instead of three indicating bimodal behavior. This is due to the small difference in the mean particle sizes of HMX Class 2 and Class 5 and the large distribution in the mean particle size of HMX Class 3. The particles in the smaller size range of HMX Class 3 contribute to the distribution of C2 and C5 adding to the height of the first curve. This is apparent for the T:1C5:1C2:4C3 system, where the amount of C3 used is four times that of C5 and C2 still giving a larger distribution curve in the smaller size range region. This is different behavior than observed for the bimodal mixtures shown in Figure 4.4.(b) as the use of two HMX systems in the smaller mean particle size range contributes to the first peak in the smaller particle size region. Similar to bimodal systems, the density distribution in the small particle size region increases as the fine-particle HMX Class 5 or HMX Class 2 mass ratio in trimodal HMX systems increases.
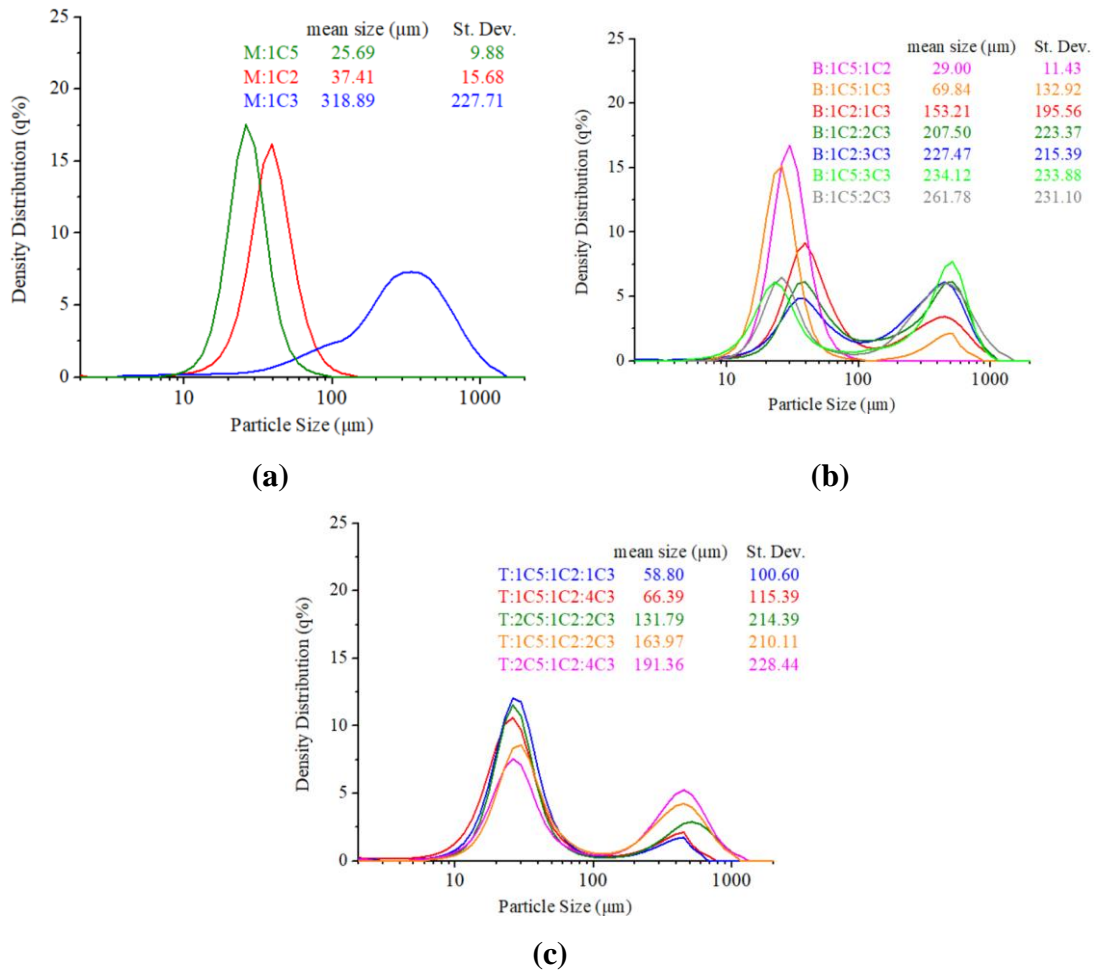
Figure 4.4. Graphical results of wetted laser diffraction particle size distribution analysis and within 95% standard deviations of (a) monomodal, (b) bimodal, (c) trimodal HMX systems listed in Table 3.7

The sphericity values of the HMX systems from based on mean size are shown in Figure 4.5. The monomodal system that has the largest mean particle size, M:1C3, attained the minimum sphericity of 0.89. The monomodal system that has the smallest mean particle size, M:1C5, attained the maximum sphericity of 0.94 amongst all the samples. The sphericities of the monomodal HMX systems M:1C5, M:1C2 and M:1C3 are found to increase with mean particle size. The sphericities of the bimodal and trimodal HMX systems do not present a significant change in behavior based on mean diameter. This may be due to agglomeration of particles of different sizes in mixtures.
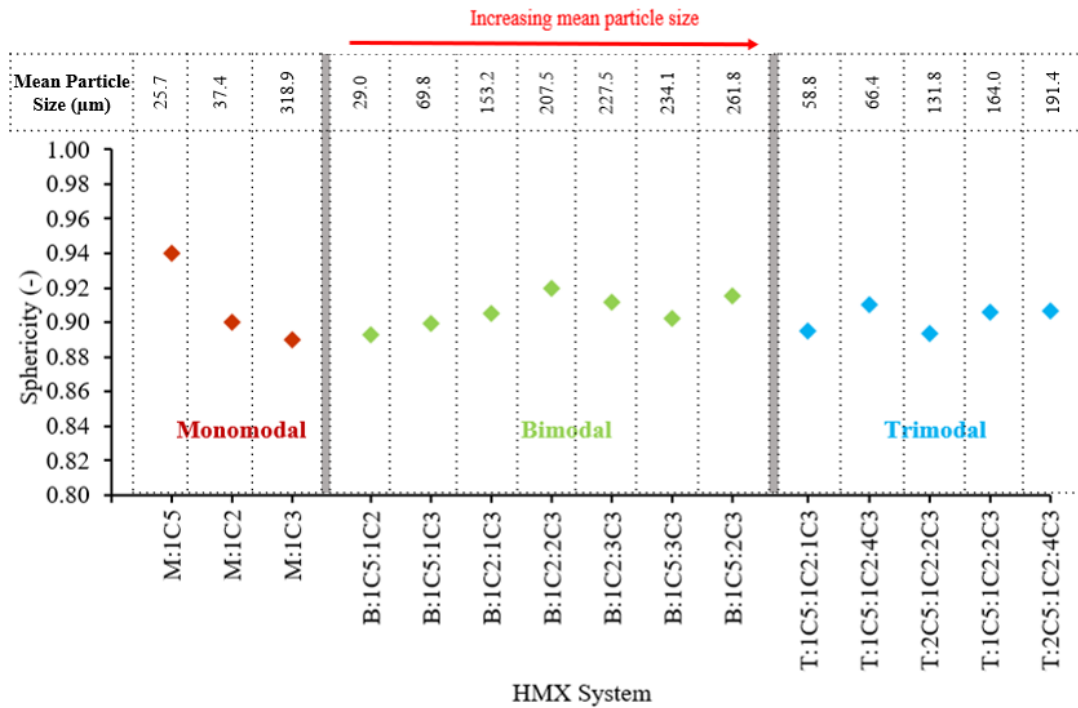
Figure 4.5. Sphericity for monomodal (red), bimodal (green), and trimodal (blue) HMX systems listed in Table 3.7

Laser diffraction mean particle size and shape results were presented in APPENDIX B.

4.1.3. Particle Geometry

Particle geometry of HMX Class 5, HMX Class 2, and HMX Class 3 were determined using scanning electron microscopy (SEM) with a magnification of 250x and 1000x as shown in Figure 4.6 and Figure 4.7, respectively. Figure 4.6. shows that the order of sphericity from high to low can be listed as follows: HMX Class 5 in Figure 4.6.(a), HMX Class 2 in Figure 4.6.(b), and HMX Class 3 in Figure 4.6.(c) supported by Figure 4.5 listing the highest sphericity of 0.94 for HMX Class 5. HMX Class 3 is observed to have very sharp corners and the lowest sphericity [41].
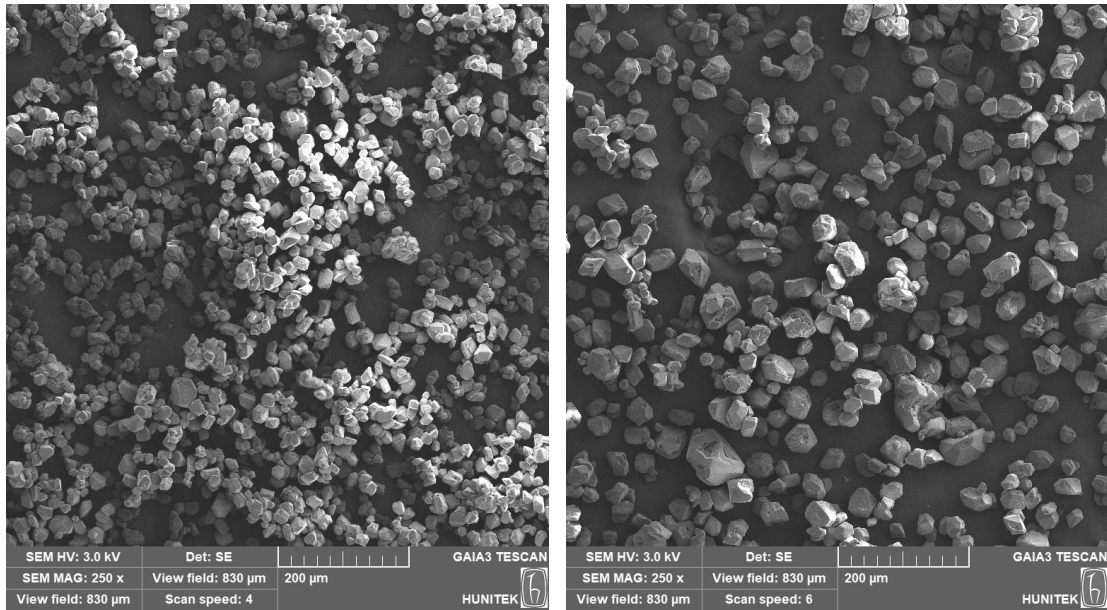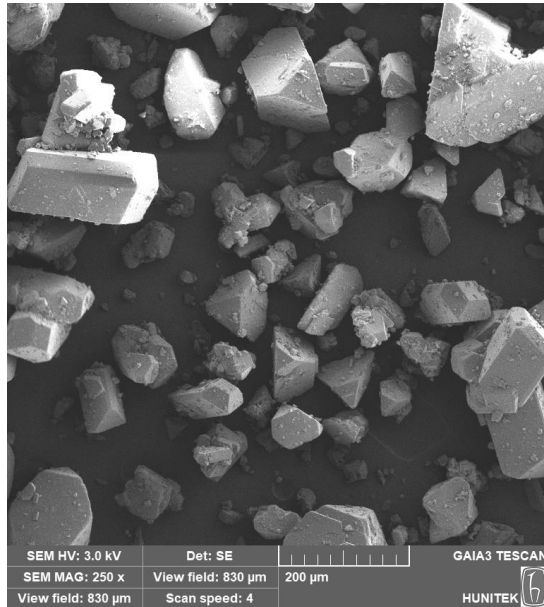
Figure 4.6. SEM micrographs at 250x magnification for (a) HMX Class 5, (b) HMX Class 2, and (c) HMX Class 3

The SEM images at 1000x magnification shown in Figure 4.7 bring forward the great differences between the sizes of the particles of HMX Class 3, which was shown to have a wide particle size distribution in Figure 4.4.(a). This sample is polydispersed with both very large and very small particles. The geometry of the large particles in HMX Class 3 that have grown in certain directions involves sharp corners, whereas the smaller particles of HMX Class 5 and Class 2 have rounded corners and, thus, higher sphericity.

SEM HV: 3.0 kV | Det: SE | 50 µm | GAIA3 TESCAN
SEM MAG: 1000 x | View field: 208 µm | |
View field: 208 µm | Scan speed: 4 | | HUNITEK

(a)

SEM HV: 3.0 kV | Det: SE | 50 µm | GAIA3 TESCAN
SEM MAG: 1.00 kx | View field: 208 µm | |
View field: 208 µm | Scan speed: 4 | | HUNITEK

(b)

SEM HV: 3.0 kV | Det: SE | 50 µm | GAIA3 TESCAN
SEM MAG: 1.00 kx | View field: 208 µm | |
View field: 208 µm | Scan speed: 4 | | HUNITEK
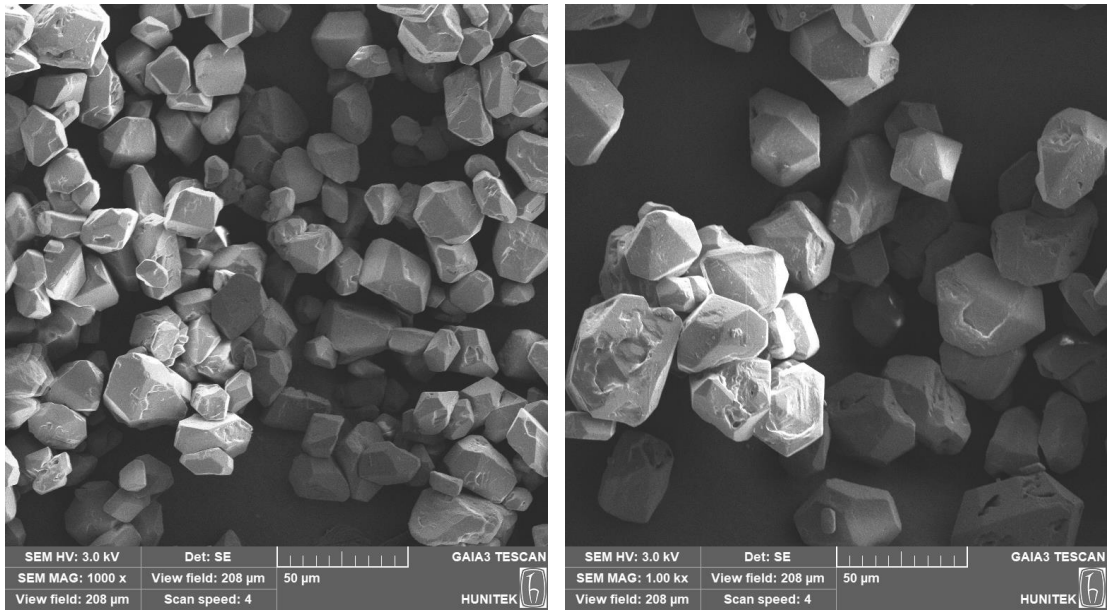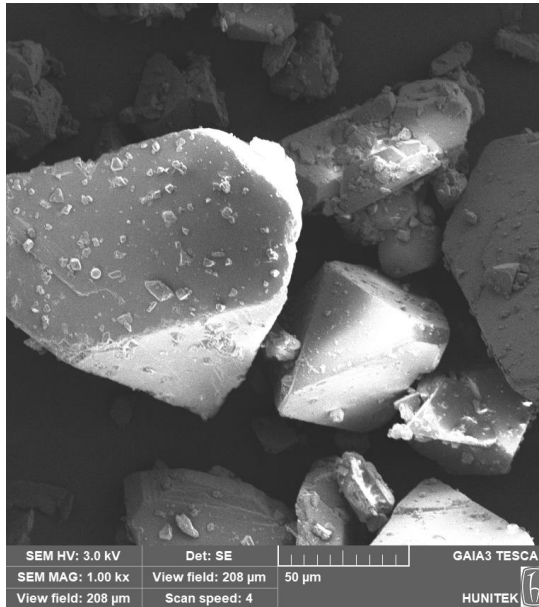
(c)

Figure 4.7. SEM micrographs at 1000x magnification for (a) HMX Class 5, (b) HMX Class 2, (c) HMX Class 3

4.2.   Properties of HMX Polymeric Suspension Prior Excluding Curing Agent

The rheological behavior of PBX samples prior to the addition of the curing agent IPDI was investigated to understand the effect of micromeritic properties of HMX.

4.2.1. Viscosity Measurement with Rheometer

The rheometer allows measurement of the viscosity by varying the shear rate. The tests were done on HMX suspensions excluding the curing agent.

Shear rate

It is well known that suspended polymer mixtures behave as shear-thinning, as proved by studies in the literature [43–48]. The results obtained for the HMX suspension system shown in Figure 4.8, applied at 30°C, 50°C and 70°C, are consistent with the literature. The viscosities have been found to decrease with increasing shear rate at all three temperatures for all suspension systems indicating non-Newtonian shear thinning (pseudoplastic) behavior, except for the monomodal M:1C2:0.36P system. Figure 4.8.(b) shows that the change in the viscosity of the M:1C2:0.36P system with respect to shear rate is positive and the viscosity reaches a maximum at a critical shear rate of 0.32 s^{-1}. The viscosity curve with respect to shear rate attains a negative slope for values above this critical shear rate. Such a transition from a shear thickening to a shear thinning behavior at a critical shear rate at all three temperatures is an unexpected behavior based on the results obtained for similar materials in this study. This odd behavior of the monomodal M:1C2:0.36P system could be due to the initial existence of particle clusters that act as larger particles in a heterogeneous mixture. Class 2 HMX has less sphericity compared to Class 5 HMX, which has slightly smaller mean particle size, and thus, may be more prone to clustering. Homogeneous mixing of HMX particles is a challenging process due to the electrostatic interactions between the energetic particles. The increasing and then decreasing behavior of the viscosity versus shear rate graph shown in Figure 4.8.(b) could be explained by two different mechanisms. One possibility is that large clusters of particles cause friction and resist the flow up to a critical shear rate, after which the clusters break up and particles get aligned in the direction of flow to reduce the viscosity. The other possibility is that these large particle clusters start to dissociate with applied shear forces causing a decrease in particle size and an increase in viscosity up to the critical shear rate when all the clusters are dissociated into original particles and the system starts to exhibit its natural behavior of decreasing viscosity with increasing shear rate.

(a)

(b)

(c)
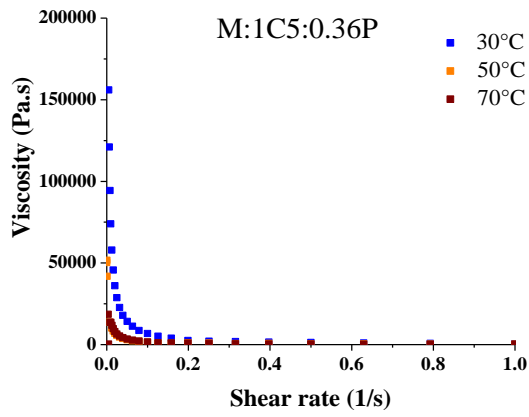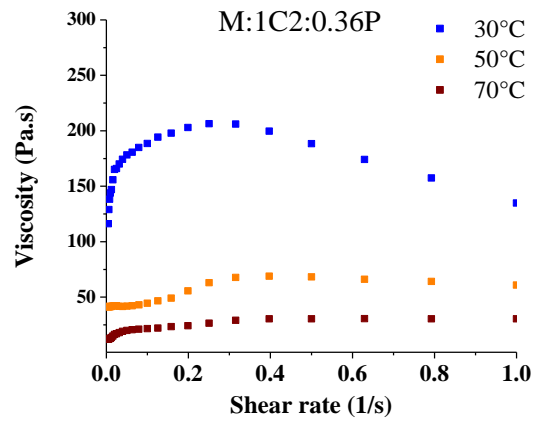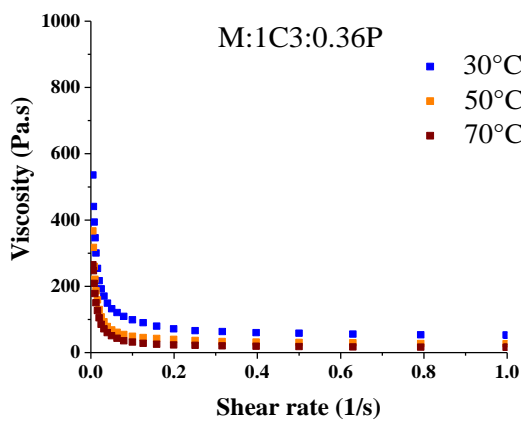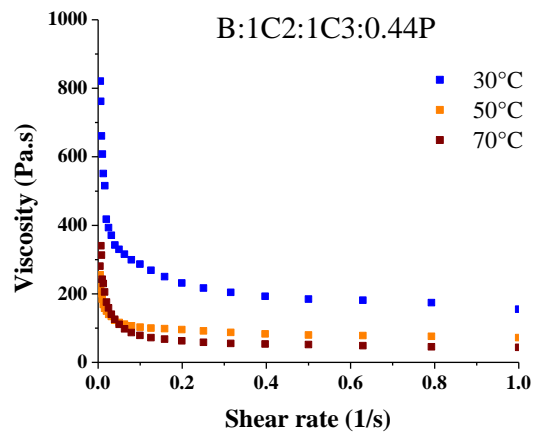
(d)
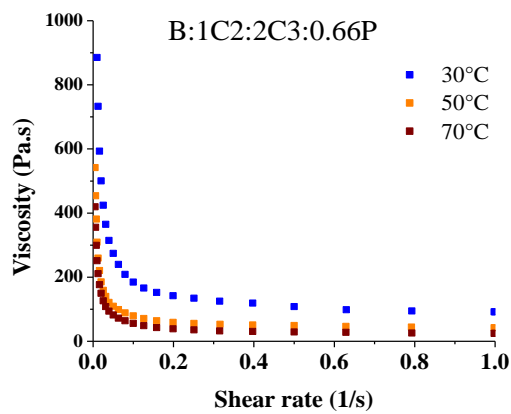
(e)
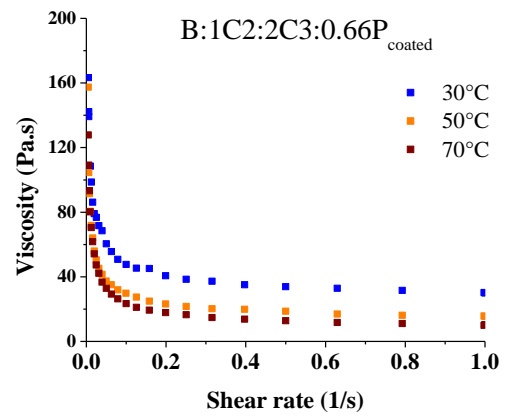
(f)
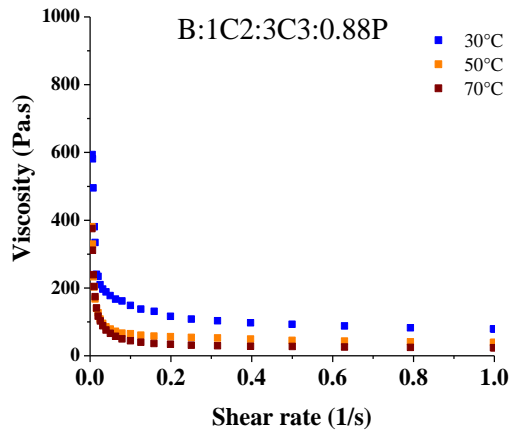
(g)
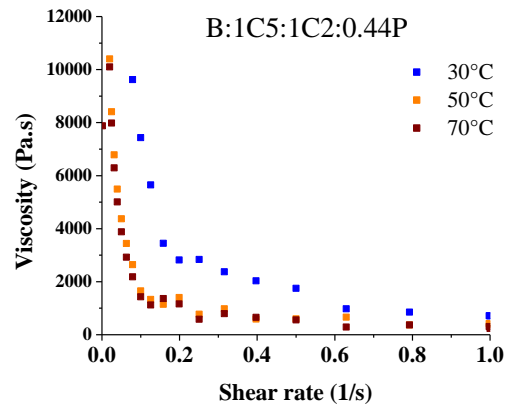
(h)
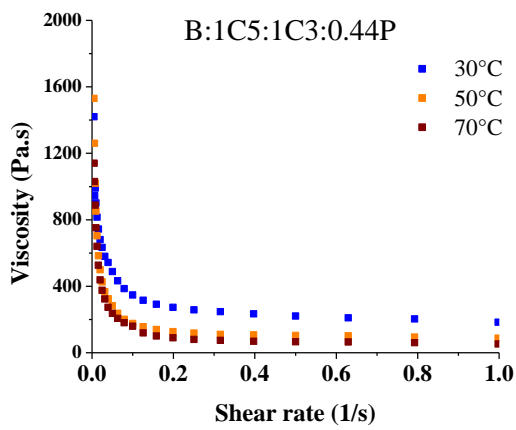
(i)
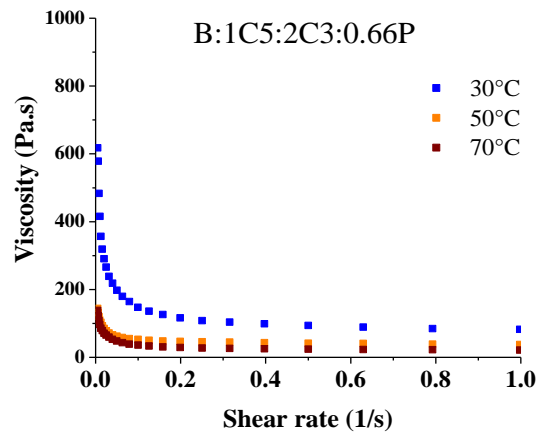
(j)
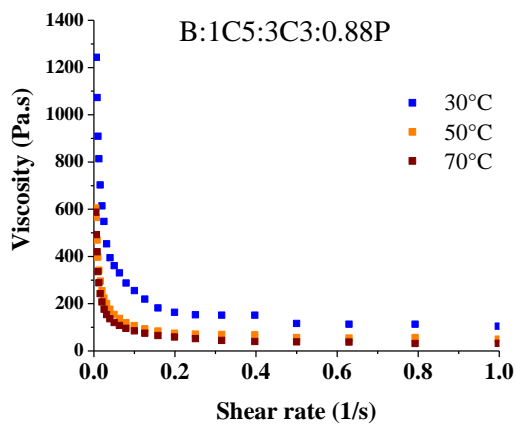
(k)
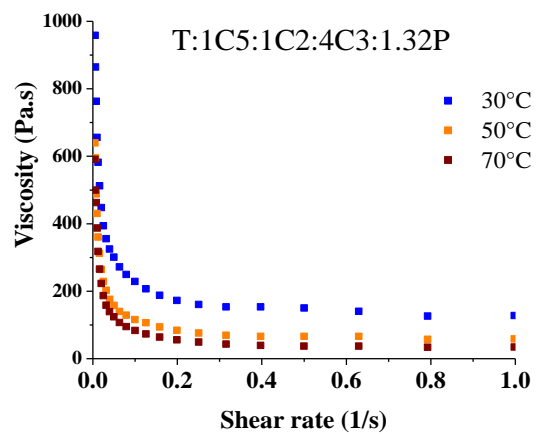
(l)
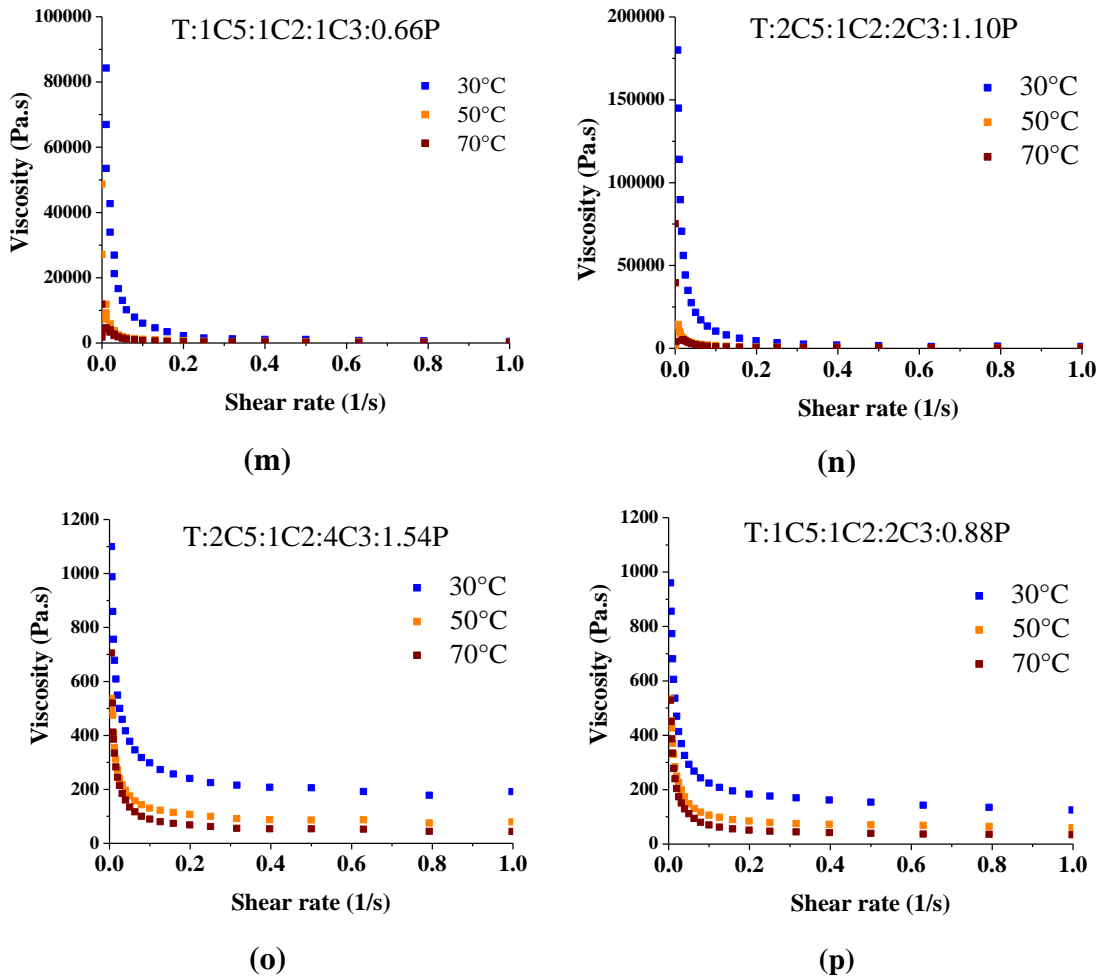
Figure 4.8. The change in viscosity with shear rate at 30°C, 50°C and 70°C for (a) monomodal M:1C5:0.36P, (b) monomodal M:1C2:0.36P, (c) monomodal M:1C3:0.36P, (d) bimodal B:1C2:1C3:0.44P, (e) bimodal B:1C2:2C3:0.66P, (f) bimodal B:1C2:2C3:0.66P$_{coated}$, (g) bimodal B:1C2:3C3:0.44P, (h) bimodal B:1C5:1C2:0.44P, (i) bimodal B:1C5:1C3:0.44P, (j) bimodal B:1C5:2C3:0.66P, (k) bimodal B:1C5:3C3:0.88P, (l) trimodal T:1C5:1C2:4C3:1.32P, (m) trimodal T:1C5:1C2:1C3:0.66P, (n) trimodal T:2C5:1C2:2C3:1.10P, (o) trimodal T:2C5:1C2:4C3:1.54P, (p) trimodal T:1C5:1C2:2C3:0.88P systems.

Modality

We investigated the effect of modality on the shear stress and viscosity with respect to shear rate between 0.005 s^{-1} and 1 s^{-1} at three different temperatures 30°C, 50°C, and 70°C as shown in Figure 4.9. The shear stress applied on the monomodal, bimodal, and trimodal HMX suspension systems have been shown to be most affected by the particle sizes used. Four of the HMX suspension systems including all three modalities have been shown to

exhibit shear stresses that are orders of magnitude higher than the others. These are the trimodal T:1C5:1C2:1C3:0.66P and T:2C5:1C2:2C3:1.10P, the bimodal B:1C5:1C2:0.44P, and the monomodal M:1C5:0.36P systems shown in the highlighted areas in Figure 4.9. The key point about these systems is that they consist of a higher amount of fine particles including C5 and C2, than coarse particles with C3. C5 and C2 type HMX have particle sizes close to each other almost forming a monomodal system as shown in Figure 4.4.(b). In this respect, the trimodal T:1C5:1C2:1C3:0.66P and T:2C5:1C2:2C3:1.10P systems can be regarded as bimodal systems with fine and coarse particles as discussed in this section and the bimodal B:1C5:1C2:0.44P system can be regarded as a monomodal system with fine particles only. These systems exhibit very high shear stresses in the order of 10^3 Pa at 30°C while the shear stresses on other systems vary between 1 and 10 Pa. The effect of temperature on these four specified HMX suspension systems is dramatic as the shear stress drops an order of magnitude to 10^2 Pa when the temperature is increased to 50°C and 70°C. This effect is subtler for the other systems. The shear stresses on all the systems drops as the viscosity decreases with temperature. High shear stresses of these four systems are based on their very high viscosities ranging between 10^5 Pa.s and 10^3 Pa.s at 30°C for shear rates between 0.005 s^{-1} and 1 s^{-1}. The viscosities of the other systems are between 10^3 Pa.s and 10^1 Pa.s at 30°C and decrease in the same order range at higher temperatures of 50°C, and 70°C (Figure 4.9 (d) and (f)).

The fluctuations observed on the shear stress and viscosity curves of the four systems that stand as a separate group on all graphs in Figure 4.9 at all temperatures are related to the limitations of the rheometer when used with materials with high viscosities and shear stresses. Figure 4.9 shows that the bimodal B:1C2:2C3:0.66P$_{coated}$ HMX suspension system with larger amount of coarse particles from C3 type HMX attains the lowest shear stresses with the lowest viscosity amongst all and presents a very smooth curve. The main factor that causes the shear stress and viscosity to increase is the larger amount of fine particles in the content.
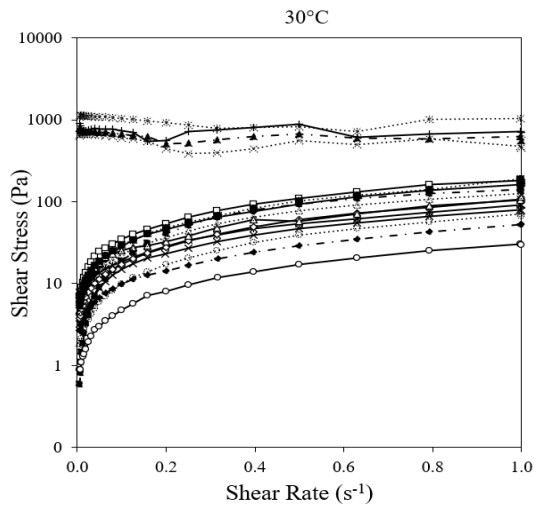
(a)
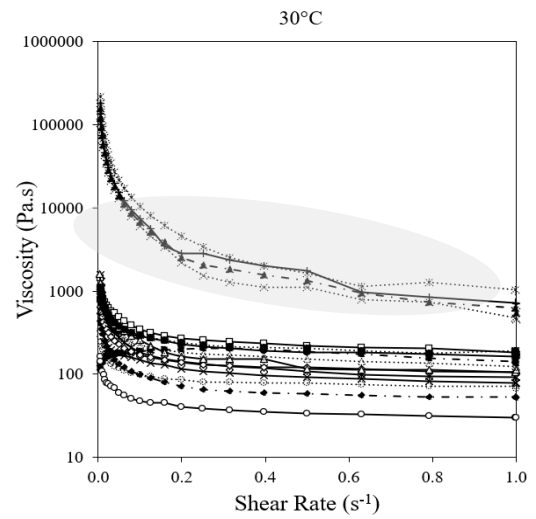
(b)
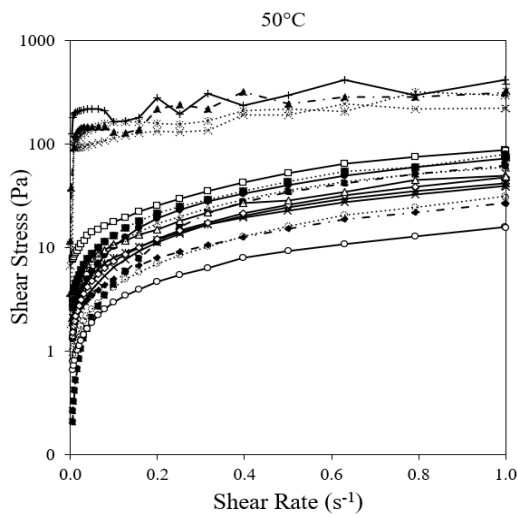
(c)
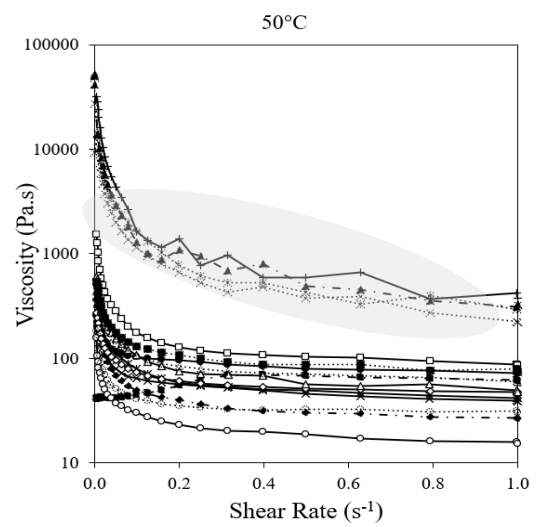
(d)
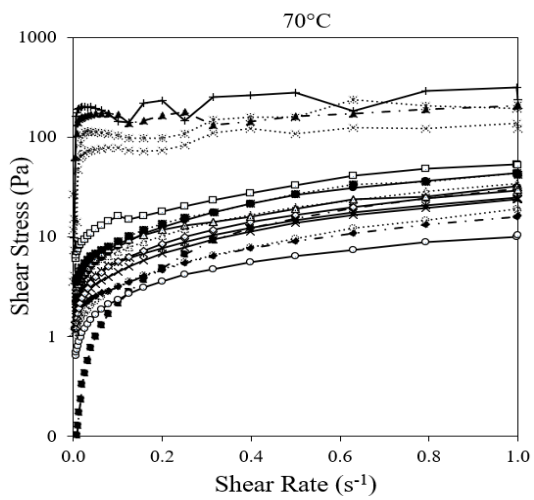
(e)
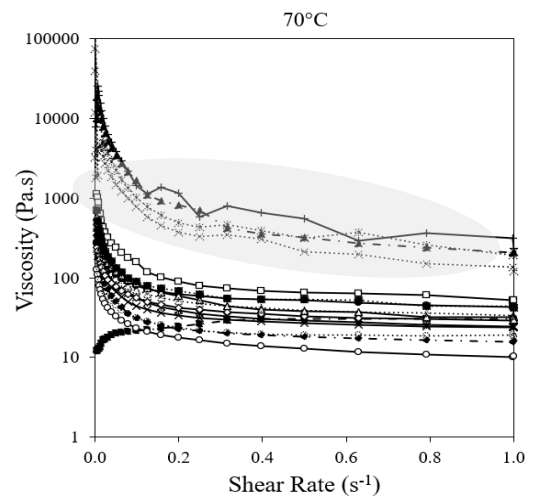
(f)
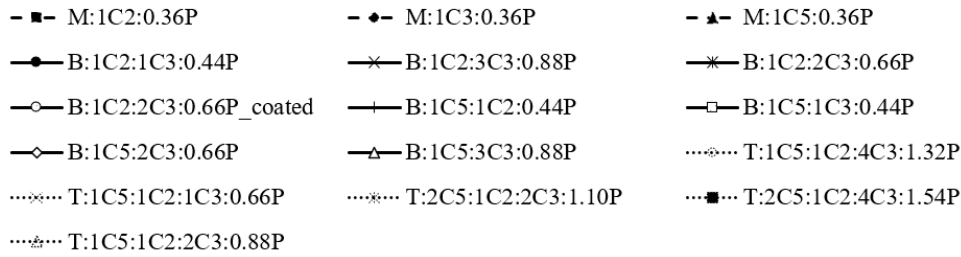
Figure 4.9. Changes of shear stress of HMX suspension systems with shear rate at (a) 30°C, (c) 50°C, and (e) 70°C and viscosity of HMX suspension systems with shear rate at (b) 30°C, (d) 50°C, and (f) 70°C

Temperature

HMX suspension systems exhibit decreasing shear stress and viscosity with increasing temperature as shown by Irgens [35], Junid et al. [42], and Sarangapani et al. [48]. This relationship between temperature and viscosity of HMX suspension systems measured at 30°C, 50°C, and 70°C can be observed in Figure 4.8 (a) to (c) for monomodal HMX suspension systems, (d) to (k) for bimodal HMX suspension systems, (l) to (p) for trimodal HMX suspension systems for shear rates between 0.005 s^{-1} and 1 s^{-1}.

A more comprehensive comparison of the effect of temperature on the variation of viscosity of the HMX suspension systems can be observed when the shear rate is kept constant. Figure 4.10 shows the change in viscosity as the temperature is increased from 30°C to 50°C, and 70°C at shear rates of 0.005 s^{-1}, 0.016 s^{-1}, 0.05 s^{-1}, and 1 s^{-1}. Viscosity has been found to decrease with increasing temperature except for two systems at the lower shear rates of 0.005 s^{-1} and 0.016 s^{-1} shown in Figure 4.10.(a) and (b), respectively. The bimodal B:1C5:1C3:0.44P and B:1C2:2C3:0.66P$_{coated}$ systems are found to have increased viscosity as the temperature is raised from 30°C to 50°C at these lower shear rates. Further increase in the temperature to 70°C has caused the viscosity to drop in both systems, which is the expected behavior. Such an increase in the viscosity with temperature, as it is raised from 30°C to 50°C, at low shear rates is unanticipated and may be caused by experimental errors from the device or nonhomogeneous mixing. The results in general indicate that the viscosity reducing effect of increasing temperature is fortified with increased shear rates at 0.5 s^{-1} and 1 s^{-1}.

Shear Rate= 0.005 s⁻¹

(a)

Shear Rate= 0.016 s⁻¹

(b)

Shear Rate= 0.5 s⁻¹

(c)

Legend:
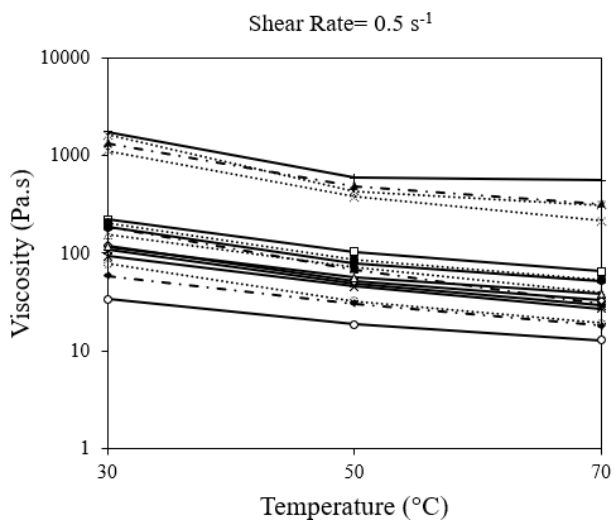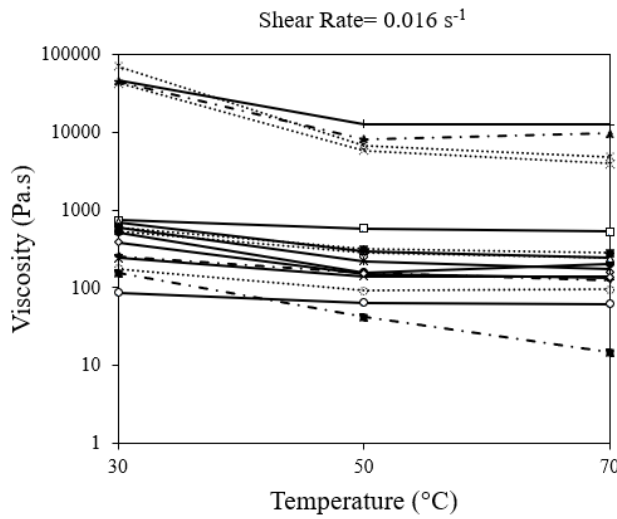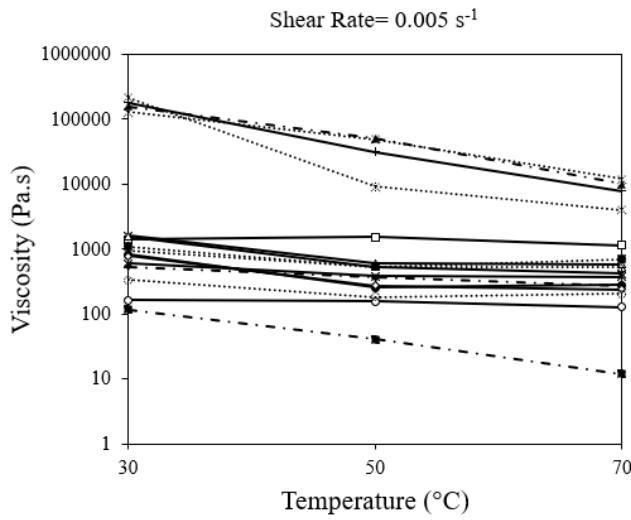
- ■ - M:1C2:0.36P
- ♦ - M:1C3:0.36P
- ▲ - M:1C5:0.36P
- ● B:1C2:1C3:0.44P
- × B:1C2:3C3:0.88P
- ✳ B:1C2:2C3:0.66P
- ○ B:1C2:2C3:0.66P_coated
- + B:1C5:1C2:0.44P
- □ B:1C5:1C3:0.44P
- ◇ B:1C5:2C3:0.66P
- △ B:1C5:3C3:0.88P
- ○ T:1C5:1C2:4C3:1.32P
- ✳ T:1C5:1C2:1C3:0.66P
- ✳ T:2C5:1C2:2C3:1.10P
- ■ T:2C5:1C2:4C3:1.54P
- △ T:1C5:1C2:2C3:0.88P
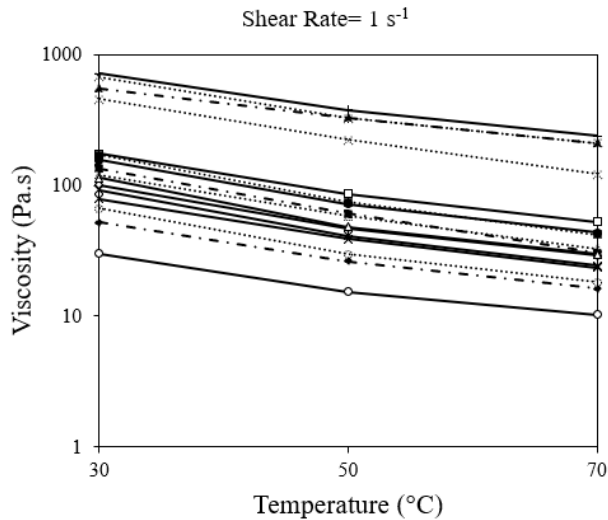
Shear Rate= 1 s⁻¹

(d)

Figure 4.10. Temperature dependent plot of viscosity at changing shear rates of (a) 0.005 s⁻¹, (b) 0.016 s⁻¹, (c) 0.5 s⁻¹, and (d) 1 s⁻¹

The non-Arrhenius temperature dependence of viscosity of the HMX suspension samples accounting for the decreasing difficulty of flow as the temperature increases is in accordance with the Vogel-Fulcher-Tammann-Hess (VFTH) viscosity model shown in Equation 2.25. The constants, A, B, and C, of this equation are found by curve fitting and presented in Table 4.1 for each HMX suspension system at constant shear rates of 0.005, 0.016, 0.5, and 1 s⁻¹. The coefficient of determination (R^2) for each system found as 1 or very close to 1 indicates an excellent fit of the viscosity of the HMX suspension samples to this temperature dependent model. Notably, the values of the constants A, B, and C are found to be strongly dependent on the shear rate for each HMX suspension system except for the monomodal M:1C2:0.36P sample that has attained the same A, B, and C values at all shear rates.

Table 4.1. Vogel-Fulcher-Tammann-Hess (VFTH) constants for HMX Polymeric Suspension System at various shear rates

HMX Polymeric Suspension Systems	Shear Rate (s⁻¹)	A (Pa.s)	B (K)	C (K)	R^2
M:1C5:0.36P	0.005	3	1250	-217	1.0000
	0.016	67	49	-7	1.0000
	0.5	0	992	-135	1.0000
	1	1	415	-71	1.0000
M:1C2:0.36P	0.005	2385	-1291	-596	1.0000
	0.016	2385	-1291	-596	1.0000

HMX Polymeric Suspension Systems	Shear Rate (s^{-1})	A (Pa.s)	B (K)	C (K)	R^2
	0.5	2385	-1291	-596	1.0000
	1	2385	-1291	-596	1.0000
M:1C3:0.36P	0.005	0	1944	-153	0.9953
	0.016	0	1858	-129	1.0000
	0.5	0	1344	-123	1.0000
	1	0	2844	-228	1.0000
B:1C2:1C3:0.44P	0.005	0	3155	-139	0.9286
	0.016	1042	0	30	0.8585
	0.5	112	73	1	1.0000
	1	0	2130	-247	1.0000
B:1C2:2C3:0.66P	0.005	370	1	29	1.0000
	0.016	142	0	31	1.0000
	0.5	1	479	-76	1.0000
	1	1	385	-65	1.0000
B:1C2:2C3:0.66P$_{coated}$	0.005	276	22	17	1.0000
	0.016	124	18	18	1.0000
	0.5	2	290	-46	1.0000
	1	2	316	-50	1.0000
B:1C2:3C3:0.88P	0.005	304	-3	33	1.0000
	0.016	243	-5	37	1.0000
	0.5	14	104	-11	1.0000
	1	4	294	-48	1.0000
B:1C5:1C2:0.44P	0.005	1	2905	-542	0.6665
	0.016	59	2	24	1.0000
	0.5	2	180	-38	1.0000
	1	2	152	-28	1.0000
B:1C5:1C3:0.44P	0.005	0	2589	-133	1.0000
	0.016	12184	1	29	1.0000
	0.5	521	3	28	1.0000
	1	10	491	-85	1.0000
B:1C5:2C3:0.66P	0.005	0	7680	-845	0.0225
	0.016	409	18	1	1.0000
	0.5	9	213	-36	1.0000
	1	3	353	-60	1.0000
B:1C5:3C3:0.88P	0.005	199	8	24	1.0000
	0.016	114	8	24	1.0000
	0.5	8	124	-15	1.0000
	1	3	233	-39	1.0000
T:1C5:1C2:4C3:1.32P	0.005	569	1	29	1.0000
	0.016	176	17	18	1.0000
	0.5	10	112	-16	1.0000

HMX Polymeric Suspension Systems	Shear Rate (s^{-1})	A (Pa.s)	B (K)	C (K)	R^2
	1	6	147	-19	1.0000
T:1C5:1C2:1C3:0.66P	0.005	225	-3	37	1.0000
	0.016	98	-1	32	1.0000
	0.5	3	199	-28	1.0000
	1	2	212	-33	1.0000
T:2C5:1C2:2C3:1.10P	0.005	0	2971	-147	0.9060
	0.016	2267	28	20	1.0000
	0.5	34	155	-15	1.0000
	1	0	1429	-159	1.0000
T:2C5:1C2:4C3:1.54P	0.005	961	77	16	1.0000
	0.016	3149	21	23	1.0000
	0.5	188	27	18	1.0000
	1	39	167	-29	1.0000
T:1C5:1C2:2C3:0.88P	0.005	797	-4	41	1.0000
	0.016	249	6	23	1.0000
	0.5	10	145	-19	1.0000
	1	2	386	-57	1.0000

Coating

Prewashing of HMX Class 2 and Class 3 particles with the plasticizer IDP liquid before application of the polymer solution has reduced the viscosity of the final product by increasing the wetting capability of the particles. The coated bimodal sample, B:1C2:2C3:0.66P$_{coated}$, proved to have smaller viscosity than its uncoated version and attained the lowest initial viscosity of 24 Pa.s. at 1 rpm shear rate and 50 °C as shown in Figure 4.11.
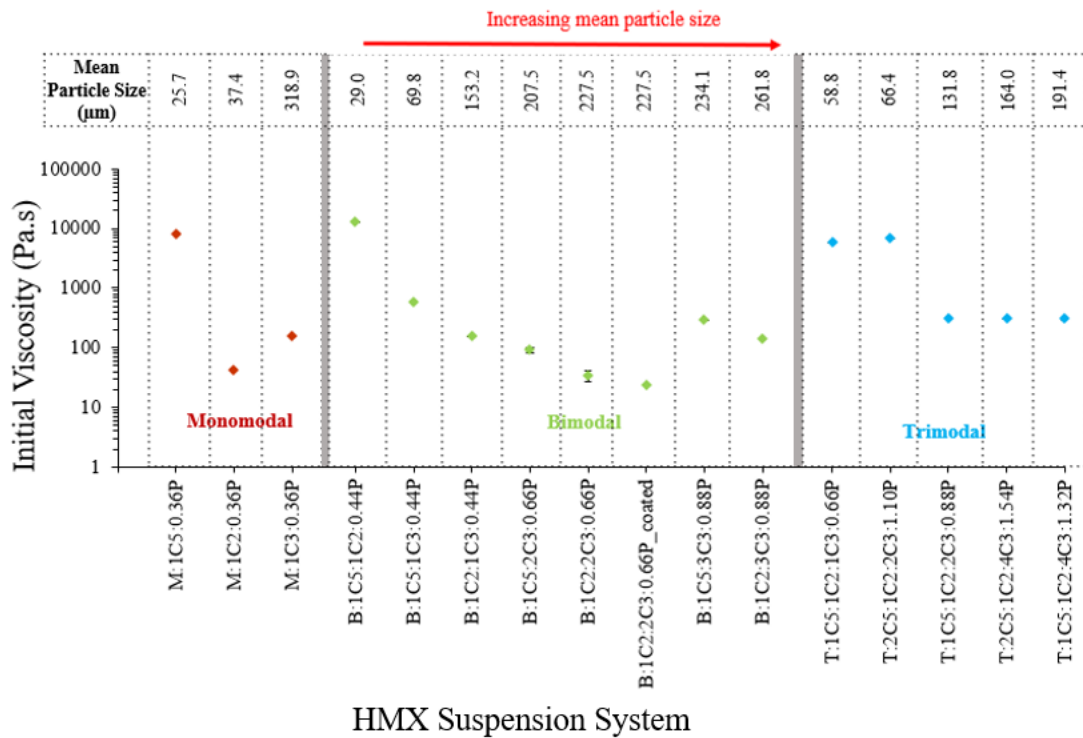
Figure 4.11. The initial viscosity for mono-, bi-, and tri-modal HMX suspension systems at 50 °C and 0.016 s^{-1} shear rate based on increasing mean particle sizes

Micromeritic parameters

The effect of modality and amounts of contents of the HMX suspension systems on the initial viscosity at fixed conditions of 50 °C and 0.016 s^{-1} shear rate are presented in Figure 4.11. The selection of temperature as 50 °C is based on the production temperature employed at the Defense Industries Research and Development Institute (SAGE). The selection of the shear rate is based on the limitation of the Brookfield viscometer, which can only operate at a maximum shear rate of 0.016 s^{-1}.

Mean particles size:

HMX suspension mixtures with larger mean particle size are observed to have lower initial viscosity as presented in Figure 4.11. The mean particle size in each HMX class can be listed in an increasing order of C5 (25.6 μm) < C2 (37.4 μm) < C3 (318.9 μm). The difference in the mean particle size of the larger Class 3 HMX and the smaller Class 2 and Class 5 HMX powders is plainly distinguishable. The smaller Class 2 and Class 5 HMX powders have been shown to behave in a mono mode as explained in Section 4.1.2.

There are some exceptions to the general behavior of decreasing viscosity with mean particle size shown in Figure 4.11. Amongst the monomodal systems, the M:1C5:0.36P and the M:1C2:0.36P systems with similar small mean particle size are expected to have similar viscosities. However, the M:1C2:0.36P system in Class 2 is observed to attain a much smaller viscosity than both the M:1C5:0.36P system and the M:1C3:0.36P system that has larger Class 3 particles. This odd behavior may be related to the clustering of small Class 2 particles creating larger particles than that of Class 3, thus reducing the viscosity further.

The bimodal HMX suspension systems that show unexpected behavior are B:1C5:3C3:0.88P and B:1C2:3C3:0.88P. These systems include a mixture of the fine particles of Class 5 or Class 2 with the coarse particles of Class 3. Notably, the bimodal B:1C5:3C3:0.88P and the B:1C2:3C3:0.88P systems, characterized by the largest mean particle size within the examined range, that have a fine to coarse ratio of 1/3 exhibited a surprisingly higher viscosity compared to their counterparts B:1C5:1C3:0.88P and B:1C2:1C3:0.88P that have a fine to coarse ratio of 1/1 and the other counterpart systems of B:1C5:2C3:0.88P and B:1C2:2C3:0.88P that have a fine to coarse ratio of 1/2. These results indicate that there exists an optimum mixing ratio of fine and large particles to achieve a minimum viscosity, which was reached at a ratio of ½ in this study. A similar result was reported by Joshi et al. [40] where a bimodal mixing ratio of 50% fine and 50% coarse HMX particles resulted in the highest bulk density and lowest viscosity.

Figure 4.12 depicts the variation of initial viscosity in bimodal and trimodal systems, subjected to a shear rate of 0.016 s^{-1} at 50 °C, plotted against the mean particle diameter. Monomodal systems are not included in this figure as they have different ratios of solid and liquid contents. As observed in previous studies [36,79,83], the initial viscosity of the suspensions generally exhibit a decline as the particle size increase. This trend aligns with the established law, suggesting its applicability to multi-modal systems. The observed behavior closely resembles the phenomena documented by Chong et al. [71] in their study of bimodal systems, strengthening the validity of the law in more complex scenarios.
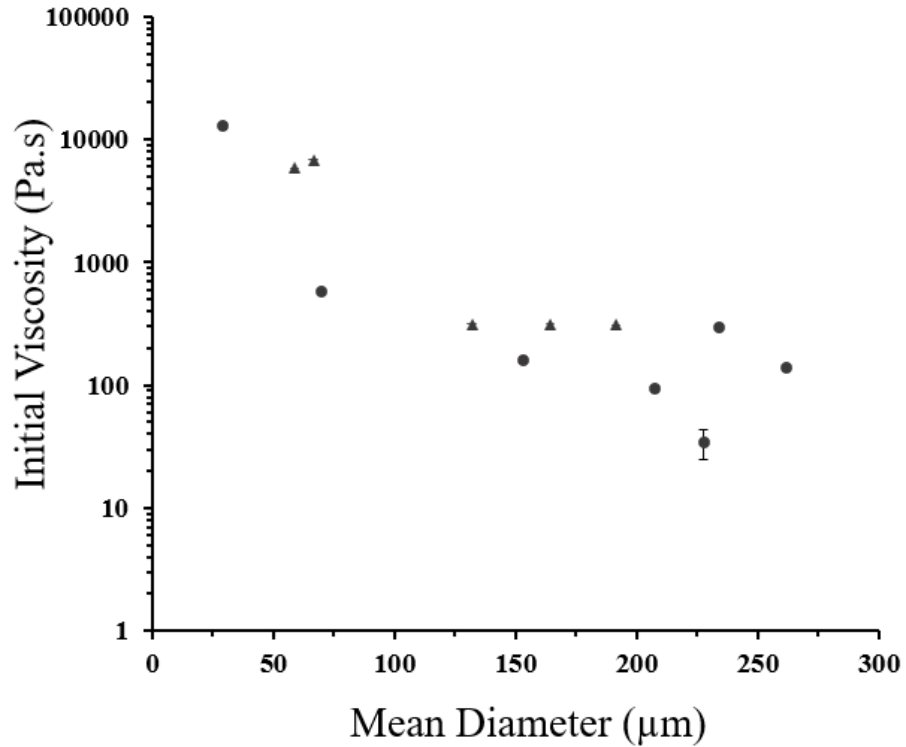
Figure 4.12. Initial (end-of-mixing) viscosity of bimodal (●, circle) and trimodal
(▲, triangle) HMX suspensions with different mean diameters at 50°C and 0.016 s^{-1}

Sphericity:

Figure 4.13 displays the initial viscosity of bimodal and trimodal HMX suspension
systems at 50 °C and shear rate of 0.016 s^{-1} as a function of particle sphericity.
Monomodal data is excluded due to different amounts of solid loading and potential
mixing inconsistencies. As observed, the initial viscosity of the suspension exhibits a
decreasing trend with increasing sphericity of the HMX particles, which is consistent with
established literature [78,89–92].
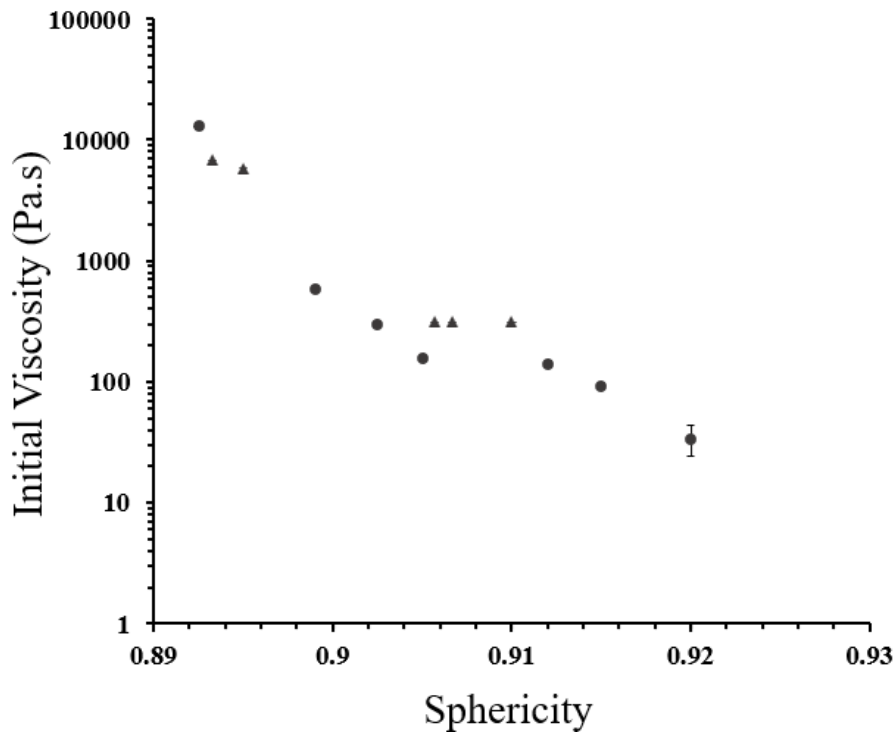
Figure 4.13. Initial (end-of-mixing) viscosities of bimodal (•, circle) and trimodal
(▲, triangle) HMX suspensions with different sphericities at 50 °C and 0.016 s^{-1}

Tapped density and bulk density:

Figure 4.14 (a) and (b) show the decreasing trend of initial viscosity with bulk density and tapped density, respectively. HMX systems that have large random particle packing, indicating a high ratio of bulk density to tapped density, have resulted with HMX suspension systems that have small initial viscosity. Initial viscosity generally decreases with increased packing as discussed in the literature [40][97][99]. The observed deviations in the rheological data presented in Figure 4.14 might be ascribed to the limited measurement scheme employed. While a single measurement was performed on most samples, the three samples exhibiting minimal viscosities were analyzed in quadruplicate. The standard deviation for these three samples is 1-5 %, thus demonstrating the repeatability of the measurements achieved in this study.
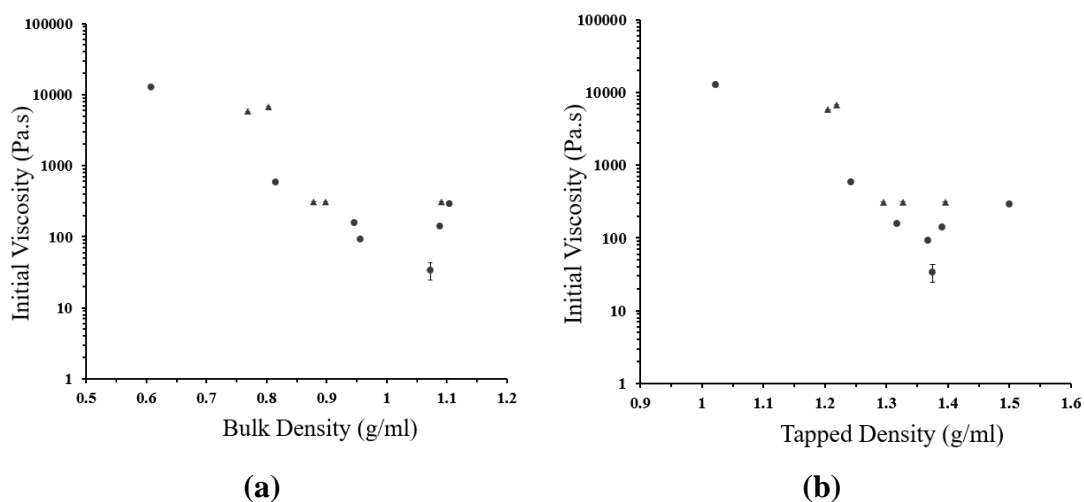
Figure 4.14. Initial (end-of-mixing) viscosity of bimodal (●, circle) and trimodal (▲, triangle) HMX suspension systems at 50 °C and 0.016 s^{-1} based on a) bulk density and b) tapped density

General comments on micromeritic properties:

HMX flowability properties, such as mean particle diameter, sphericity, and tapped and bulk densities are found to be influential factors affecting the initial viscosity in multimodal PBX systems formulated with HMX classes 5, 2, and 3 as supported by Figure 4.12, Figure 4.13, and Figure 4.14, respectively. Systems formulated as B:1C2:2C3:0.66P, B:1C5:2C3:0.66P, and T:1C5:1C2:4C3:1.32P display the lowest initial viscosities compared to the other investigated systems. These systems exhibit both increased sphericity and larger mean particle size and demonstrate superior powder flowability as evidenced by CI and HR measurements.

All initial viscosity data are presented in APPENDIX C.

4.3. Properties of Product: PBX

Modified PBXN-110 systems were investigated for their rheological, mechanical, and physical properties, such as initial viscosity, hardness, tensile strength, and true density. The monomodal and multimodal systems used in this study include different mass percent of HMX due to initial viscosity restrictions based on standards for PBX systems as explained in Section 3.3.2. The monomodal systems include a maximum HMX loading of 75.8%, whereas the multi modal systems include a maximum HMX loading of 82% to

attain an initial viscosity below 1000 Pa.s. The results presented below should be considered based on this information.

4.3.1. Viscosity of IPDI Added Samples Determined via Viscometer

The addition of curing agent IPDI to the PBX suspensions indicates the beginning of the curing process. Change in viscosity with time for the IPDI added monomodal, bimodal, and trimodal modified PBX suspensions measured via a Brookfield viscometer is presented in Figure 4.15. The current data cannot definitively identify rheopectic or thixotropic behavior. The addition of the curing agent inherently alters viscosity, reflecting the initial curing stages rather than the intrinsic rheological properties of the uncured suspension.

Several formulations failed to be cast, preventing the collection of viscosity data (Figure 4.15). M:1C2:0.36Pi exhibited constant viscosity, suggesting Newtonian behavior. Conversely, M:1C3:0.36Pi showed a rapid viscosity increase, possibly due to a fast-curing reaction. Formulations with small HMX particles, M:1C2:0.36Pi and M:1C5:0.36Pi, displayed potential dispersion issues likely due to agglomeration. Inconsistencies in measurement times suggest sample agglomeration, with solids settling and polymers rising.

An analysis of viscosity for bimodal PBX suspensions containing small HMX Class 2 or Class 5 particles with coarse Class 3 particles showed that the viscosity ranking from low-to-high for the HMX Class 2 systems was observed as B:1C2:2C3:0.66Pi, B:1C2:3C3:0.88Pi, and B:1C2:1C3:0.44Pi with C2/C3 mass ratios of 1/2, 1/3, and 1/1, respectively. This trend shows that increasing the amount of coarse HMX Class 3 particles decreases the viscosity and doubling it resulted in the lowest viscosity. Similarly, for the HMX Class 5 systems, the viscosity ranking from low to high was B:1C5:2C3:0.66Pi, B:1C5:3C3:0.88Pi, and B:1C5:1C3:0.44Pi with C5:C3 mass ratios of 1/2, 1/3, and 1/1, again demonstrating a decrease in viscosity with an increase in the coarse HMX Class 3 particle fraction. In both cases, systems with a higher fraction of coarse particles, HMX Class 3, exhibited lower viscosity.

Viscosity measurement of B:1C5:1C2:0.44Pi was hindered by the excessively high viscosity of the 1/1 (wt/wt) HMX Class 5/Class 2 system due to their similar fine particle size distribution (Figure 4.4).

A bimodal HMX particle system composed of HMX Class 5 and HMX Class 3 exhibited a 100 Pa.s reduction in suspension viscosity compared to a system using HMX Class 2 and HMX Class 3. This suggests that the HMX Class 5 to Class 3 combination promotes the lowest viscosity. Enhanced packing efficiency due to the finer Class 5 particles and their superior sphericity are hypothesized as contributing factors.

Trimodal T:1C5:1C2:1C3:0.66Pi and T:2C5:1C2:2C3:1.10Pi PBX samples had a viscosity that was too high to be measured because the amount of fine HMX contained in these systems is higher than the amount of coarse HMX particles. These systems can be treated as bimodal systems consisting only of fine and coarse HMX particles.

Among trimodal PBX suspensions, the T:1C5:1C2:4C3:1.32Pi system with C5/C2/C3 ratio as 1/1/4 , initially exhibited the lowest viscosity, likely due to its bimodal behavior due to a 1/2 fine-to-coarse ratio. This result confirms the optimum 1/2 fine-to-coarse ratio and the trend that higher fine particle (HMX Class 5 and Class 2) content leads to increased viscosity in PBX suspensions.
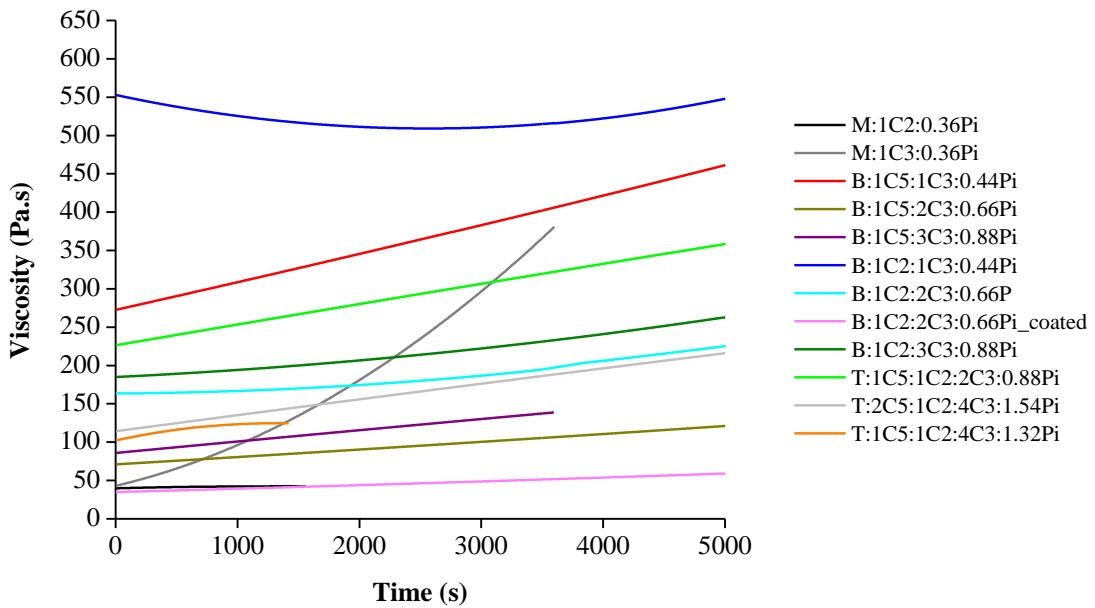
Figure 4.15. Change in viscosity with time measured via Brookfield viscometer for monomodal, bimodal, trimodal PBX systems following the addition of IPDI at 50°C. Curves are smoothed based on the Savitzky-Golay method

Brookfield viscometer results presented in Figure 4.11 show that B:1C5:2C3:0.66Pi, B:1C5:3C3:0.88Pi, T:1C5:1C2:4C3:1.32Pi, and B:1C2:2C3:0.66Pi have the lowest viscosities, which disagree with the rheometer measurements shown in Figure 4.15. High

measurement fluctuations up to 150 Pa.s inherent to the Brookfield instrument reduced its sensitivity. Consequently, rheometer data with greater precision was used for statistical analysis in this study.

Figure 4.15 indicates that the IDP-coated system exhibits the lowest viscosity. This means that a significant reduction in initial viscosity may be achieved by adding polymer coating on HMX particles during PBX production.

Figure 4.16 depicts the pot life, defined as the time to reach 1000 Pa.s viscosity, of various formulations measured with the Brookfield viscometer. Detailed calculations of pot life is given in Appendix D. PBX formulations that exceed the instrument's viscosity limit, such as M:1C5:0.36Pi, B:1C5:1C2:0.44Pi, T:1C5:1C2:1C3:0.66Pi, and T:2C5:1C2:2C3:1.10Pi, were deemed uncastable, resulting in zero pot life. Notably, pre-coating HMX Class 2 and Class 3 with IDP plasticizer (B:1C2:2C3:0.66Picoated) significantly extended pot life of uncoated HMX systems from 15 hours to 52 hours, a nearly 350% increase. This suggests the effectiveness of pre-coating in enhancing pot life. Overall, bimodal and trimodal systems generally had lower initial viscosity and consequently, shorter pot life.
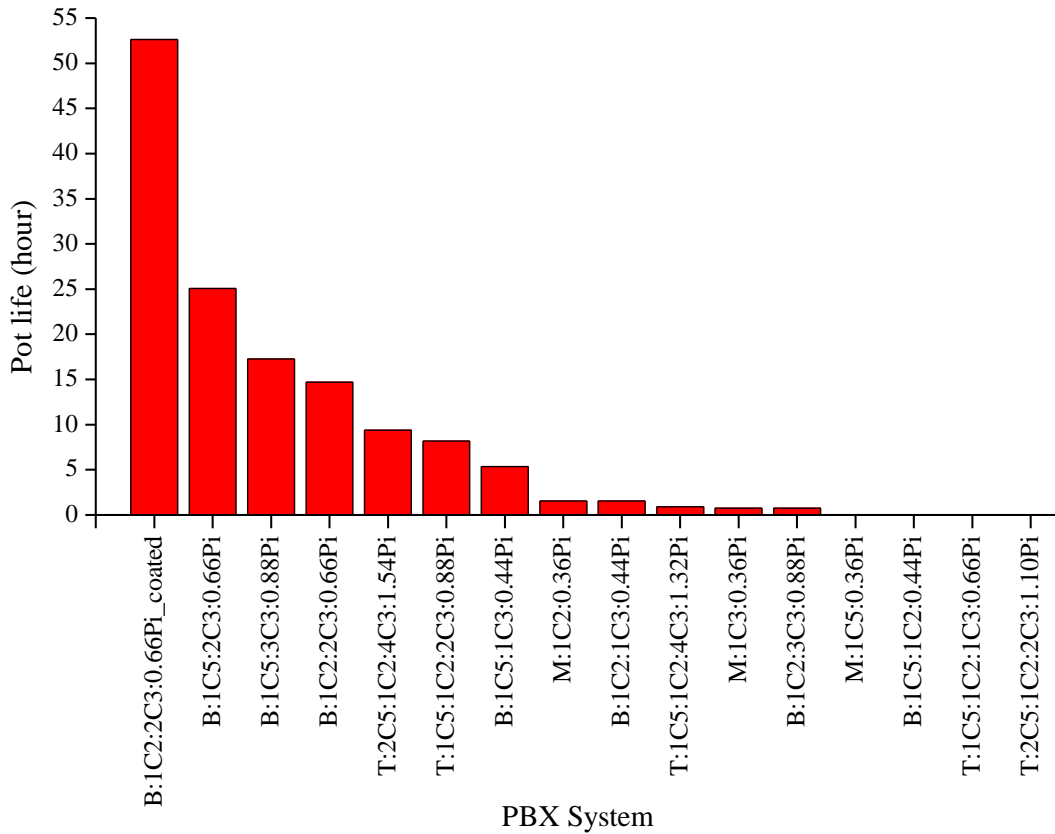
Figure 4.16. Pot life of IPDI added PBX suspensions based on Brookfield
viscometer measurements at 50 °C for monomodal, bimodal, and trimodal systems
listed in Table 3.7

4.3.2. Hardness

Figure 4.17 displays the curing times of modified PBXN-110 suspensions measured by
Shore A hardness according to MIL-DTL-82901A [14]. The data is presented in
APPENDIX E. Due to their high initial viscosities, data for M:1C5:0.36Pi and
B:1C5:1C2:0.44Pi are unavailable. Curing times for most systems are comparable, as
expected. However, M:1C2:0.36Pi exhibits a significantly longer cure time. As discussed
in Chapter 4.1.1, this is likely due to low packing density, hindering the formation of a
homogeneous structure. The material may reach the desired hardness only after a
substantial delay due to particle settling. Similarly, B:1C5:1C3:0.44Pi's low packing,
potentially caused by unseen agglomeration, may also delay curing, and disrupt system
homogeneity. While the packing density of T:1C5:1C2:1C3:0.66Pi is also low, further
investigation is needed to determine if a similar agglomeration mechanism is affecting its
curing behavior.
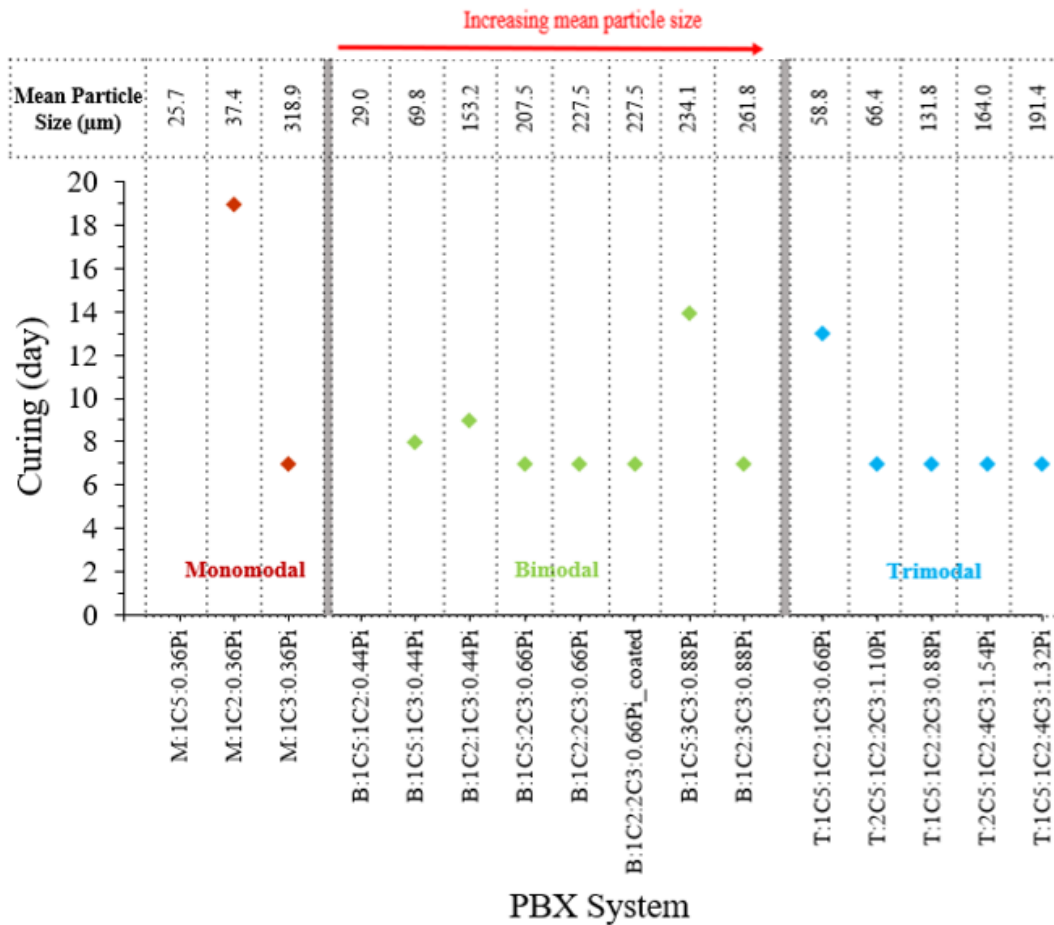
Figure 4.17. Curing time for monomodal, bimodal, and trimodal PBX systems listed in Table 3.7

4.3.3. Tensile Strength

The results of uniaxial tensile test are presented in APPENDIX G**.** All measured tensile strains exceeded the minimum 9% requirement of the standard [14]. The uniaxial tensile strain and stress are presented in Figure 4.18 and Figure 4.19, respectively. Pre-coating HMX with IDP plasticizer (B:1C2:2C3:0.66Pi$_{coated}$) increased tensile strain by approximately 20% compared to the non-coated counterpart (B:1C2:2C3:0.66Pi). Data is unavailable for M:1C5:0.36Pi and B:1C5:1C2:0.44Pi due to their high initial viscosities. Fluctuations observed in this figure likely stem from the small-scale production. Notably, pre-coating HMX with IDP plasticizer (B:1C2:2C3:0.66Pi$_{coated}$) increased tensile strain by approximately 20% compared to the non-coated counterpart (B:1C2:2C3:0.66Pi).

Data is unavailable for M:1C5:0.36Pi and B:1C5:1C2:0.44Pi due to their high initial viscosities.
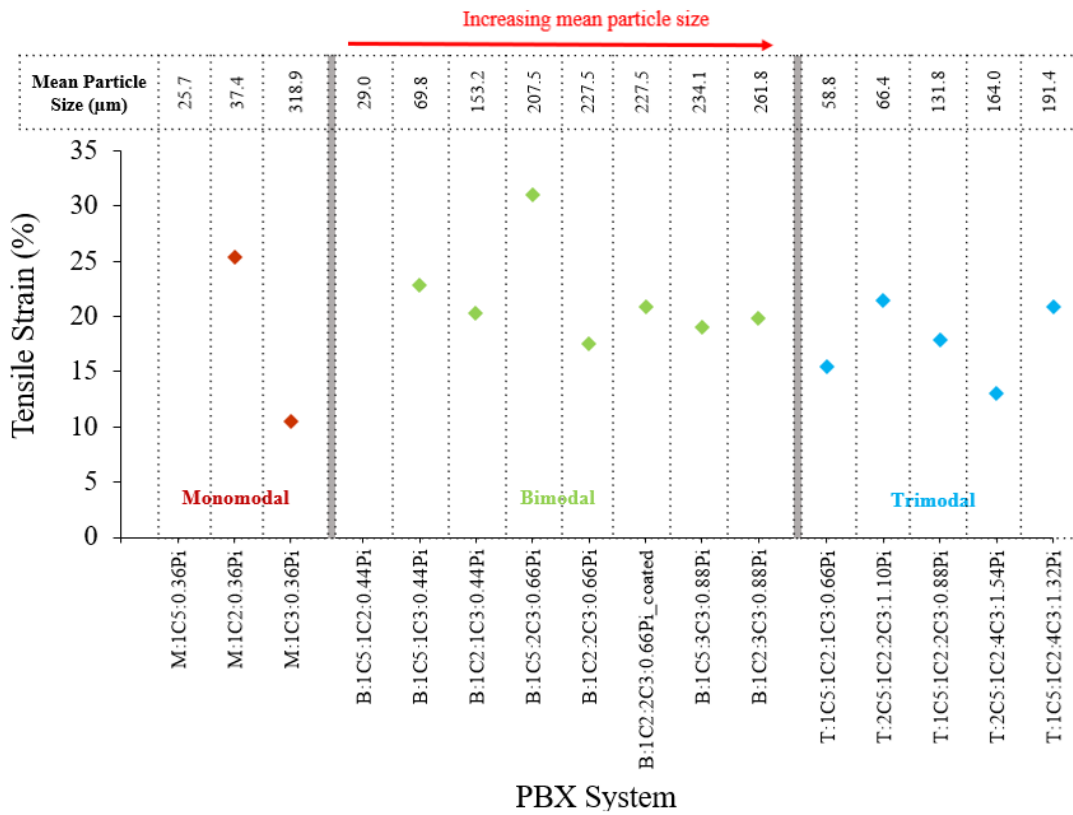
Figure 4.18. Uniaxial tensile following one-day of curing for monomodal, bimodal, and trimodal PBX systems listed in Table 3.7

All tensile stress values in Figure 4.19 are greater than 0.14 MPa, which is the requirement in the military standard [14], shows that the mechanical properties can be improved with large-scale production to be carried out in the future.
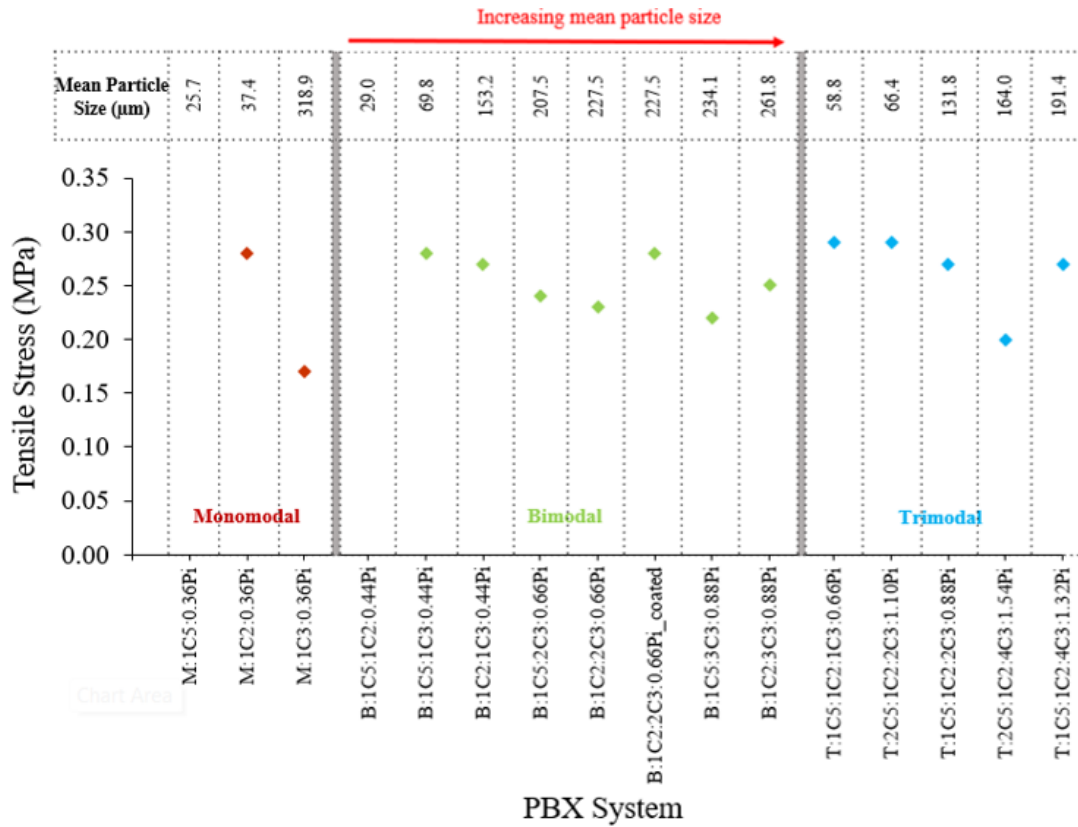
Figure 4.19. Uniaxial tensile stress following one-day of curing for monomodal, bimodal, and trimodal PBX systems listed in Table 3.7

4.3.4. True Density

Raw data used in the calculation of true density was shown in APPENDIX F. Figure 4.20 shows the true density of modified PBX suspensions around 1.60 g/ml. This is smaller than the 1.62 g/cm³ requirement for PBXN-110 [14] with a solid content of 86-89%.

The bimodal and trimodal systems used in this study have a solid loading of 82% and the monomodal systems have a solid content of 75.8%, both less than the PBXN-110 requirement causing a small reduction in true density. The true densities for the bimodal and trimodal systems are found to be similar. True density data for the two systems, M:1C5:0.36Pi and B:1C5:1C2:0.44Pi, is unavailable due to the high initial viscosity of these systems.
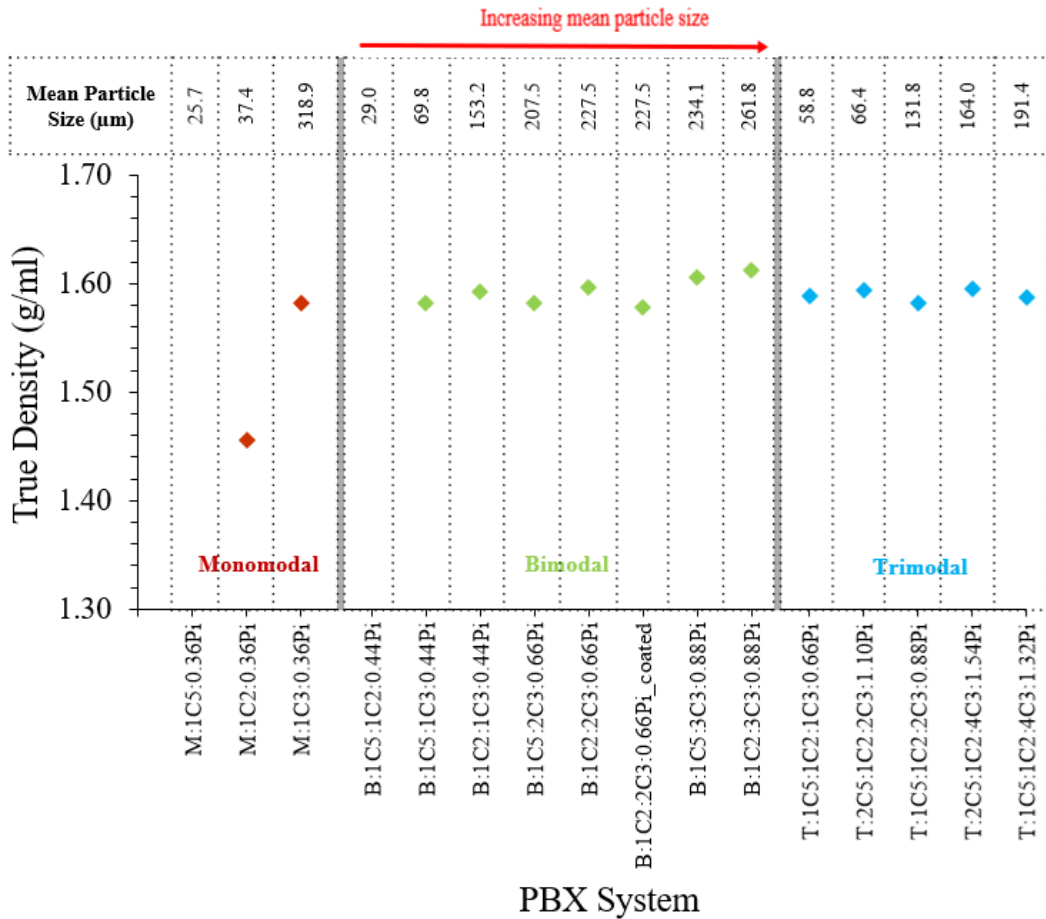
Figure 4.20. Post-curing true density of monomodal, bimodal, and trimodal PBX systems listed in Table 3.7

4.4.   Viscosity Models

This chapter presents the results of three approaches we used to estimate the viscosity value as a function of single or multiple parameters. These three approaches are listed as follows:

1.   Viscosity models as a function of solid loading,
2.   Viscosity models as a function of shear stress and shear rate,
3.   Complex statistical methods based on multiple data.

4.4.1. Comparison of Viscosity Models as a Function of Solid Loading

Figure 4.21 shows the relative viscosity were calculated based on Equation 2.1 of the HMX suspension at 0.016 s^{-1} at 50°C for increasing HMX loadings from 82% to 86% in a bimodal system with a Class 2:Class 3 mass ratio of 1:2 (black dots). As observed, the

relative initial viscosity exhibits an exponential increase with increasing HMX content. This aligns with established literature findings [40,71,78,79] demonstrating that higher solid particle loading in suspensions leads to a rise in viscosity.

Figure 4.21 presents the various mathematical models in the literature for relative viscosity in such suspensions are tabulated in the figure, along with their R^2 values. Experimental relative viscosity data for increasing solid loading (black dots) alongside a newly developed exponential model fit (dark blue line) was shown in the equation below:

$$\eta_r = 3.06 \times 10^{-12} \times exp\left(\frac{2.5 \times \varphi}{1-40.01 \times \varphi}\right) \tag{4.1}$$

The Mooney model [65] with an R^2 value of 0.9448 (red line) emerged as the best fit among existing literature models and shown the equation below:

$$\eta_r = exp\left(\frac{2.5 \times \varphi}{1-0.8471 \times \varphi}\right) \tag{4.2}$$

Interestingly, the fitting constant (k) in the Mooney equation, which reflects the geometrical particle characteristics, yielded a value of approximately 0.85. This value deviates significantly from the expected range of 1.35-1.91 for spherical particles. This discrepancy, along with the SEM micrographs in Figure 4.6 and Figure 4.7, suggests that the actual sphericity of the HMX particles used in this study might be lower than previously determined. Furthermore, the obtained experimental k value (0.85) can be interpreted as a crowding factor in the suspension.
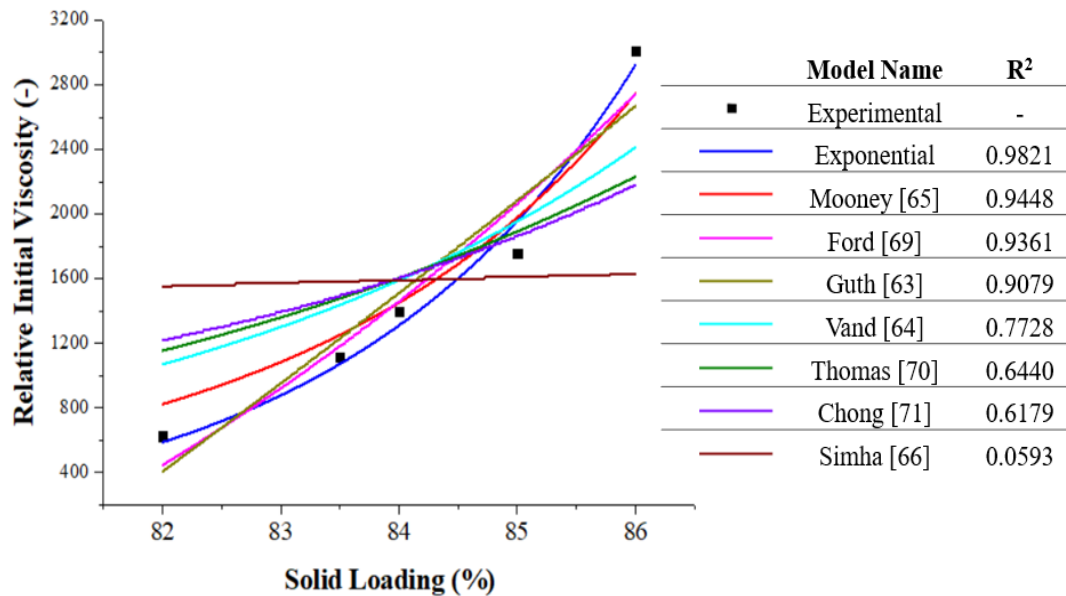
Figure 4.21. Comparison of the relative initial (end-of-mixing) viscosities predicted with mathematical models in the literature and the experimental data for PBX suspensions with different HMX loading (%) at 50 °C and 0.016 s^{-1}

4.4.2. Comparison of Viscosity Models as a Function of Shear Rate

We employed the Oswald model (PLM) to fit the shear stress vs. shear rate curves for the lowest viscosity B:1C2:2C3:0.66P, B:1C5:2C3:0.66P, and T:1C5:1C2:4C3:1.32P HMX suspensions at 30 °C, 50 °C, and 70 °C in Figure 4.22. The model's fit was satisfactory, with R² values exceeding 0.98 in

Table *2.2*. Pseudoplasticity index (n) that were in between 0.62 and 0.89 confirmed shear-thinning behavior, aligning with literature on composite propellants (0.6-1.0) [37,38]. Notably, n values increased with temperature for each system, but inconsistencies were observed at 70 °C (lower R²). The consistency coefficient (K) decreased with temperature for all systems, reflecting the viscosity-dependence of n and K in the Oswald equation. We know that the K value and the n value are proportional to the viscosity [79,123]. While B:1C5:2C3:0.66P had a higher K than the other two, its lower n value resulted in the expected viscosity sequence.
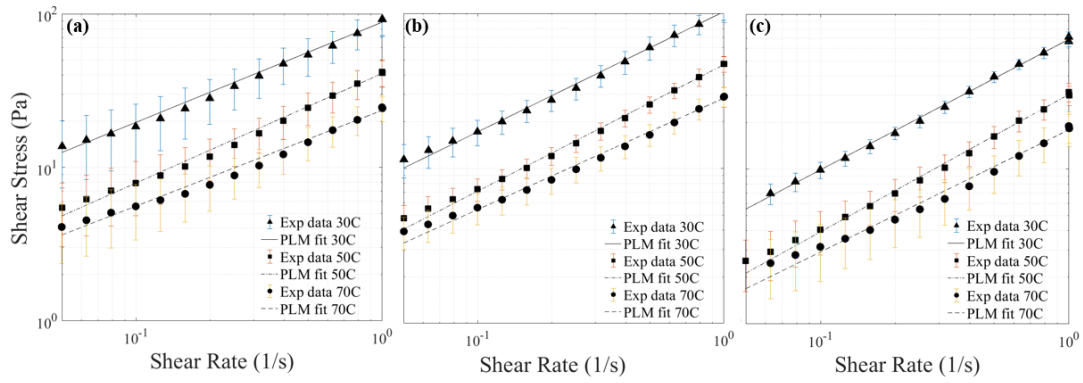
Figure 4.22. Comparison of the shear stresses predicted with the Oswald model (power law model, PLM) and the experimental data for HMX suspension systems with changing shear rates of systems (a) B:1C2:2C3:0.66P, (b) B:1C5:2C3:0.66P, (c) T:1C5:1C2:4C3:1.32P

Table 4.2. Fitting results of the 3 models with the lowest viscosity according to the Oswald model (Power Law Model, PLM)

Product Name	Temperature (°C)								
	30			50			70		
	n	K (Pa.s^n)	R^2	n	K (Pa.s^n)	R^2	n	K (Pa.s^n)	R^2
B:1C2:2C3:0.66P	0.65	88	0.9870	0.71	41	0.9922	0.62	24	0.9841
B:1C5:2C3:0.66P	0.78	100	0.9967	0.82	47	0.9978	0.72	28	0.9952
T:1C5:1C2:4C3:1.32P	0.84	69	0.9982	0.89	30	0.9964	0.79	18	0.9848

4.4.3. Statistical Estimation of Viscosity Based on Multiple Data

Firstly, exploratory data analysis (Figure 7.1 from APPENDIX H) confirmed the normality of independent variable distributions. Figure 4.23 shows the diverging heatmap of viscosity results from rheometer at 30°C, 50°C, 70°C and from Brookfield at 50°C. The raw data of this heatmap is tabulated in

Table *7.11* from APPENDIX H. The viscosity results from the rheometer measurements have a high correlation, indicating that any one of the temperatures (30°C, 50°C or 70°C) may be used to represent the others. Conversely, poor correlation between rheometer and Brookfield measurements excludes Brookfield data from further statistical analysis. Based on the heatmap, rheometer data at 50 °C is chosen for subsequent analysis.
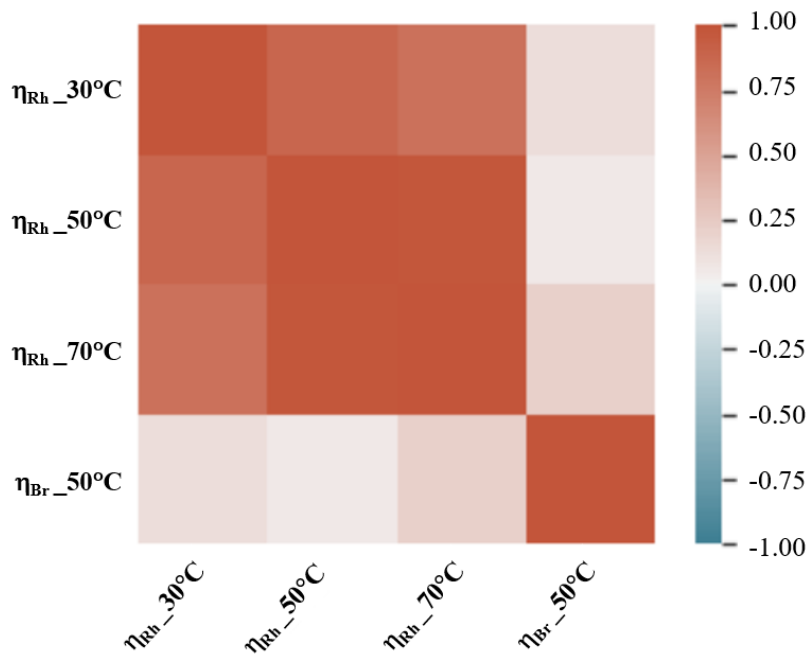
Figure 4.23. Diverging heatmap of viscosity (Pa.s) from rheometer analysis at 30°C, 50°C, 70°C and Brookfield viscometer at 50°C

The diverging heatmap in Figure 4.24 depicts correlations among rheometer result at 50 °C, mean diameter, sphericity, tapped density, and bulk density. Notably, tapped and bulk density exhibit a near-perfect correlation as 96%, suggesting they are highly dependent. Consequently, tapped density is excluded from further analysis, and only bulk density is retained as an independent variable. The raw data of this heatmap is tabulated in

Table *7.12* from APPENDIX H.
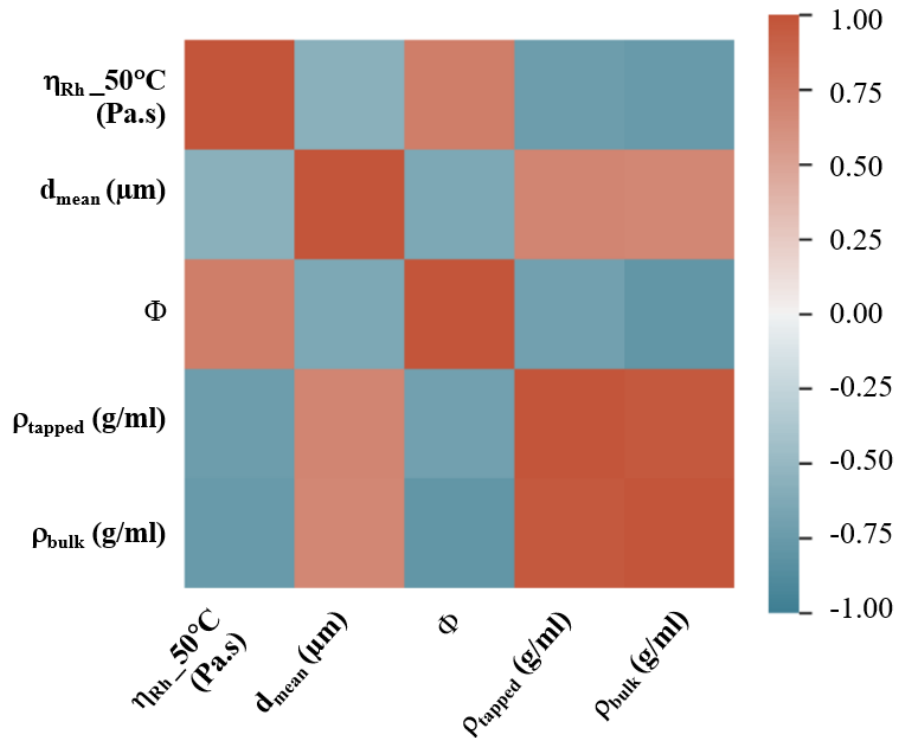
Figure 4.24. Diverging heatmap of viscosity from rheometer measurement at 50°C η_{Rh}_50°C, mean diameter d_{mean}, sphericity Φ, tapped density ρ_{tapped} , and bulk density ρ_{bulk}

Mean diameter, bulk density and sphericity values were analyzed with the viscosity results measured by rheometer at 50°C for regression.

Multiple linear regression was applied to the sphericity, mean diameter and bulk density data, and the results are in Table 4.3 below. Variables: sphericity Φ, mean diameter d_{mean} and bulk density ρ_{bulk}; are not able to explain the variation in the rheometer measurements. This is because the p-value is greater than 0.05.

Table 4.3. Multiple linear regression results

	coefficient	std err	t	P>|t|
x1 (Φ)	1.1954	1.417	0.843	0.421
x2 (d_{mean})	1.6509	1.625	1.016	0.336
x3 (ρ_{bulk})	-1.5714	1.412	-1.113	0.294

The multiple linear regression model exhibited low accuracy due to limited data (15 data set). Consequently, a random forest regression was employed. Table 4.4 shows the random forest model yielded a higher accuracy compared to the multiple linear regression model, approximately 8% improvement. This improved accuracy justifies using the random forest model to analyze the correlations between initial viscosity from rheometer results at 50 °C and the independent variables.

Table 4.4. Comparison of linear regression and random forest model

Model Name	Model Accuracy (%)
Multiple Linear Regression	71.6967
Random Forest	77.2540

Figure 4.25 shows the importance of independent micromeritic parameters on initial viscosity results taken by the rheometer at 50 °C and 0.016 s^{-1} from random forest regression. Random forest regression identified sphericity as the most influential parameter for initial viscosity. According to the correlations with the initial viscosity at 50°C obtained from the rheometer, the effects of micromeritic properties are as follows, from high to low: sphericity (58%), bulk density (31%), and mean diameter (11%). The results of monomodal systems were also included in the analysis since a minimum of 15 data were needed to apply statistical analysis. There may be a deviation in the results because the solid loading in the monomodal system is lower than in the bimodal and trimodal systems Table 3.7.
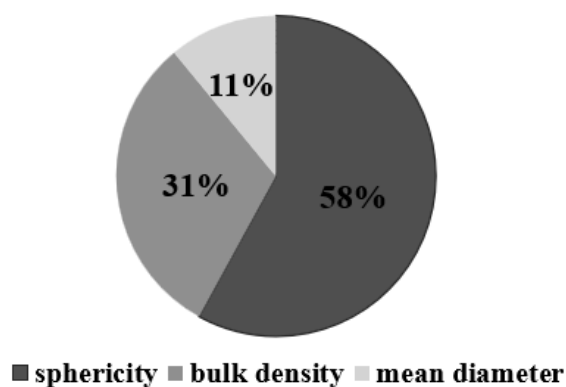
Figure 4.25. Effect values (importance) of variables on the initial viscosity (from Rheometer result at 50 °C and 0.016 s^{-1}) according to random forest model

The statistical analysis presented in Figure 4.24 reveals a strong positive correlation (nearly 96%) between tapped density and bulk density. As shown in Figure 4.25, bulk density emerged as the second most significant factor influencing the initial viscosity of the PBX mixture, accounting for 31% of the observed variation. Therefore, it is anticipated that systems with the lowest initial viscosities (B:1C2:2C3:0.66P, B:1C5:2C3:0.66P, and T:1C5:1C2:4C3:1.32P) will also exhibit the highest values for both bulk density and tapped density.

The combined results demonstrate a negative correlation between initial viscosity and sphericity, signifying that increased sphericity leads to decreased viscosity, confirming the established literature referenced in [78,89–92]. This observation aligns with the dominant influence of sphericity on initial viscosity i.e., 58%, as highlighted by the statistical analysis in Figure 4.25.

The statistical results further reveal a moderate correlation between the initial viscosity and the mean diameter i.e., 11%. This suggests a lesser, but still observable, influence of mean diameter compared to sphericity.

In this study, initial viscosity of PBX mixture was fitted the chosen curve in 2 different ways: 1. The effect of HMX loading in the PBX suspension at 50 °C on the relative viscosity, 2. The effect of shear rate applied in the range of $0.005 - 1$ s^{-1} on shear stress. Initial viscosity for systems B:1C2:2C3:0.66P, B:1C5:2C3:0.66P and T:1C5:1C2:4C3:1.32P that gave the minimum initial viscosity value obtained at 30 °C, 50 °C and 70 °C.

5.   CONCLUSIONS

In the defense industry, optimizing resource allocation is essential for castable polymer-bonded explosives (PBX) like PBXN-109 and -110 as their rheology, heavily influenced by component properties, and initial post-mixing viscosity directly impact casting quality. In this study, the effect of micromeritic parameters of HMX energetic particles on the initial viscosity of a modified PBX-110 formulation was investigated. Initial viscosity, following the mixing of the particles and the liquid polymer right before casting, needs to be minimized to improve casting and, thus, the quality of the final product. The rheological behavior of fifteen different HMX-polymer suspensions was studied at different solid loadings, temperatures, and shear rates prior to the addition of the curing agent towards production of PBX. It was found that the following conditions favor a reduction in the initial viscosity of the HMX suspensions:

-       High sphericity, as spherical particles demonstrate lower resistance to flow,

-       Low Hausner ratio and low compressibility index, indicating less particle interaction and interlock during flow,

-       High packing factor, not allowing for air entrapment,

-       Multi-modality, allowing for a broader and polydisperse particle size distribution since larger and more diverse particle sizes can promote better packing efficiency and reduce particle interactions.

The initial viscosity exhibited a direct relationship with the proportion of fine particles within the HMX suspension. Among bimodal systems, the combination of HMX Class 2 and Class 3 particles in a 1:2 mass ratio resulted in the lowest viscosity. This phenomenon is potentially attributable to the enhanced packing achieved when the finer Class 2 particles fill the interstitial spaces between the larger Class 3 particles efficiently. The HMX Class 2-Class 3 combination exhibited lower viscosity compared to the HMX Class 5-Class 3 combination, likely due to the superior packing density achieved in the former.

Pre-coating the HMX energetic particles with the curing agent isodecyl pelargonate (IDP) improved the processability and mechanical properties of HMX-based explosives. Pot life of the IDP coated bimodal HMX Class 2-Class 3 formulation was enhanced up to 350% and its tensile strain increased by 20%.

The thesis presents various viscosity models employed to predict the initial viscosity as a function of single or multiple parameters. These models can be categorized into: 1. Solid loading-dependent models, 2. Temperature-dependent but non-Arrhenius-type models, 3. Viscosity models depend on shear stress and shear rate, and 4. Complex statistical methods based on multiple parameters.

Solid loading-dependent models were applied on bimodal HMX Class 2-Class 3 systems, which resulted with 115% increase in relative initial viscosity. The exponential Mooney model was found to give the best fits within the applied HMX loading range of 82%-86%.

The Oswald model, which is a power law model relating the initial viscosity to shear stress and shear rate, was shown to predict the pseudoplastic shear thinning behavior of the modified PBXN-110 suspensions effectively. The pseudo-plasticity index n of HMX suspensions were found to be between 0.61 and 0.89 consistent with the literature.

The temperature dependent non-Arrhenius Vogel-Fulcher-Tammann-Hesse (VFTH) model was found to represent the relation between viscosity and temperature effectively for all suspension systems studied. As expected, the model predicts a decrease in viscosity with increasing temperature, consistent with experimental rheometer data.

Random forest stochastic analysis revealed that among the investigated micromeritic parameters, sphericity exhibited the strongest correlation at 58% with the initial viscosity measured via rheometer at 50 °C, followed by bulk or tapped density at 31%, and mean diameter at 11%. This result is specifically valuable in showing the significance of multiple variables on initial viscosity.

In conclusion, this thesis study underscores the crucial role of the multi-micromeritic properties of HMX particles in determining the initial viscosity of HMX suspensions. By optimizing these micromeritic properties, researchers and manufacturers can achieve efficient casting processes and enhance the final quality of PBX products.

6. REFERENCES

[1]   Q.L. Yan, S. Zeman, A. Elbeih, Recent advances in thermal analysis and stability evaluation of insensitive plastic bonded explosives (PBXs), Thermochim. Acta 537 (**2012**) 1–12.

[2]   M.A. Daniel 1980-, Polyurethane binder systems for polymer bonded explosives, (**2006**).

[3]   T. Chai, Y.C. Liu, H. Ma, Y.W. Yu, Rheokinetic analysis on the curing process of HTPB-DOA- MDI binder system, in: IOP Conf. Ser. Mater. Sci. Eng., **2016**.

[4]   J.P. Agrawal, High Energy Materials: Propellants, Explosives and Pyrotechnics, Jai Prakash Agrawal, **2010**.

[5]   Y. Bu, C. Chen, F. Jiang, X. Wang, D. Che, H. Nan, Experimental and Numerical Analysis of Single Screw Extrusion Process for Thermoplastic PBX Based on PVT Properties, Propellants, Explos. Pyrotech. (**2022**) 1–15.

[6]   Q. Xia, Y. Wu, F. Huang, Effect of interface behaviour on damage and instability of PBX under combined tensioneshear loading, Def. Technol. (**2022**) 1–15.

[7]   R.S. Norris, H.M. Kristensen, J. Handler, The B61 family of bombs, Bull. At. Sci. 59 (**2003**) 74–76.

[8]   X. Zhu, X. Zhang, W. Li, W. Yao, Strain Rate and Temperature Effects of the JOXL-1 Explosive, Propellants, Explos. Pyrotech. (**2022**) 1–10.

[9]   A. Barua, Y. Horie, M. Zhou, Energy localization in HMX-Estane polymer-bonded explosives during impact loading, J. Appl. Phys. 111 (**2012**) 1–11.

[10]   A. Barua, S. Kim, Y. Horie, M. Zhou, Ignition criterion for heterogeneous energetic materials based on hotspot size-temperature threshold, J. Appl. Phys. 113 (**2013**) 1–22.

[11]   Detail Specification RDX (Cyclotrimethylenetrinitramine) MIL-DTL-398D, Mod. Large Cult. Dimens. Glob. 00 (**1962**) 3–41.

[12]   MIL-DTL-45444C Detail Specification HMX, United States Department of

Defense, **1996**.

[13] MIL-E-82886 Explosive, Plastic-Bonded, Cast PBXN-109, United States Department of Defense, **1993**.

[14] MIL-DTL-82901A (OS) Explosive, Plastic-Bonded, Cast PBXN-110, United States Department of Defense, **2002**.

[15] U. Teipel, Energetic Materials: Particle Processing and Characterization, Wiley-VCH, **2005**.

[16] B.L. Hamshere, I.J. Lochert, R.M. Dexter, Evaluation of PBXN-109: the explosive fill for the penguin anti-ship missile warhead, Dsto-Tr-1471 (**2003**) 45.

[17] B. Le Roux, M. Golfier, M. Rat, S. Lecume, Development of a cast plastic bonded explosive with high CL20 content, in: Insensitive Munitions Energ. Mater. Technol., **2006**: pp. 1–10.

[18] R. Muthiah, V.N. Krishnamurthy, B.R. Gupta, Rheology of HTPB propellant: Development of generalized correlation and evaluation of pot life, Propellants, Explos. Pyrotech. 21 (**1996**) 186–192.

[19] M.T. Cucksee, H.C. Allen, Extension of pot life of HTPB composite propellants by phosphine oxides, US3974004A, **1976**.

[20] B. Florczak, R. Bogusz, W. Skupiński, M. Chmielarek, A. Dzik, Study of the effect of nitrated hydroxyl-terminated Polybutadiene (NHTPB) on the properties of heterogeneous rocket propellants, Cent. Eur. J. Energ. Mater. 12 (**2015**) 841–854.

[21] C. Erişken, A. Göcmez, Ü. Yilmazer, F. Pekel, S. Özkar, Modeling and rheology of HTPB based composite solid propellants, Polym. Compos. 19 (**1998**) 463–472.

[22] Y. Liang, J. Zhang, X. Jiang, HMX content in PBX booster measured by visible spectro-photometric method, Chinese J. Energ. Mater. 16 (**2008**) 531–534.

[23] L. Chen, New explosive charge of warhead, Chinese J. Explos. Propellants 25 (**2002**) 26–27.

[24] B.M. Bandgar, V.N. Krishnamurthy, T. Mukundan, K.C. Sharma, Mathematical

modeling of rheological properties of hydroxyl-terminated polybutadiene binder and dioctyl adipate plasticizer, J. Appl. Polym. Sci. 85 (**2002**) 1002–1007.

[25] L. Nucci, D. Narvaez, T. Krettenauer, ACS Symposium Series, Appl. Polym. Sci. (**2014**) 1–542.

[26] A. Seifolazadeh, M. Edrissi, Determination of the rheological properties of hydroxyl terminated polybutadiene (HTPB) mixtures with energetic materials and presenting empricial models, Int. J. Eng. Trans. B Appl. 18 (**2005**) 413–420.

[27] H. Abou-Rachid, L.S. Lussier, S. Ringuette, X. Lafleur-Lambert, M. Jaidann, J. Brisson, On the correlation between miscibility and solubility properties of energetic plasticizers/polymer blends: Modeling and simulation studies, Propellants, Explos. Pyrotech. 33 (**2008**) 301–310.

[28] M. Kohga, Y. Hagihara, Efects of addition of surfactants on viscosity of uncured ammonium perchlorate/hydroxyl-terminated polybutadiene propellant, Kayak. Gakkaishi 59 (**1998**) 167–173.

[29] J.S. Gharia, R.K. Sinha, V. V. Tadas, V. Prakash, V.K. Phadke, Studies on physico-mechanical and explosive characteristics of RDX/HMX-based castable plastic-bonded explosives, Def. Sci. J. 48 (**1998**) 125–130.

[30] C. Montealegre, V. Verardo, M.L. Marina, M.F. Caboni, Analysis of glycerophospho- and sphingolipids by CE, Electrophoresis 35 (**2014**) 779–792.

[31] S. Lee, J.H. Choi, I.K. Hong, J.W. Lee, Curing behavior of polyurethane as a binder for polymer-bonded explosives, J. Ind. Eng. Chem. 21 (**2015**) 980–985.

[32] L.D. Villar, T. Cicaglioni, M.F. Diniz, M.F.K. Takahashi, L.C. Rezende, Thermal aging of HTPB/IPDI-based polyurethane as a function of NCO/OH ratio, Mater. Res. 14 (**2011**) 372–375.

[33] K.H. Sweeny, R.D. Geckler, The rheology of suspensions, J. Appl. Phys. 25 (**1954**) 1135–1144.

[34] F. Guidotti, K.P.D. Käser, S. Junod, R. Gagnaux, Rheology of Cast-Cured Insensitive Plastic-Bonded Explosives - Part Ii an Approach of Viscoelastic

Behaviour Using Reaction Kinetics, 35th Int. Annu. Conf. Fraunhofer Inst. Chem. Technol. (**2004**).

[35] F. Irgens, Rheology and Fluids, (**2014**).

[36] F. Sta, C. Boulnois, C. Lemaitre, P. Marchal, Rheological Behaviour of Energetic Concentrated Suspensions Lynked to Their Components Physico-Chemical Properties, Propellants, Explos. Pyrotech. 47 (**2022**) 1–14.

[37] A. Restasari, R.S. Budi, K. Hartaya, Pseudoplasticity of Propellant Slurry with Varied Aluminium Content for Castability Development To, J. Phys. Conf. Ser. 1005 (**2018**).

[38] G. Dombe, M. Jain, P. Singh, K. Radhakrishnan, B. Bhattacharya, Pressure casting of composite propellant, Indian J. Chem. Technol. (**2008**).

[39] M. Szycher, Szycher's handbook of polyurethanes, **2013**.

[40] V.S. Joshi, S. Vadali, R.D. Wasnik, S.K. Jangid, M. Maurya, Studies on rheological properties and process parameters of TNT based castable high explosive compositions, Sci. Technol. Energ. Mater. 78 (**2017**) 87–92.

[41] D. Zhu, L. Zhou, X. Zhang, Rheological Behavior of DNAN/HMX Melt-Cast Explosives, Propellants, Explos. Pyrotech. 44 (**2019**) 1583–1589.

[42] R. Junid, J.P. Siregar, N.A. Endot, J.A. Razak, A.N. Wilkinson, Optimization of glass transition temperature and pot life of epoxy blends using response surface methodology (Rsm), Polymers (Basel). 13 (**2021**).

[43] M.R. Kamal, A. Mutel, Rheological Properties Of Suspensions In Newtonian And Non-Newtonian Fluids, J. Polym. Eng. 5 (**1985**) 293–382.

[44] T.G. Mezger, The Rheology Handbook, **2014**.

[45] J. Izdebska, S. Thomas, Z. Żołek-Tryznowska, Printing on Polymers. Chapter 6 Rheology of printing inks, Print. Polym. (**2016**) 87–99. http://www.sciencedirect.com/science/article/pii/B9780323374682000063.

[46] J. V. Koleske, Paint and Coating Testing Manual: 15th. Edition of the Gardner-

Sward Handbook, **2012**.

[47]   S. Mueller, E.W. Llewellin, H.M. Mader, The rheology of suspensions of solid particles, Proc. R. Soc. A 466 (**2010**) 1201–1228.

[48]   R. Sarangapani, V. Ramavat, S.Reddy, P. Subramanian, A.K. Sikder, Rheology studies ofNTO–TNT based melt-cast dispersions and influence of particle–dispersant interactions, Powder Technol. 273 (**2015**) 118–124.

[49]   B. Xia, P.S. Krueger, Rheology of particulate suspensions with non-Newtonian fluids incapillaries, Proc. R. Soc. A 478 (**2022**) 20.

[50]   A. Malkin, A. Iyasev, Rheology: Concepts, Methods and Applications, ChemTec Publishing, Toronto, **2017**.

[51]   L. Naeun, K. Youngdae, S. Jaehan, H. Sangkeun, S. Jeongseob, L. Keundeuk, L. Sangmook, L. Jaewook, Rheological properties comparison between polymer bonded explosives (PBX) and its simulant, AIP Conf. Proc. 1713 (**2016**) 1–6.

[52]   O. von Wolkenstein, Über die Geschwindigkeitsfunktion der Viskosität disperser Systeme, (**1925**).

[53]   E.C. Bingham, An investigation of the laws of plastic flow, Bull. U.S. Bur. Stand. (**1916**).

[54]   N. Casson, A flow equation for pigment-oil suspensions of the printing ink type, Pergamon Press (**1959**).

[55]   W.H. Herschel, R. Bulkley, Measurement of consistency as applied to rubber benzene solutions, Proc. ASTM 82 (**1925**).

[56]   A.W. Sisko, The flow of lubricating greases, Ind. Eng. Chem. (**1958**).

[57]   M.M. Cross, Rheology of non-Newtonian fluids: A new flow equation for pseudoplastic systems, J. Colloid Interface Sci. (**1965**).

[58]   S.B. Ellis, Thesis, Lafayette College, (**1927**).

[59]   P.J. Carreau, Rheological equations from molecular network theories,

Transactions Soc. Rheol., 1972, Trans. Soc. Rheol. (**1972**).

[60] K. Yasuda, R.C. Armstrong, R.E. Cohen, Shear flow properties of concentrated solutions of linear and star branched polystyrenes, Rheol. Acta 20 (**1981**) 163–178.

[61] D.-M. Liu, Particle packing and rheological property of highly-concentrated ceramic suspensions: φm determination and viscosity prediction, J. Mater. Sci. 35 (**2000**) 5503–5507.

[62] A. Einstein, Eine neue Bestimmung der Moleküldimensionen, Ann. Phys. 324 (**1906**) 289–306.

[63] E. Guth, R. Simha, Untersuchungen über die Viskosität von Suspensionen und Lösungen. 3. Über die Viskosität von Kugelsuspensionen, Kolloid-Zeitschrift 74 (**1936**) 266–275.

[64] V. Vand, Viscosity of Solutions and Suspensions. I. Theory, J. Phys. Chem. A 1 (**1948**) 277–299.

[65] M. Mooney, The Viscosity of a Concentrated Suspension of Spherical Particles, Phys. Rev. 80 (**1950**) 580–594.

[66] R. Simha, A Treatment of the Viscosity of Concentrated Suspensions, J. Appl. Phys. 23 (**1952**) 1020–1024.

[67] H.C. Brinkman, The viscosity of concentrated suspensions and solutions, J. Chem. Phys. 20 (**1952**) 571.

[68] I.M. Krieger, T.J. Dougherty, A Mechanism for NonNewtonian Flow in Suspensions of Rigid Spheres, J. Rheol. (N. Y. N. Y). 3 (**1959**) 137–152.

[69] T.F. Ford, Viscosity-Concentration and Fluidity-Concentration Relationships for Suspensions of Spherical Particles in Newtonian Liquids, J. Phys. Chem 64 (**1960**) 1168–1174.

[70] D.G. Thomas, Transport characteristics of suspension: VIII. A note on the viscosity of Newtonian suspensions of uniform spherical particles, J. Colloid Sci. 20 (**1965**) 267–277.

[71] J.S. Chong, E.B. Christiansen, A.D. Baer, Rheology of Concentrated Suspensions, J. Appl. Polym. Sci. 15 (**1971**) 2007–2021.

[72] P.K. Senapati, B.K. Mishra, A. Parida, Modeling of viscosity for power plant ash slurry at higher concentrations: Effect of solids volume fraction, particle size and hydrodynamic interactions, Powder Technol. 197 (**2010**) 1–8.

[73] D. Chauhan, L. Khan, S.K. Mandal, A. Jauhari, S.C. Bhattacharyya, Studies on the processing of HTPB-based fast-burning propellant with trimodal oxidiser distribution and its rheological behaviour, Asia-Pac J Chem Eng (**2022**).

[74] R. Muthiah, R. Manjari, V.. N. Krishnamurth, Rheology of HTPB Propellant: Effect of Mixing Speed and Mixing Time, Def. Sci. J. 43 (**1993**) 167–172.

[75] D.H. Vogel, Das Temperaturabhaengigkeitsgesetz der Viskositaet von Fluessigkeiten, Phys. Zeitschrift 22 (**1921**) 645.

[76] G.S. Fulcher, Analysis of recent measurements of the viscosity of glasses, J. Am. Ceram. Soc. 8 (**1925**) 339.

[77] G. Tammann, W. Hesse, Die Abhängigkeit der Viscosität von der Temperatur bie unterkühlten Flüssigkeiten, Zeitschrift Für Anorg. Und Allg. Chemie 156 (**1926**) 245.

[78] Z. An, Y. Zhang, Q. Li, H. Wang, Z. Guo, J. Zhu, Effect of particle shape on the apparent viscosity of liquid– solid suspensions, Powder Technol. 328 (**2018**) 199–206.

[79] Y. Liu, Q. Zhang, R. Liu, Effect of particle size distribution and shear rate on relative viscosity of concentrated suspensions, Rheol. Acta (**2021**).

[80] J.M. DallaValle, Micromeritics: the technology of fine particles, **1948**.

[81] R. Sarangapani, V. Ramavat, R. T.S., R.S. Patil, G.M. Gore, A.K. Sikder, Effect of particle size and shape of NTO on micromeritic characteristics and its explosive formulations, Powder Technol. 253 (**2014**) 276–283.

[82] E.C. Abdullah, D. Geldart, The use of bulk density measurements as flowability

indicators, Powder Technol. 102 (**1999**) 151–165.

[83] C.C. Furnas, Grading Aggregates, Ind. Eng. Chem. 23 (**1931**) 1052–1058.

[84] R.A. Layton, W.R. Murray, J.L. Garbini, The control of power for efficient batch mixing, Propellants, Explos. Pyrotech. 22 (**1997**) 269–278.

[85] B. Singh, D.R. Kaushik, Spheroidization of RDX and Its Effect on the Pourability of RDX/TNT Slurries, 39 (**1989**) 95–98.

[86] D.P. Haughey, G.S.G. Beveridge, Structural properties of packed beds — A review, Can. J. Chem. Eng. 47 (**1969**) 130–140.

[87] M. Marine, K. Ramohalli, Processing Experiments on Model Composite Propellants, in: AIAA 90-2313 26th Jt. Propuls. Conf., Arizona Tucson, **1990**.

[88] S.J. Blott, K. Pye, Particle size distribution analysis ofsand-sized particles by laser diffraction: an experimental investigation of instrument sensitivity and the effects of particle shape, 53 (**2006**) 671–685.

[89] H.D. Keith, F.J. Padden, A Phenomenological Theory of Spherulitic Crystallization, J. Appl. Phys. 34 (**1963**) 2409–2421.

[90] P.W. Cleary, The effect of particle shape on simple shear flows, Powder Technol. 179 (**2008**) 144–163.

[91] K.J. Kim, Spherulitic crystallization of 3-nitro-1,2,4-triazol-5-one in water N-methyl-2-pyrrolidone, J. Cryst. Growth 208 (**2000**) 569–578.

[92] R.J. Hudson, M. Moniruzzaman, P.P. Gill, Investigation of Crystal Morphology and Shock Sensitivity of Cyclotrimethylenetrinitramine Suspension by Rheology, Propellants, Explos. Pyrotech. 40 (**2015**) 233–237.

[93] Y. Bayat, M. Eghdamtalab, V. Zeynali, Control of the Particle Size of Submicron HMX Explosive by Spraying in Non-Solvent, J. Energ. Mater. 28 (**2010**) 273–284.

[94] R.L. Brown, J.C. Richards, Principles of Powder Mechanics, **1970**.

[95] R. 0. Grey, J.K. Beddow, On the Hausner Ratio and its Relationship to Some

Properties of Metal Powders, Powder Technol. 2 (**1969**) 323–326.

[96]   R.P. Zou, A.B. Yu, Evaluation of the packing characteristics of mono-sized non-spherical particles, Powder Technol. 88 (**1996**) 71–79.

[97]   R.L. Carr, Evaluating the flow properties of solids, Chem. Eng. J. 72 (**1965**) 163–168.

[98]   M.M. Gupta, B. Srivastava, S. Monika, A. Vinita, Spherical crystallization: a tool of particle engineering for making drug powder suitable for direct compression, Int. J. Pharm. Res. Dev. 1 (**2010**) 5.1-5.10.

[99]   R. Muthiah, V.N. Krishnamurthy, B.R. Gupta, Rheology of HTPB Propellant. 1. Effect of Solid Loading, Oxidizer Particle Size, and Aluminum Content, J. Appl. Polym. Sci. 44 (**1992**) 2043–2052.

[100] J.J. Stickel, R.L. Powell, Fluid mechanics and rheology of dense suspensions, Annu. Rev. Fluid Mech. 37 (**2005**) 129–149.

[101] G.R. Miller, A.N. Garroway, A Review of the Crystal Structures of Common ExplosivesPart 1: RDX, HMX, TNT, PETN, and Tetryl, Security (**2001**) 33.

[102] National Center for Biotechnology Information, PubChem Compound Summary for CID 66957, 8-Methylnonyl nonanoate, (n.d.). https://pubchem.ncbi.nlm.nih.gov/compound/8-Methylnonyl-nonanoate.

[103] ASTM-D974-12 Standard Test Method for Acid and Base Number by Color-Indicator Titration, (n.d.).

[104] ASTM-E203-08 Standard Test Method for Water Using Volumetric Karl Ficher Titration, (n.d.).

[105] ASTM-D-1217-12 Standard Test Method for Density and Relative Density (Spesific Gravity) of Liquids by Bingham Pycnometer, (n.d.).

[106] ASTM-D-2983-15 Standard Test Method for Low-Temperature Viscosity of Lubricanta Measured by Brookfield, (n.d.).

[107] MIL-P-82809 Military Specification, Polymer, Liquid, Hydroxyl-Terminated

Polybutadiene with Antioxidant, United States Department of Defense, **1989**.

[108] ASTM-D-4274-11 Standard Test Methods for Testing Polyurethane Raw Materials: Determination of Hydroxly Numbers of Polyols, (**2021**).

[109] MIL-H-85497 Military Specification, Hydroxyl-Terminated Polybutadiene, United States Department of Defense, **1981**.

[110] National Center for Biotechnology Information, PubChem Compound Summary for CID 16682738, Dibutyltin dilaurate., (**2023**). https://pubchem.ncbi.nlm.nih.gov/compound/Dibutyltin-dilaurate.

[111] DOD-D-82727 Military Specification Dibutyltin Dilaurate, (**1983**).

[112] National Center for Biotechnology Information, PubChem Compound Summary for CID 5287971, Lecithin., (**2023**). https://pubchem.ncbi.nlm.nih.gov/compound/Lecithin.

[113] MIL-L-3061B Military Spesification, Lecithin, United States Department of Defense, **2003**.

[114] National Center for Biotechnology Information, PubChem Compound Summary for CID 169132, Isophorone diisocyanate., (**2023**). https://pubchem.ncbi.nlm.nih.gov/compound/Isophorone-diisocyanate.

[115] MIL-C-85498 Military Specification, Curing Agents, United States Department of Defense, **1981**.

[116] MIL-C-82813 Military Specification, Curing Agent, Isophrone Diisocyanate, United States Department of Defense, **1989**.

[117] MIL-STD-650 Sampling, Inspection and Testing to all Holders, **1973**.

[118] Brookfield Laboratory Viscometer Accessories, (n.d.). https://www.brookfieldengineering.com/-/media/ametekbrookfield/product-cut-sheets/lab-cut-sheets/lab-accessories-cut-sheets/helipath-stand.pdf?dmc=1&la=en&hash=2C8115BC8AE4AE452211BF4298E03B3A.

[119] STANAG 4506 ED-11 (Tensile Test), (n.d.).

[120] AOP, Ordnance Publication North Atlantic Treaty Organization Manual Of Data Requirements And Tests For The Qualification Of Explosive Materials, Pfp Unclassif. Publ. Allied Ordnance 7 (**2003**).

[121] T. Hastie, R. Tibshirani, G. James, D. Witten, An Introduction to Statistical Learning, **2006**.

[122] M.H. Kutner, C.J. Nachtsheim, J. Neter, W. Li, Applied Linear Statistical Models, **2005**.

[123] M.A. K., G. Monika, P.D. D., Empirical Modeling of Chemoviscosity of Hydroxy Terminated Polybutadiene Based Solid Composite Propellant Slurry, Malaysian Polym. J. (**2010**) 1–16.

7.   APPENDICES

A.   Average Bulk and Tapped density, Hausner Ratio, Compressibility Indices and Random Packing Results of HMX Systems

Table 7.1. Average bulk density results of all HMX systems

Modality	Product Name	Average Bulk Density (g/mL)
Monomodal	M:1C5	0.5435 ± 0.0008
	M:1C2	0.7437 ± 0.0011
	M:1C3	0.9124 ± 0.0005
Bimodal	B:1C2:1C3	0.9456 ± 0.0031
	B:1C2:2C3	1.0723 ± 0.0003
	B:1C2:3C3	1.0884 ± 0.0005
	B:1C5:1C2	0.6078 ± 0.0030
	B:1C5:1C3	0.8143 ± 0.0012
	B:1C5:2C3	0.9556 ± 0.0016
	B:1C5:3C3	1.1033 ± 0.0024
Trimodal	T:1C5:1C2:4C3	1.0905 ± 0.0002
	T:1C5:1C2:1C3	0.7684 ± 0.0036
	T:2C5:1C2:2C3	0.8027 ± 0.0025
	T:2C5:1C2:4C3	0.8978 ± 0.0013
	T:1C5:1C2:2C3	0.8785 ± 0.0021

Table 7.2. Average tap density (V1250) results of all HMX systems

Modality	Product Name	Average Tapped Density (g/mL)
Monomodal	M:1C5	0.9592 ± 0.0003
	M:1C2	1.0852 ± 0.0006
	M:1C3	1.2548 ± 0.0007
Bimodal	B:1C2:1C3	1.3173 ± 0.0023
	B:1C2:2C3	1.3749 ± 0.0004
	B:1C2:3C3	1.3897 ± 0.0010
	B:1C5:1C2	1.0213 ± 0.0021
	B:1C5:1C3	1.2423 ± 0.0008
	B:1C5:2C3	1.3669 ± 0.0002
	B:1C5:3C3	1.4990 ± 0.0011
Trimodal	T:1C5:1C2:4C3	1.3953 ± 0.0007
	T:1C5:1C2:1C3	1.2052 ± 0.0002
	T:2C5:1C2:2C3	1.2188 ± 0.0007
	T:2C5:1C2:4C3	1.3261 ± 0.0002
	T:1C5:1C2:2C3	1.2945 ± 0.0005

Table 7.3. Hausner ratio, compressibility indices and random packing results of all HMX systems

Modality	Product Name	Hausner Ratio	Comp. Index (%)	Random Packing
	M:1C5	1.7649	43.3393	0.5666
Monomodal	M:1C2	1.4592	31.4692	0.6853
	M:1C3	1.3753	27.2886	0.7271
	B:1C2:1C3	1.3931	28.2161	0.7178
	B:1C2:2C3	1.2822	22.0084	0.7799
	B:1C2:3C3	1.2769	21.6858	0.7831
Bimodal	B:1C5:1C2	1.6803	40.4880	0.5951
	B:1C5:1C3	1.5256	34.4532	0.6555
	B:1C5:2C3	1.4304	30.0871	0.6991
	B:1C5:3C3	1.3587	26.4018	0.7360
	T:1C5:1C2:4C3	1.2795	21.8451	0.7815
	T:1C5:1C2:1C3	1.5686	36.2470	0.6375
Trimodal	T:2C5:1C2:2C3	1.5185	34.1442	0.6586
	T:2C5:1C2:4C3	1.4771	32.2983	0.6770
	T:1C5:1C2:2C3	1.4735	32.1345	0.6787

B. Laser Diffraction Mean Particle Size and Shape Results

Table 7.4. Laser diffraction mean particle size results of all HMX systems

Modality	Product Name	Mean Particle Size (µm)
Monomodal	M:1C5	25.6883 ± 9.88
	M:1C2	37.4131 ± 15.68
	M:1C3	318.8903 ± 227.71
Bimodal	B:1C2:1C3	153.2083 ± 195.56
	B:1C2:2C3	227.4693 ± 215.39
	B:1C2:3C3	261.7759 ± 231.10
	B:1C5:1C2	28.9970 ± 11.43
	B:1C5:1C3	69.8436 ± 132.92
	B:1C5:2C3	207.4964 ± 223.37
	B:1C5:3C3	234.1159 ± 233.88
Trimodal	T:1C5:1C2:4C3	191.3649 ± 228.44
	T:1C5:1C2:1C3	58.7965 ± 100.60
	T:2C5:1C2:2C3	66.3882 ± 115.39
	T:2C5:1C2:4C3	163.9672 ± 210.11
	T:1C5:1C2:2C3	131.7943 ± 214.39

Table 7.5. Sphericity results of all HMX systems

Modality	Product Name	Sphericity
Monomodal	M:1C5	0.9400 ± 0.0002
	M:1C2	0.9000 ± 0.0002
	M:1C3	0.8900 ± 0.0001
Bimodal	B:1C2:1C3	0.9050 ± 0.0001
	B:1C2:2C3	0.9200 ± 0.0002
	B:1C2:3C3	0.9120 ± 0.0002
	B:1C5:1C2	0.8925 ± 0.0001
	B:1C5:1C3	0.8990 ± 0.0001
	B:1C5:2C3	0.9150 ± 0.0002
	B:1C5:3C3	0.9025 ± 0.0001
Trimodal	T:1C5:1C2:4C3	0.9100 ± 0.0001
	T:1C5:1C2:1C3	0.8950 ± 0.0001
	T:2C5:1C2:2C3	0.8933 ± 0.0001
	T:2C5:1C2:4C3	0.9067 ± 0.0001
	T:1C5:1C2:2C3	0.9057 ± 0.0001

C. Viscosity Results from Rheometer

Table 7.6. Initial viscosity results of all products from rheometer at 50 °C, 0.016 s^{-1}

Modality	Product Name	Initial Viscosity (Pa.s.) (Rheometer @50 °C, 0.016 s^{-1})
Monomodal	M:1C5:0.36P	8247
	M:1C2:0.36P	42
	M:1C3:0.36P	159
Bimodal	B:1C2:1C3:0.44P	158
	B:1C2:2C3:0.66P	34
	B:1C2:2C3:0.66P$_{coated}$	24
	B:1C2:3C3:0.88P	140
	B:1C5:1C2:0.44P	12910
	B:1C5:1C3:0.44P	584
	B:1C5:2C3:0.66P	93
	B:1C5:3C3:0.88P	296
Trimodal	T:1C5:1C2:4C3:1.32P	311
	T:1C5:1C2:1C3:0.66P	5850
	T:2C5:1C2:2C3:1.10P	6834
	T:2C5:1C2:4C3:1.54P	312
	T:1C5:1C2:2C3:0.88P	313

D. Pot Life Calculation

Table 7.7. Calculation of pot life and results of all products

Product Name	Equation	R^2	Pot life (hours)
M:1C5:0.36Pi	No data was available	-	0
M:1C2:0.36Pi	$y = -2E\text{-}06x^2 + 0.004x + 39.841$	0.9990	2
M:1C3:0.36Pi	$y = 2E\text{-}05x^2 + 0.0378x + 42.856$	1.0000	1
B:1C2:1C3:0.44Pi	$y = -2E\text{-}06x^2 + 0.004x + 39.841$	0.9990	2
B:1C2:2C3:0.66Pi	$y = 0.0161x + 146.76$	0.9645	15
B:1C2:2C3:0.66Pi$_{coated}$	$y = 0.0051x + 33.956$	0.9980	53
B:1C2:3C3:0.88Pi	$y = 2E\text{-}05x^2 + 0.0378x + 42.856$	1.0000	1
B:1C5:1C2:0.44Pi	No data was available	-	0
B:1C5:1C3:0.44Pi	$y = 0.0379x + 270.42$	0.9997	5
B:1C5:2C3:0.66Pi	$y = 0.0103x + 70.019$	0.9995	25
B:1C5:3C3:0.88Pi	$y = 0.0147x + 86.124$	1.0000	17
T:1C5:1C2:4C3:1.32Pi	$y = -1E\text{-}05x^2 + 0.0344x + 102.29$	0.9998	1
T:1C5:1C2:1C3:0.66Pi	No data was available	-	0
T:2C5:1C2:2C3:1.10Pi	No data was available	-	0
T:2C5:1C2:4C3:1.54Pi	$y = 0.02x + 115.54$	0.9998	9
T:1C5:1C2:2C3:0.88Pi	$y = 0.0262x + 227.52$	0.9999	8

E. Shore A Hardness Results

Table 7.8. Shore A hardness results of all products

Modality	Product Name	Curing (Day)	Hardness (Shore A)
Monomodal	M:1C5:0.36Pi	-	-
	M:1C2:0.36Pi	19	20 ± 2
	M:1C3:0.36Pi	7	21.5 ± 2
Bimodal	B:1C2:1C3:0.44Pi	9	20 ± 1
	B:1C2:2C3:0.66Pi	7	20 ± 1
	B:1C2:2C3:0.66Pi$_{coated}$	7	20 ± 1
	B:1C2:3C3:0.88Pi	7	20 ± 1
	B:1C5:1C2:0.44Pi	-	-
	B:1C5:1C3:0.44Pi	8	20 ± 2
	B:1C5:2C3:0.66Pi	7	20 ± 1
	B:1C5:3C3:0.88Pi	14	21 ± 2
Trimodal	T:1C5:1C2:4C3:1.32Pi	7	20 ± 1
	T:1C5:1C2:1C3:0.66Pi	13	23 ± 2
	T:2C5:1C2:2C3:1.10Pi	7	20 ± 2
	T:2C5:1C2:4C3:1.54Pi	7	21 ± 2
	T:1C5:1C2:2C3:0.88Pi	7	22 ± 3

F.   True Density Results

Table 7.9. True density results of all products

| Modality	Product Name	TRUE DENSITY (g/cm^3)
		Value
Monomodal	M:1C5:0.36Pi	-
	M:1C2:0.36Pi	1.4557 ± 0.0004
	M:1C3:0.36Pi	1.5818 ± 0.0004
Bimodal	B:1C2:1C3:0.44Pi	1.5921 ± 0.0006
	B:1C2:2C3:0.66Pi	1.5964 ± 0.0006
	B:1C2:2C3:0.66Pi$_{coated}$	1.5782 ± 0.0012
	B:1C2:3C3:0.88Pi	1.6118 ± 0.0006
	B:1C5:1C2:0.44Pi	-
	B:1C5:1C3:0.44Pi	1.5827 ± 0.0006
	B:1C5:2C3:0.66Pi	1.5824 ± 0.0003
	B:1C5:3C3:0.88Pi	1.6063 ± 0.0008
Trimodal	T:1C5:1C2:4C3:1.32Pi	1.5877 ± 0.0003
	T:1C5:1C2:1C3:0.66Pi	1.5882 ± 0.0004
	T:2C5:1C2:2C3:1.10Pi	1.5941 ± 0.0004
	T:2C5:1C2:4C3:1.54Pi	1.5957 ± 0.0015
	T:1C5:1C2:2C3:0.88Pi	1.5826 ± 0.0004

G.   Uniaxial Tensile Test Results

Table 7.10. Uniaxial tensile test results of all products

| Modality	Product Name	Tensile Strain (%)	Tensile Stress (MPa)
Monomodal	M:1C5:0.36Pi	-	-
	M:1C2:0.36Pi	25.35	0.28
	M:1C3:0.36Pi	10.54	0.17
Bimodal	B:1C2:1C3:0.44Pi	20.34	0.27
	B:1C2:2C3:0.66Pi	17.5	0.23
	B:1C2:2C3:0.66Pi$_{coated}$	20.91	0.28
	B:1C2:3C3:0.88Pi	19.8	0.25
	B:1C5:1C2:0.44Pi	-	-
	B:1C5:1C3:0.44Pi	22.83	0.28
	B:1C5:2C3:0.66Pi	31.05	0.24
	B:1C5:3C3:0.88Pi	19.08	0.22
Trimodal	T:1C5:1C2:4C3:1.32Pi	20.84	0.27
	T:1C5:1C2:1C3:0.66Pi	15.47	0.29
	T:2C5:1C2:2C3:1.10Pi	21.42	0.29
	T:2C5:1C2:4C3:1.54Pi	12.98	0.2
	T:1C5:1C2:2C3:0.88Pi	17.82	0.27

H. Results of Statistical Analysis

(a)

(b)

(c)
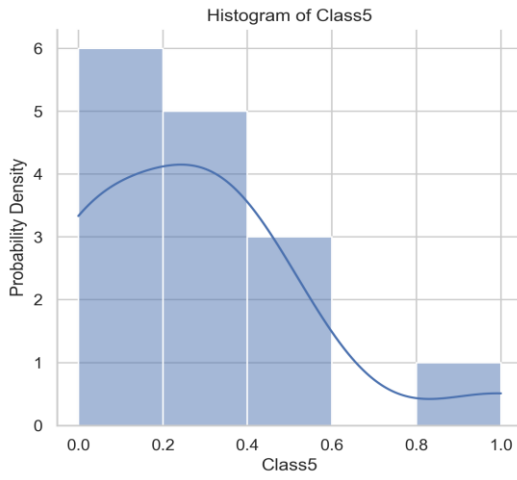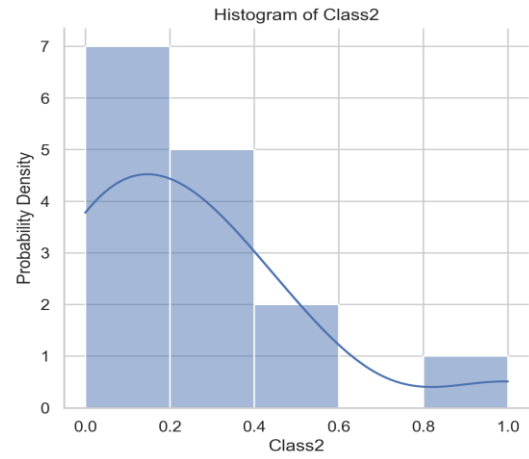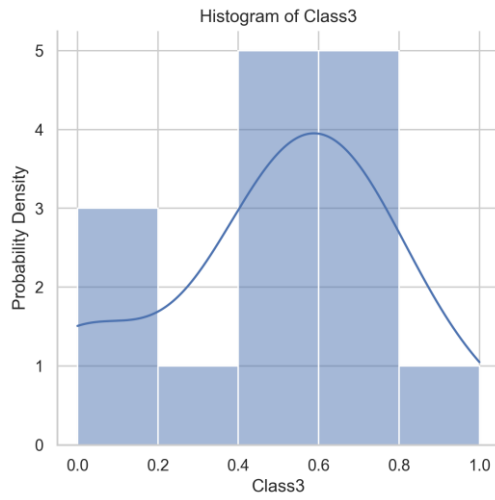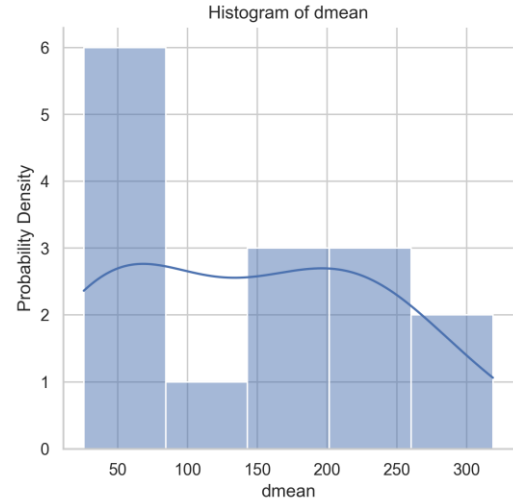
(d)
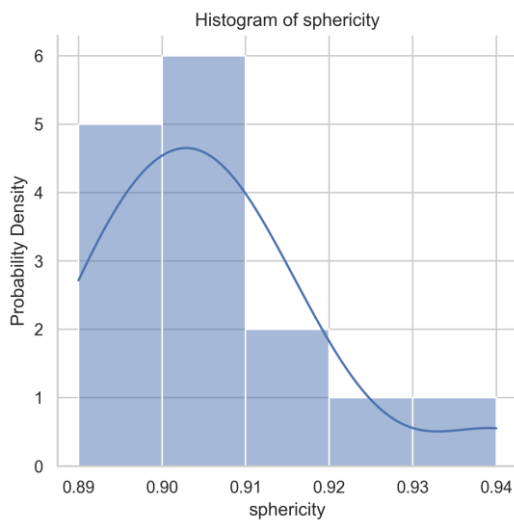
(e)
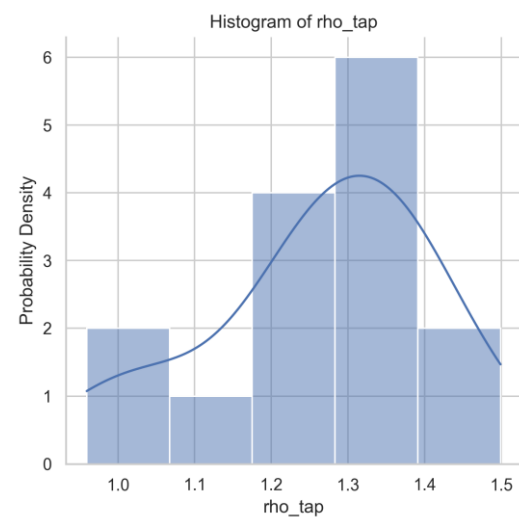
(f)
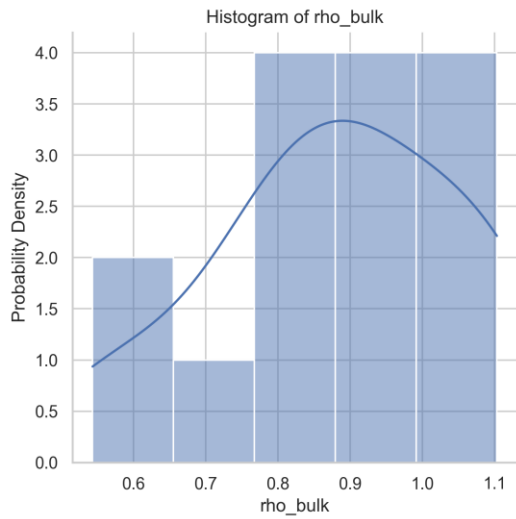
(g)
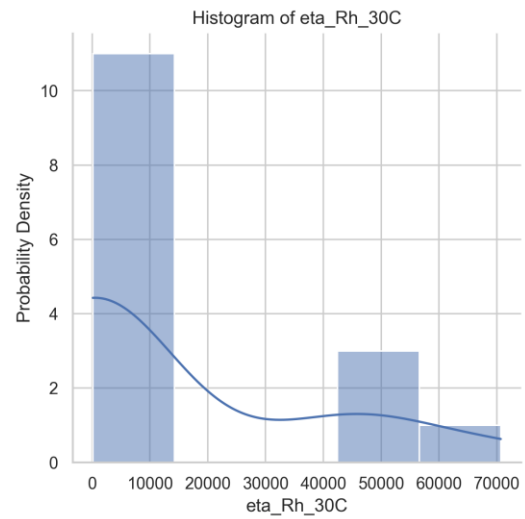
(h)
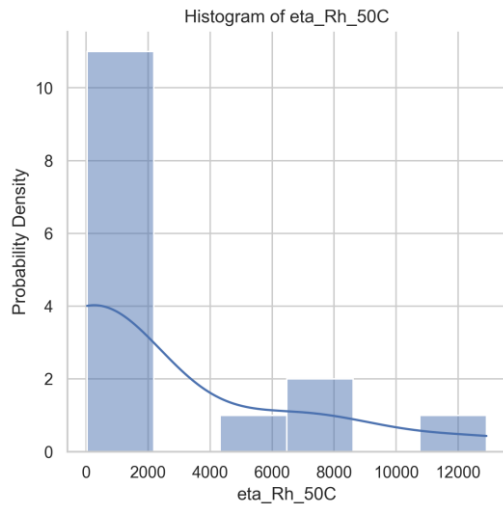
(i)

(j)

(k)
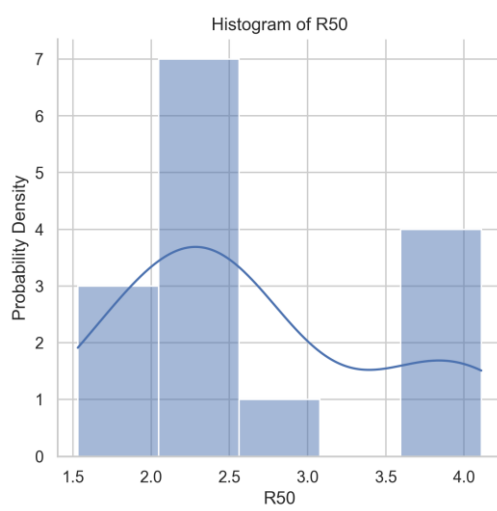
(l)

Figure 7.1. Probability distributions of (a) mass ratio of HMX Class 5, (b) mass ratio of HMX Class 2, (c) mass ratio of HMX Class 3, (d) mean diameter (μm), (e) sphericity, (f) tapped density (g/ml), (g) bulk density (g/ml), (h) vi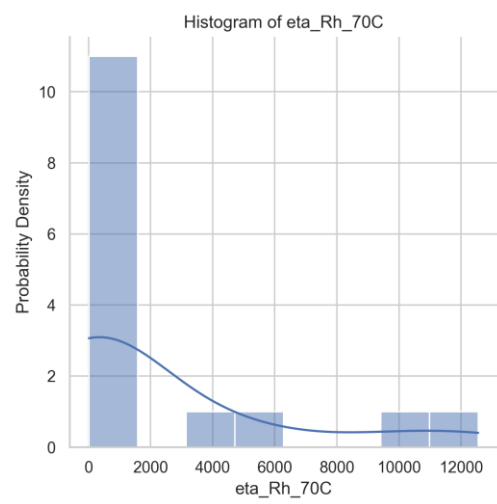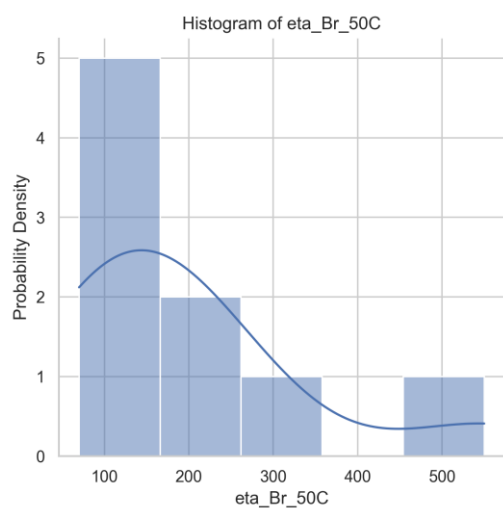scosity from rheometer at 30°C (Pa.s), (i) viscosity from rheometer at 50°C (Pa.s), (j) viscosity from rheometer at 70°C (Pa.s), (k) viscosity from Brookfield at 50°C (Pa.s), (l) logarithm of viscosity from rheometer at 50°C (Pa.s).

Table 7.11. Raw data for diverging heatmap of rheometer viscosity (Pa.s) results at 30°C, 50°C, 70°C

	η_{Rh} at 30 °C	η_{Rh} at 50 °C	η_{Rh} at 70 °C
η_{Rh} at 30 °C	1.0000	0.8821	0.8091
η_{Rh} at 50 °C	0.8821	1.0000	0.9802
η_{Rh} at 70 °C	0.8091	0.9802	1.0000
η_{Br} at 50 °C	0.1027	0.0128	0.1710

Table 7.12. Raw data of diverging heatmap of Rheometer result at 50°C, mean diameter, sphericity, tapped density and bulk density

	η_{Rh} at 50 °C (Pa.s)	d_{mean} (μm)	φ	ρ_{tapped} (g/ml)	ρ_{bulk} (g/ml)
η_{Rh} at 50 °C (Pa.s)	1.0000	-0.5763	0.7271	-0.7285	-0.7578
d_{mean} (μm)	-0.5763	1.0000	-0.6434	0.6854	0.6726
φ	0.7271	-0.6434	1.0000	-0.6967	-0.7925
ρ_{tapped} (g/ml)	-0.7285	0.6854	-0.6967	1.0000	0.9622
ρ_{bulk} (g/ml)	-0.7578	0.6726	-0.7925	0.9622	1.0000

Table 7.13. Second table of Results of test of normality

Control Group	Test Group	MW Test Result	KS Test Result
η_{Rh} at 30 °C	η_{Rh} at 50 °C	MW-Not Significant	KS-Not Significant
η_{Rh} at 30 °C	η_{Rh} at 70 °C	MW-Not Significant	KS-Not Significant
η_{Rh} at 50 °C	η_{Rh} at 70 °C	MW-Not Significant	KS-Not Significant
η_{Rh} at 30 °C	η_{Br} at 50 °C	MW-Significant	KS-Significant
η_{Rh} at 50 °C	η_{Br} at 50 °C	MW-Not Significant	KS-Not Significant
η_{Rh} at 70 °C	η_{Br} at 50 °C	MW-Not Significant	KS-Not Significant

Table 7.14. First table of results of test of normality

Control Group	Test Group	Group Sizes	Mean of Control	Mean of Test	St. Dev. of Control	St. Dev. of Test
η_{Rh} at 30 °C	η_{Rh} at 50 °C	15	14016	2417	23269	3905
η_{Rh} at 30 °C	η_{Rh} at 70 °C	15	14016	2222	23269	3819
η_{Rh} at 50 °C	η_{Rh} at 70 °C	15	2417	2222	3905	3819
η_{Rh} at 30 °C	η_{Br} at 50 °C	9	478	197	197	140
η_{Rh} at 50 °C	η_{Br} at 50 °C	9	246	197	154	140
η_{Rh} at 70 °C	η_{Br} at 50 °C	9	224	197	134	140

Table 7.15 Second table of results of test of normality

Control Group	Test Group	Shapiro test p-value		Levene's test p-value	MW P-value	KS P-value
		control set	test set			
η_{Rh} at 30 °C	η_{Rh} at 50 °C	0.0000	0.0001	0.0791	0.1057	0.1844
η_{Rh} at 30 °C	η_{Rh} at 70 °C	0.0000	0.0000	0.0746	0.0680	0.1844
η_{Rh} at 50 °C	η_{Rh} at 70 °C	0.0001	0.0000	0.8998	0.6187	0.6781
η_{Rh} at 30 °C	η_{Br} at 50 °C	0.5733	0.0167	0.3276	0.0104	0.0336
η_{Rh} at 50 °C	η_{Br} at 50 °C	0.3332	0.0167	0.6457	0.3772	0.3517
η_{Rh} at 70 °C	η_{Br} at 50 °C	0.3370	0.0167	0.9946	0.5365	0.7301